RADICAL FORMATION AND FUNCTIONS IN MYCOBACTERIUM TUBERCULOSIS CATALASE-PEROXIDASE (KatG) AND IN CRYPTOCOCCUS NEOFORMANS MELANIN.

by

Abdelahad Khajo

A dissertation submitted to the Graduate Faculty in Chemistry in partial fulfillment of
the requirements for the degree of Doctor of Philosophy,
The City University of New York

2012

This manuscript has been read and accepted for the Graduate Faculty in Chemistry in satisfaction of the dissertation requirement for the degree of Doctor of Philosophy.

Date

Chair of Examining Committee
Dr. Richard S. Magliozzo

Date

Executive Officer
Dr. Maria D. Tamargo

Supervisory Committee:

Dr. Roberto Sanchez-Delgado

Dr. Ruth E. Stark

Dr. Johannes J. P. Schelvis

THE CITY UNIVERSITY OF NEW YORK

ABSTRACT

RADICAL FORMATION AND FUNCTIONS IN MYCOBACTERIUM TUBERCULOSIS CATALASE-PEROXIDASE (KatG) AND IN CRYPTOCOCCUS NEOFORMANS MELANIN.

by

Abdelahad Khajo

Adviser: Dr. Richard S. Magliozzo

The dual-function heme enzyme catalase-peroxidase, KatG, is found in many microorganisms but in the human pathogen *M. tuberculosis* it is the only catalase ($2H_2O_2 \rightarrow O_2 + 2H_2O$) and plays an important role in protecting this organism against oxidative stress. The structural and functional origins of its high catalase activity are therefore of special interest. KatG also exhibits a broad-spectrum peroxidase activity ($ROOH + 2AH \rightarrow 2ROH + 2A^{\bullet}$) and in *M. tuberculosis* it is responsible for peroxidative activation of the *pro-drug* isoniazid used to treat tuberculosis infection.

Previous studies have shown that the catalase activity of KatG depends upon a unique adduct structure consisting of three conserved amino acids (Met255, Tyr229 and Trp107, M-Y-W) on the distal side of the heme pocket and that this adduct enables formation of a unique radical intermediate required for efficient turnover of H_2O_2. Here, EPR measurements along with site-directed mutagenesis and isotope labeling experiments allowed assignment of the 'narrow doublet' radical signal found during catalase turnover to Tyr229 of the M-Y-W adduct, explained the operation of this radical in KatG using optical and stopped-flow spectrometry, and elucidated a function for this unique cofactor and a role for neighboring residues in the enzyme's

catalase activity. Based on these findings, a new radical-dependent catalase reaction mechanism in KatG could be proposed.

Previous studies also showed formation of other amino acid-based radicals in KatG upon reaction with alkyl peroxides. Gaining insights into the poorly-understood peroxidase reaction mechanism in KatG through identifying the location and the possible function of the ‘wide doublet’ radical signal was among the goals of this thesis. Mutagenesis and rapid freeze-quench EPR experiments revealed the involvement of several residues in an electron transfer pathway including Tyr229, Tyr597, Tyr678, Trp90, Trp135, and Trp149. Other important aspects regarding the peroxidase function of KatG such as the electronic structure of its initial hypervalent heme species and the role of proximal Trp321 were studied. While details of the peroxidase reaction in KatG are far from being resolved, a mechanism was presented based on the available data.

The second part of this work was devoted to studying another biologically-relevant free radical, which occurs in eumelanin from the fungus *C. neoformans*. With the application of EPR spectroscopy, UV-Vis spectrometry, chemical analyses, and other physico-chemical techniques to investigate how high-dose gamma irradiation under aqueous aerobic conditions interacts with the semiquinone radical and affects the physical and chemical properties of natural and synthetic melanins, the studies aimed to gain insights into a radioprotective role of melanin in fungal cells.

Findings here revealed a shielding function for melanin in live fungal cells from high-dose ionizing radiation by attenuating the destructive effects of radiolysis-induced hydroxyl radicals and serving as a sacrificial barrier in the cell wall. Chemical analysis of irradiated samples showed that hydroxyl radical attack on susceptible sites in melanin subunits lead to C-C bond cleavage and the release of low molecular weight aldehydes.

ACKNOWLEDGMENTS

I would like to thank my supervisor Professor Richard S. Magliozzo for his generous help and guidance throughout the duration of my doctoral studies. At many stages in the course of this dissertation, his advice, new ideas, positive outlook and confidence inspired me and gave me the courage to continue and reach my research goals. Furthermore, his careful editing contributed enormously to the production of this thesis.

I want to express my sincere gratitude to all the people working in Dr. Magliozzo's laboratory at Brooklyn College over the past few years who helped me in the completion of my thesis studies. In particular, I wish to thank Dr. Javier Suarez and Dr. Xiangbo Zhao who offered me great help with the KatG project. In addition, the help of Dr. Richard M. Burger and Mr. Yan Levitsky with the melanin project is highly appreciated.

I would like to thank the medical scientists from Albert Einstein College of Medicine: Dr. Ruth A. Bryan, Dr. Ekaterina Dadachova, and Dr. Arturo Casadevall for their collaboration on the melanin project. I also want to acknowledge all the other collaborators on projects that were not mentioned in this thesis: Dr. Kalina Ranguelova, Dr. Roberto Colangeli, and Dr. Kalle Levon.

I also wish to thank all the members of my doctoral thesis committee: Dr. Roberto Sanchez-Delgado, Dr. Ruth E. Stark, and Dr. Johannes J. P. Schelvis for their valuable discussions, input, and accessibility during the past few years.

Finally, I would like to thank all my friends and family members for their continuous support and encouragement.

TABLE OF CONTENTS

LIST OF TABLES

LIST OF SCHEMES

LIST OF FIGURES

PART I

The formation, consumption, and potential catalytic role of amino acid-based radicals in catalase-peroxidase (KatG) from *Mycobacterium tuberculosis.*

Chapter 1: Introduction, background, and current research objectives.

Chapters 1-3 of this thesis are focused on studying the structural and catalytic features of the overexpressed heme enzyme catalase-peroxidase (KatG) from *Mycobacterium tuberculosis* (*Mtb*) upon turnover of peroxides. This study gains its significance because of the widely-accepted involvement of KatG in the activation of the first-line anti-tuberculosis antibiotic, isoniazid (isonicotinic acid hydrazide, INH). Special attention throughout this thesis research is centered on the identification of amino acid-based radicals formed in KatG upon turnover of different peroxides and explaining the role of these radicals in KatG catalysis and possibly in INH activation by KatG. Consequently, this study aims to gain an insight into the mechanistic reasons behind the failure of the INH therapy in bacterial strains carrying mutant *katG* genes by examining the structure and function of wild-type (WT) KatG enzyme and some specific mutants of interest.

The application of electron paramagnetic resonance (EPR) spectroscopy is the main tool utilized throughout this section. Other physico- and biochemical techniques including optical and stopped-flow spectrophotometry, site-directed mutagenesis, isotope-labeling, and the rapid freeze-quench technique, along with theoretical calculations (collaboration with Dr. A. Jarzecki), have also been applied in parallel with EPR to explain the radical behavior and role in KatG.

1.1 *M. tuberculosis*: an old enemy with new defenses.

Although the clinical and microbiological aspects of *M. tuberculosis* are beyond the scope of this thesis, a general historical overview about the disease is necessary to express the significance of the research and the urgency of the health issue behind it.

Tuberculosis (TB) is an old infectious disease in humans caused by the *M. tuberculosis* pathogen. Just until a few decades ago, TB was thought to have been nearly eradicated as the number of cases in the United States and the world was dropping [1]. However, in the last 20 years or so, the disease has made a quick comeback, reenergized by the reduced immune response among HIV-positive patients and spread quickly in urban areas with overcrowding, new immigrants, homelessness, and poverty. Currently, according to World Health Organization (WHO) estimates, TB kills nearly 2 million people a year worldwide and introduces millions of new infections (over 9 million in 2010). The WHO approximates that 36 million people will die of TB by 2020 if it is not controlled. The overall TB case rate in the United States in 2010 was 3.5 per 100,000 people, with rates of infection and disease being higher among foreign-born individuals. The annual cost of TB in the United States in the recent past has exceeded $1 billion. Globally, as shown in Figure 1.1, the largest number of new TB cases occurs in sub-Saharan Africa, South-East Asia, and the Eastern Mediterranean regions at nearly 350 cases per 100,000 populations in some areas [1].

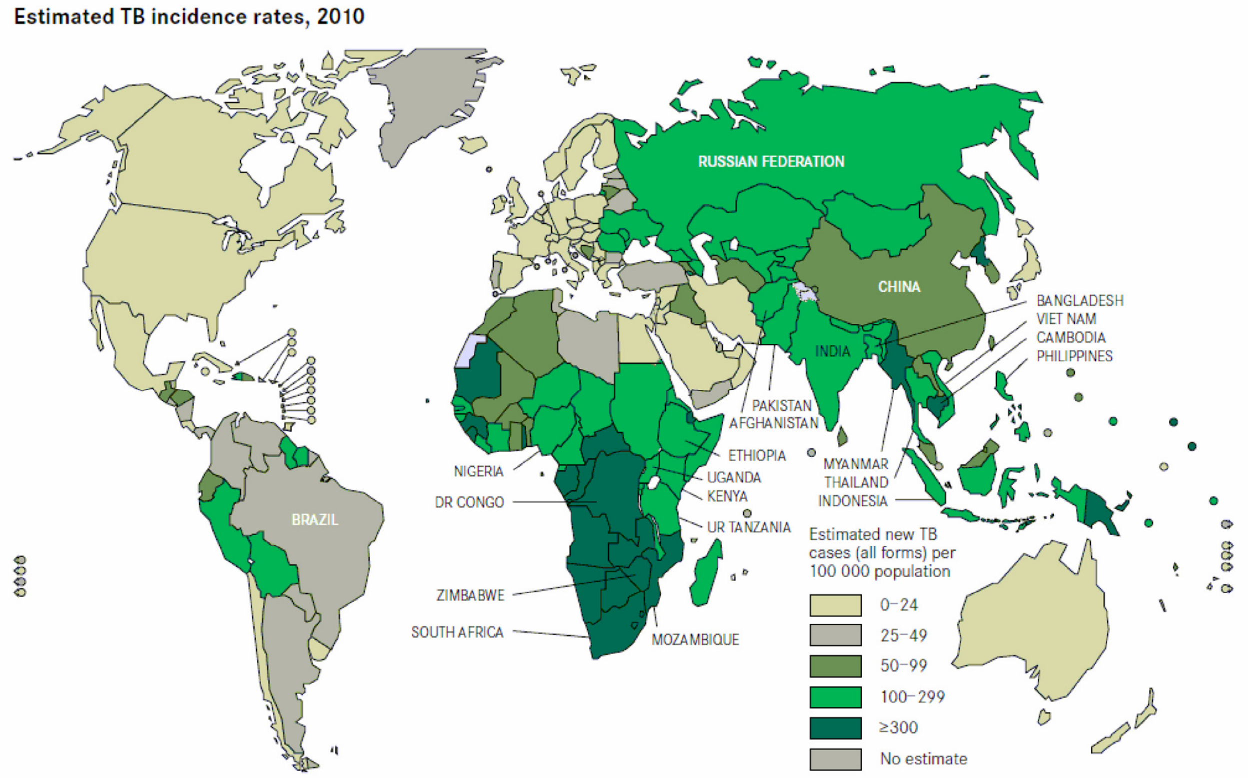

Figure 1.1. World map showing WHO estimates for rates of new TB cases by country in 2010. (Adapted from WHO [1]).

The *Mtb* pathogen is a bacillus that typically attacks the lungs (pulmonary TB) but it can affect other sites as well (extra pulmonary TB). The TB infection is highly contagious with the ability of each untreated person carrying the active disease to transmit the infection to between 10 and 15 other individuals. The disease is spread when an individual who is sick with pulmonary TB coughs, sneezes, talks, or spits forcing the TB germs (bacilli) into the air where an unlucky person needs only to inhale a small number of the TB bacilli to become infected [2-3].

1.2 Tuberculosis treatment, antibiotic resistance, and role of KatG in INH function.

The *Mtb* pathogen has been infecting humans since ancient times, and evidence of tubercular decay has been found in the spinal columns of Egyptian mummies from several thousand years B.C [4]. Understanding of the true etiologic origin of TB began in 1882 when *Mtb* was first isolated by the German microbiologist Robert Koch who discovered a staining technique that enabled him to see the TB bacterium [3]. Although the TB treatment methodologies began in the late 19th century, the effective antibiotic treatment did not start until 1944 as streptomycin purified from *Streptomyces griseus* was first administered to humans and the results were extremely remarkable as the disease immediately stopped its development, the bacteria disappeared from the patient's sputum, and he recovered fully. Not surprisingly, a series of anti-TB drugs started to appear in the following years. This was very necessary because with the continuing streptomycin treatment, resistant mutants began appearing within a few months, risking the success of the antibiotic therapy. However, it was soon proven that using a combination of drugs could solve that problem [5].

Since 1952 until the present, isoniazid (INH) has been the most-successful, safest, and most-affordable first-line antibiotic against *Mtb* [6]. The structures of INH and other first-line drugs including rifampicin (RMP), pyrazinamide (PZA), ethambutol (EMB), and streptomycin (STM) are shown in Figure 1.2.

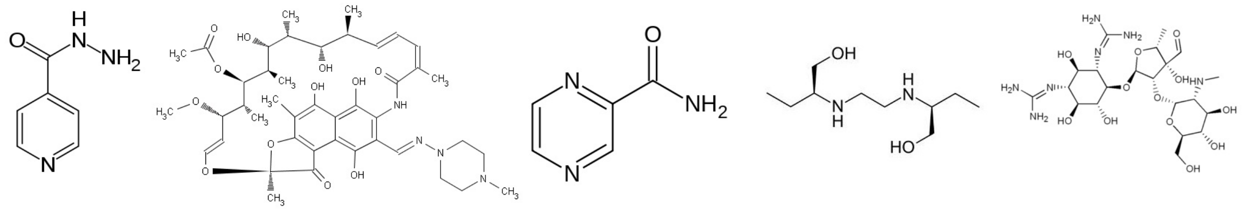

INH **RMP** **PZA** **EMB** **STM**

Figure 1.2. First-line drugs used to treat TB disease. From left to right: isoniazid, rifampin, pyrazinamide, ethambutol, and streptomycin. (Adapted from CDC [7]).

Nevertheless, the management of the disease is complicated by the fact that *Mtb* strains have been increasingly acquiring and accumulating mutations that confer resistance to INH and other first-line drugs. Furthermore, the emergence of multi-drug resistant (MDR) and extensively-drug resistant (XDR) TB, which make the individuals carrying these bacterial strains nearly untreatable, have made the treatment more difficult [8-10]. Some INH-resistant *Mtb* strains exhibited either a decrease or a complete lack of catalase activity. DNA sequence analysis of these strains revealed the presence of mutations in or deletions of the gene that encodes the KatG enzyme, which is the only catalase in *Mtb*. In addition, the introduction of the WT *katG* gene was shown to be sufficient to confer INH sensitivity to INH-resistant strains of *Mtb*. All together, these facts provide direct evidence for the importance of KatG to the *Mtb* pathogen [11-13].

Although not fully-understood, the widely-accepted mechanism of action of INH can be explained as follows: the *pro-drug* becomes activated by serving as a single-electron donor to one of KatG's radical intermediates, forming a hydrazyl radical which decomposes into an isonicotinic acyl radical ($IN^\bullet$) that reacts with a nicotinamide adenine dinucleotide (NAD^+) molecule to form an IN-NAD adduct (Figure 1.3). This adduct is a potent inhibitor of the *Mtb* enoyl-acyl carrier protein reductase, InhA, which is an enzyme necessary for the synthesis of mycolic acids, essential components of the bacterial cell wall. Interrupting the synthesis of mycolic acids disrupts the cell wall structure, consequently, killing the bacterial cells [14-17].

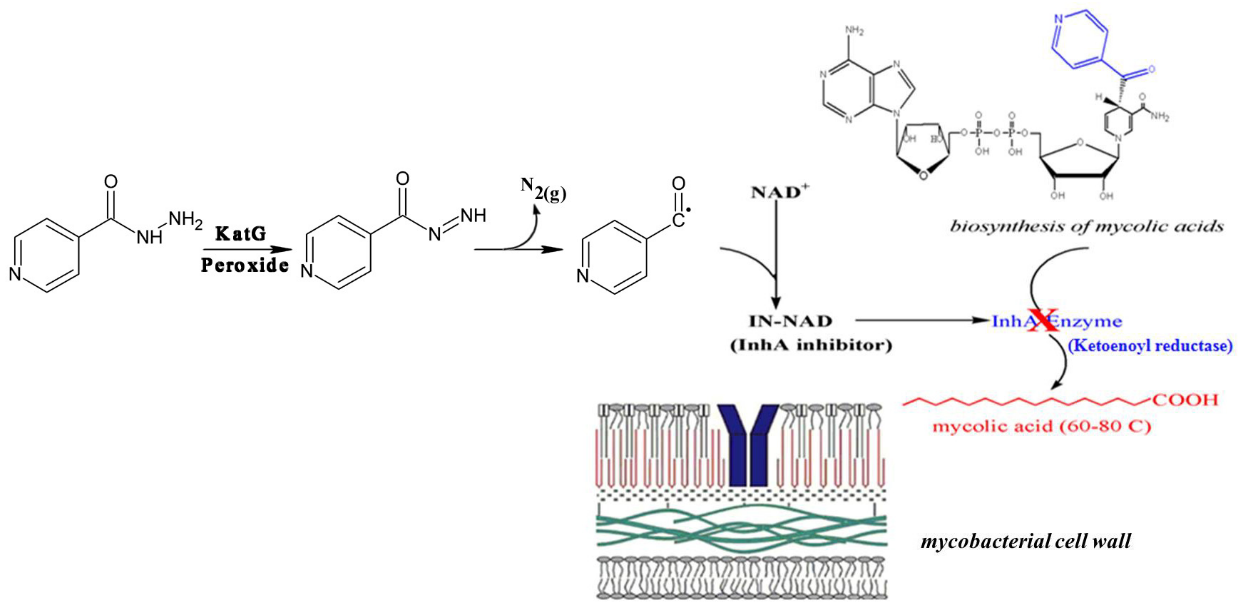

Figure 1.3. Proposed schematic mechanism of INH activation by KatG and its action on bacterial cell wall.

1.3 Structural and functional characteristics of M. tuberculosis catalase-peroxidase.

Mtb KatG is a member of a relatively new family of bifunctional bacterial heme enzymes, catalase-peroxidase, different from the monofunctional heme catalases, initially isolated from *E. coli* about 30 years ago [18-19]. Shortly after their initial identification, KatGs were found in several other microorganisms, all with a protein sequence showing little homology with typical catalases but high homology with prokaryotic peroxidases, including fungal cytochrome c peroxidase (CCP) and plant ascorbate peroxidase (APX) and were, therefore, classified in the Class I superfamily of peroxidases [20].

Mtb KatG, whose crystal structure is shown in Figure 1.4, is a homodimeric protein with a total molecular weight of ~160 kDa and each monomer consists of 740 amino acid residues and one heme group. This heme group in KatG is deeply buried in the N-terminal domain and this active site shares great structural similarity with those of monofunctional peroxidases. A small substrate access channel was defined that connects the surface of the protein with the active site and allows the passage of H_2O_2 and small aromatic molecules [20].

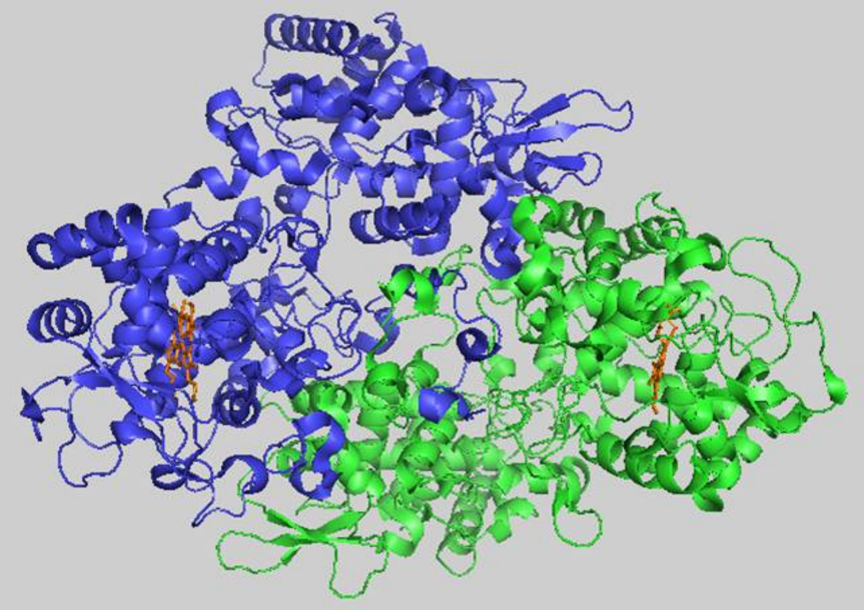

Figure 1.4. Crystal structure of *M. tuberculosis* catalase-peroxidase (2cca.pdb [21]). KatG structure is colored by protein subunits (blue and green), and heme groups are shown in orange.

Since KatG is the only catalase in *Mtb* [22], it is expected to be at least partially responsible for survival in macrophages by protecting the pathogen against oxidative stress. One of the first studies on the relationship between KatG and virulence of *Mtb* showed that INH-resistant isolates of *Mtb* were catalase-deficient and noticeably attenuated in guinea pigs [23]. This relationship was further supported by work done to clarify the role of KatG in the replication and persistence of *Mtb in vivo*, where a *katG* null strain of *Mtb* (*ΔkatG*) had a greatly reduced ability to replicate and persist in infected macrophages and mice [24].

The key functions of *Mtb* KatG are determined by its catalase and peroxidase activities. KatG possesses a broad-spectrum peroxidase activity that allows it to perform reactions similar to monofunctional peroxidases. It also exhibits a robust catalase activity despite having low structural homology with monofunctional catalases. KatG protects *Mtb* from oxidative damage within host macrophages by eliminating hydrogen peroxide (catalase reaction): $2H_2O_2 \rightarrow 2H_2O + O_2$, while it can also oxidize an organic reducing substrate through a peroxidase mechanism ($ROOH + 2AH \rightarrow 2ROH + 2A^{\bullet}$) [25-26].

In the typical catalase cycle in monofunctional enzymes (Scheme 1.1, top), a molecule of H_2O_2 reacts with the resting ferric enzyme to form a very reactive intermediate: ferryl heme porphyrin π-cation radical, $Fe(IV)=O(Por^{\pi+\bullet})$, referred to as Compound I, which contains two oxidizing equivalents relative to the ferric enzyme. Compound I then is reduced by a second molecule of H_2O_2 bringing the enzyme back to the resting state [27]. The details of this reaction (proton and electron transfers) are still not fully-understood.

The peroxidase cycle (Scheme 1.1, bottom) shares the same first step with the catalase cycle but the highly reactive species, Compound I, returns to the resting state by a different pathway involving first a reaction with a single-electron donor (usually a small aromatic molecule) to yield ferryl heme porphyrin, Fe(IV)=O(Por), known as Compound II. A second single electron reduction of Compound II reduces the enzyme back to the resting state [28].

The classical monofunctional heme catalase and heme peroxidase reaction pathways are illustrated in Scheme 1.1.

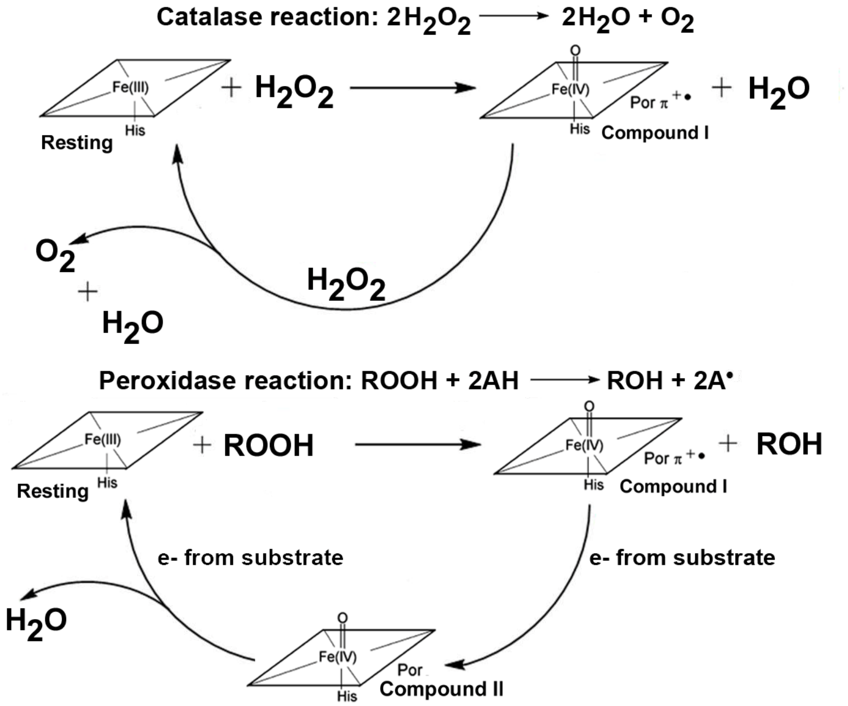

Scheme 1.1. The catalytic cycles of classical monofunctional heme catalases and monofunctional heme peroxidases.

A major difference from monofunctional peroxidases (but in common with classical catalases) is that KatG shows a rapid decay of the hypervalent heme (Compound I) intermediate (KatG Compound I shares some optical features with typical peroxidase Compound I) to the ferric state without the formation of the typical peroxidase Compound II. This happens even in the absence of a reducing substrate most probably due to the rapid formation of amino acid-based radicals and the possible participation of the radical intermediate(s) in the catalytic cycle [29-30].

Our research group has started investigating these aspects in the catalytic cycles of *Mtb* KatG and has made an important contribution demonstrating the presence of a catalytically-active amino acid-based radical during the catalase cycle in KatG [31]. Furthermore, in contrast to the reactions in the presence of H_2O_2, it has been observed that during the turnover of alkyl peroxide such as peroxyacetic acid (PAA), a series of radicals are formed in KatG through a single-electron oxidation of tyrosine and/or tryptophan residues (later chapters). Based on previous results from this lab, it is suggested that some of the redox-active residues involved in the electron transfer reactions in KatG include Tyr229 and Trp107. Tryptophan residues including W321, W300, W91, W135, and W149 were suggested elsewhere to be involved in radical formation in KatG and reaction with INH [32-33]. Therefore, identifying the radical-forming sites in KatG and understanding the catalytic relevance of these species are of great interest.

1.4 ***Main research goals.***

Explaining a role of the radicals in KatG catalysis (and possibly in INH activation) is among the goals of this thesis. Furthermore, understanding the structure of KatG is important toward elucidating its catalytic mechanisms especially since the correlation between the unusual features of its structure and particular mechanistic steps which involve radical species is not fully defined or understood yet. One of these remarkable structural features is the post-translational covalent modification Met255-Tyr229-Trp107 (M-Y-W adduct) found on the distal side of the heme pocket (Figure 1.5) that is required for catalase activity and formation of a catalytically-competent amino acid-based radical. The role of the M-Y-W adduct in catalysis and in radical formation in KatG is addressed in Chapter 2 of this thesis.

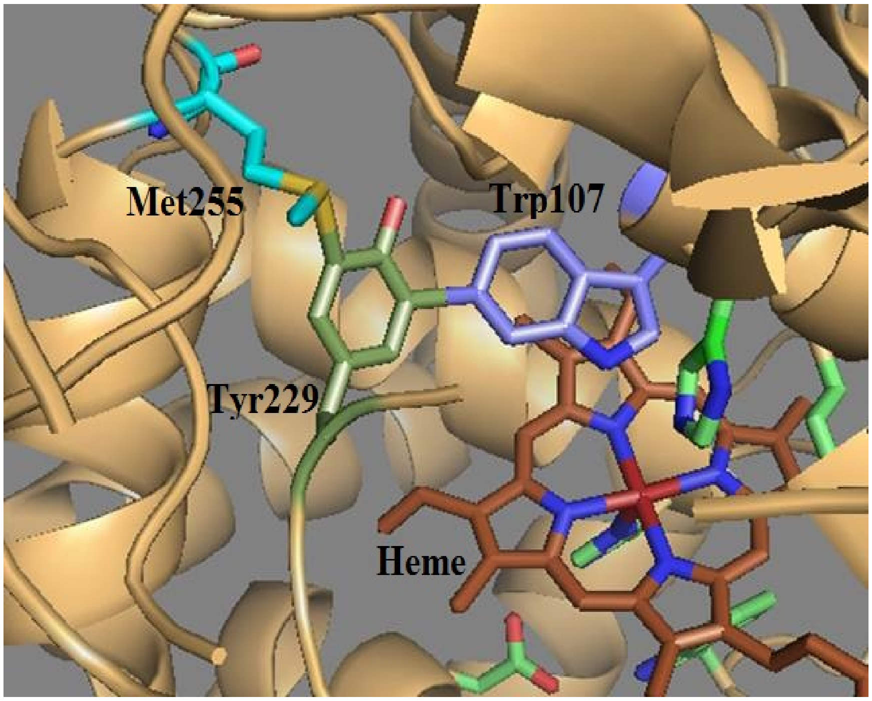

Figure 1.5. The active site (distal side) structure of *M. tuberculosis* KatG featuring the covalent methionine-tyrosine-tryptophan (M-Y-W) adduct and the heme group. This figure was generated using PyMOL (The PyMOL Molecular Graphics System, version 1.2r3pre, Schrödinger, LLC.) based on published KatG crystal structure (2cca.pdb).

Also among the important structure/function issues that are believed to be misunderstood about catalytic mechanisms in KatG is the electronic structure of the initial intermediate produced from a single turnover of peroxide. This species is not necessarily equivalent to typical peroxidase Compound I (Fe(IV)=O(Por$^{\pi+\bullet}$)) as in horseradish peroxidase (HRP). Is the catalytically-active radical that has been recently assigned to the unique M-Y-W adduct [34] part of Compound I or is proximal residue Trp321 also involved as a radical site, as in CCP Compound I; or can both species appear at the same time? Theoretical (DFT) calculations predict a 'versatile' Compound I structure for KatG such that both protein-based radicals exist simultaneously, along with a fraction of the typical Fe(IV)=O(Por$^{\pi+\bullet}$). Experimentally, very different conditions (excess H_2O_2 or excess alkyl peroxide) provide evidence for each of these species separately (later chapters).

The data in Chapters 2 and 3 is devoted to filling in details for mechanisms we now understand reasonably well (catalase) and not so well (peroxidase) that could be changed by site-directed mutagenesis at positions of interest.

Summary of the major findings includes: the formation of a catalytically-competent amino acid-based radical during the catalase reaction confirmed on Tyr229 of the heme distal side adduct of KatG; the participation of remote residues including Arg418 and Asp137, not required for the initial turnover of hydrogen peroxide, along with a steady-state dioxyheme intermediate in the catalase activity in KatG; the existence of a collection of secondary radicals formed upon turnover of alkyl peroxides involving several Tyr and Trp residues starting, likely, close to the heme and terminating at the surface of the enzyme in the absence of reducing substrate (to force the enzyme to reveal potential electron transfers); and an evidence for a radical formed on the proximal Trp321 (analogous to residue W191 in CCP) during turnover of alkyl peroxides.

EPR spectroscopy and the rapid freeze-quench methods have been used as the main tools for formation and detection of transient intermediates (radicals) that form during the fast catalytic reactions in KatG. Other techniques have been applied to obtain the data presented in this thesis including site-directed mutagenesis, isotopic-labeling, optical and stopped-flow spectrophotometry, computer simulations, and DFT calculations (collaboration).

Chapter 2: The catalase reaction mechanism in KatG and role of M-Y-W radical and remote amino acid residues.

2.1 ***Background.***

Heme enzymes contain an iron protoporphyrin IX in their active site (Figure 2.1) but, in general, heme proteins may contain other cofactors. The protoporphyrin ring is made up of 4 pyrrole rings linked by methene bridges. Four methyl, 2 vinyl, and 2 propionate side chains are attached to the pyrrole rings. The iron, which can either be in the ferrous, ferric, or ferryl oxidation states, has 6 possible coordination sites. The porphyrin ring has 4 nitrogen atoms that bind to the iron, while the 5th coordination positions of the iron is available for bonding to the proximal amino acid residue of the protein and the distal 6th position is vacant (as in most peroxidases) and available for coordination with exogenous or exchangeable ligands. The heme group allows the protein to carry out a biological function that the polypeptide alone cannot do. The iron in this group is capable of undergoing oxidation and reduction reactions; therefore this metal is the key player in the catalytic activity carried out by metalloproteins, except when a radical is also involved [28].

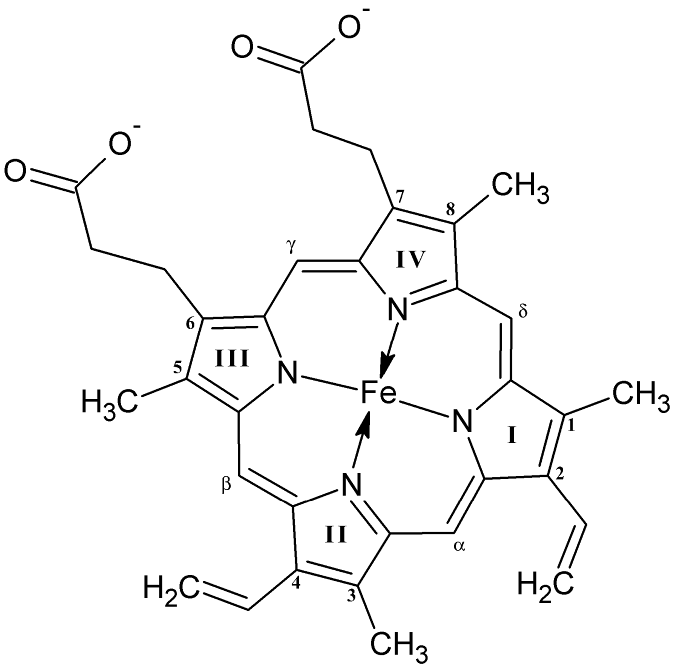

Figure 2.1. Structure of iron protoporphyrin IX. (Adapted from Dunford [28]).

Based on the mechanism of action of several heme enzymes, these unusual proteins can utilize amino acid-based radicals for catalysis [35]. In fact, immediately after the development of detection techniques for paramagnetic species, such as EPR spectroscopy, radicals were discovered in heme enzymes [36]. More recently, tyrosyl and tryptophanyl radicals in many other heme enzymes such as bovine catalase [37], turnip peroxidase [38], ribonucleotide reductase [39], prostaglandin H synthase [40], lignin peroxidase [41], and *Mtb* catalase-peroxidase [42-43] were detected. In many of these proteins, the radicals are associated with catalytic function, while in others the catalytic role of the radicals has not been identified yet. In the case of *Mtb* KatG, the work on amino acid-based radical locus assignment and catalytic function identification is still ongoing and is of special interest in this thesis.

2.2 <u>M-Y-W radical formation in Mtb KatG.</u>

In a recently-published work on the catalase reaction mechanism of KatG [31], our group reported the formation of a tyrosyl-like radical during the turnover of hydrogen peroxide, which was tentatively assigned to the unique distal side adduct consisting of three amino acid residues (Met255-Tyr229-Trp107, M-Y-W), covalently linked to each other through their side chains (Figure 1.5). The radical assignment was based on characterizations of X- and D-band EPR signals (Figures 2.2 and 2.3), DFT calculations, and site-directed mutagenesis of the adduct residues.

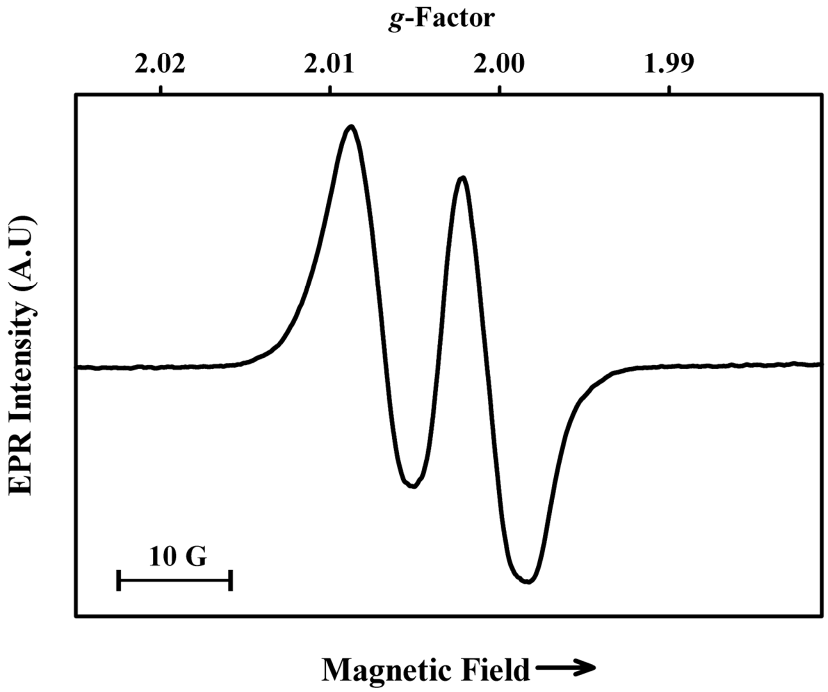

Figure 2.2. X-band RFQ-EPR spectrum of WT KatG (50 µM, final concentration) treated with 1000-fold molar excess of H_2O_2 at pH 8.5 frozen 20 ms after mixing. Experimental conditions: T = 77 K; microwave frequency = 9.45 GHz; microwave power = 0.1 mW; modulation amplitude = 1 G; average of 9 scans.

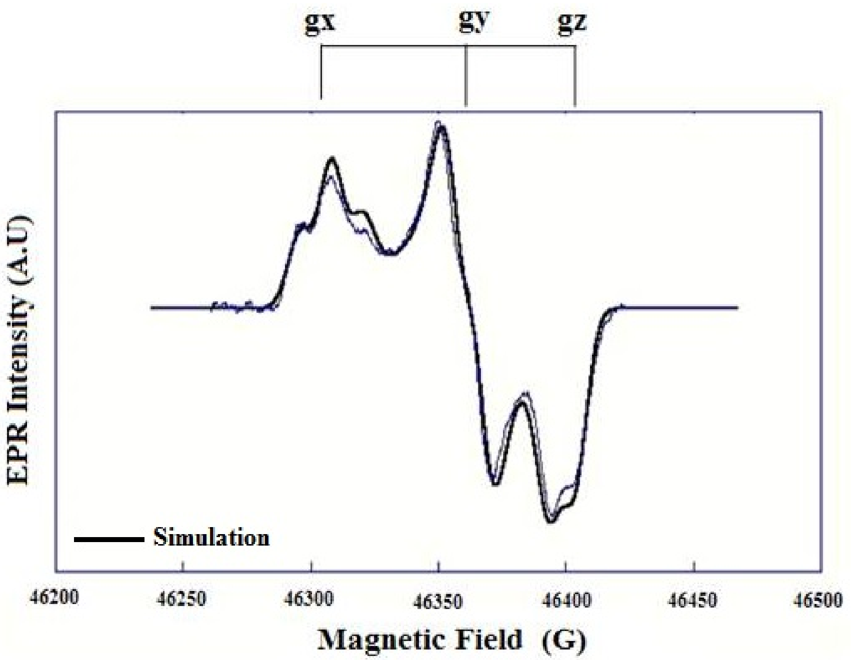

Figure 2.3. D-band (130 GHz) RFQ-EPR spectrum of WT KatG (75 µM) treated with 4000-fold molar excess of H_2O_2 at pH 8.5 frozen 35 ms after mixing. (Adapted from Suarez [31]).

Some of the primary experimental data (and calculations) pointed to Tyr229 as a site of radical formation in KatG but it was not clear whether Tyr229 was the only participant or there were other Tyr residues involved in a radical pathway. Therefore, each Tyr residue in KatG was mutated. Furthermore, WT KatG with deuterium-labeled tyrosine was prepared with the aim to unquestionably confirm the identity of the amino acid-based radical in KatG.

Part of the results presented below about the adduct radical are reproduced, with permission, from the article: "A radical on the Met-Tyr-Trp modification required for catalase activity in catalase-peroxidase is established by isotopic labeling and site-directed mutagenesis." Zhao, X., Suarez, J., Khajo, A., Yu, S., Metlitsky, L., and Magliozzo, R. S. (2010) *J. Am. Chem. Soc.* **132**(24):8268-8269. Copyright © 2010 American Chemical Society [34].

More recent data about the catalase reaction mechanism and function of remote residues including experimental and theoretical findings, presented later in this chapter, were in review at the time of this writing.

All EPR sample preparations, measurements, and simulations of spectra, optical and stopped-flow spectrometry, and KatG activity assays shown in this section were carried out by the author, while site-directed mutagenesis, enzyme purification, and the isotope-labeling of tyrosines in KatG were done with the help of Dr. J. Suarez and Dr. X. Zhao.

*2.3 **Construction and characterization of tyrosine mutants in Mtb KatG.***

The KatG monomer contains 21 tyrosine residues. As stated earlier, a major part of this thesis study is devoted to identifying the specific tyrosine residue(s) at which amino acid-based radical is formed upon turnover of peroxides and defining a possible radical role in catalytic function of KatG. For this purpose, KatG enzymes with a single mutant at every tyrosine residue (in most cases a tyrosine to phenylalanine modification) were prepared and characterized by measuring the catalase and peroxidase activities and, more importantly, inspecting the EPR spectra upon turnover of hydrogen peroxide and alkyl peroxides.

Purified overexpressed Tyr-mutant KatG enzymes (prepared according to the procedure for bacterial culture and protein purification described in [44]) showed normal optical purity ratio (Reinheitzahl or Rz, defined as A_{405}/A_{280}) of ~0.50 similar to that for WT KatG (0.55). The spectroscopic features are consistent with a mixture of 5- and 6-coordinate high-spin ferric heme in the resting mutant enzymes similar to WT KatG. The catalase-specific activity of most of the Tyr mutants was normal compared to WT, with the notable exception of KatG[Y229F] which showed reduction in rate of more than 1000-fold, and KatG[Y678S] with ~22% of the activity of WT KatG.

All tyrosine mutants exhibited close to normal peroxidase activity (evaluated according to [44] using tert-butyl hydroperoxide and *o*-dianisidine) with the only exception found in KatG[Y678S] which demonstrated activity of ~26% of WT KatG. Preparation of KatG[Y678F] was attempted but the protein was highly unstable (Dr. J. Suarez, personal communication). Therefore, KatG[Y678S] mutant was prepared instead. KatG[Y678S] mutant was also relatively unstable but a small yield of partially purified protein was obtained. This amount was enough to characterize for catalase and peroxidase activities and perform some EPR experiments.

The catalase and peroxidase specific activities of WT KatG and the Tyr mutants, measured by the author and colleagues in the laboratory, are summarized in Table 2.1.

KatG mutant	Catalase activity (unit/mg)	Peroxidase activity (unit/mg)
Y28F	3191	0.98
Y64F	3999	1.75
Y95F	3582	1.86
Y98F	3594	0.73
Y113F	3895	2.40
Y155S	3588	0.93
Y197F	3268	0.88
Y210F	3181	1.23
Y229F	2.7	2.80
Y304F	3374	1.85
Y337F	3548	1.36
Y339F	2320	0.94
Y353F	3800	1.58
Y390F	2839	0.98
Y413F	3033	1.03
Y426F	3841	2.12
Y597F	2587	1.27
Y608F	3196	1.73
Y638F	3065	1.20
Y678S	894.5	0.29
Y711F	2357	1.86
WT	4000	1.10

Table 2.1. Catalase and peroxidase activity characterizations of tyrosine mutants in KatG.

2.4 Formation of the 'narrow doublet' EPR signal in KatG.

Upon manual mixing of ferric WT KatG with excess H_2O_2 followed by freezing the reaction in liquid nitrogen within ~1.5 sec, the X-band EPR spectrum recorded at 77 K exhibited a 'narrow doublet' signal characterized by a *g*-factor of 2.0036, linewidth of 17 Gauss (peak to trough), and a principal hyperfine splitting of 11 Gauss (Figure 2.4).

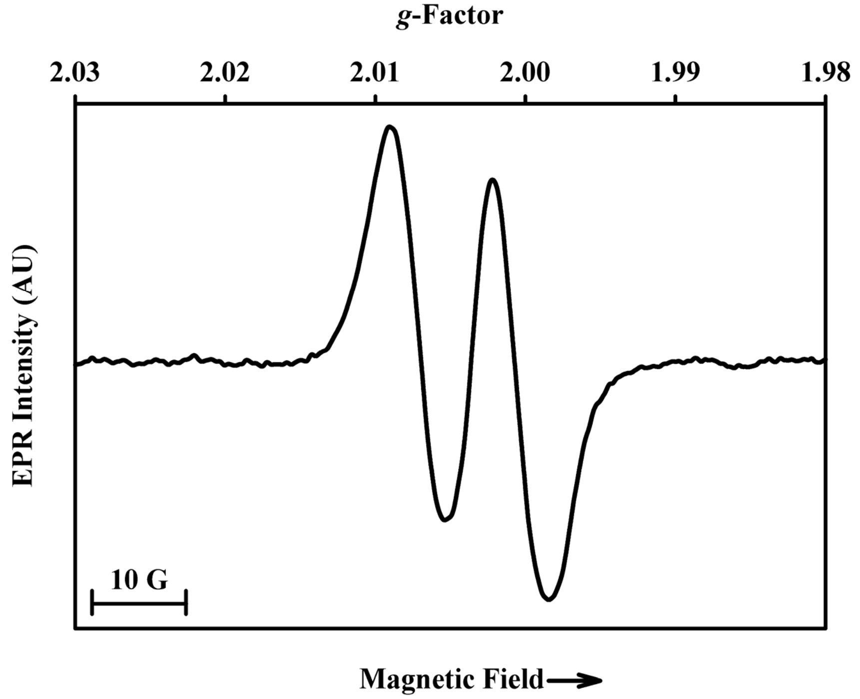

Figure 2.4. X-band EPR spectrum of WT KatG (50 µM) treated with 8000-fold molar excess of H_2O_2 at pH 8.5 frozen manually within 1.5 sec after mixing. Experimental conditions: T = 77 K; microwave frequency = 9.45 GHz; microwave power = 0.1 mW; modulation amplitude = 1 G; average of 9 scans.

The large excess of peroxide was routinely used to produce a detectable yield of the radical during rapid turnover. The narrow doublet was the only signal observed in the *g* = 2 region and had an intensity of ~0.05 spins/heme for WT KatG under the experimental conditions of manual mixing and freezing. Much greater yields are reported below using the rapid freeze-quench method. According to a simulation (published before this work) of the X-band EPR signal, the simple shape with a single splitting is characteristic of a protein-based radical with one strong hyperfine coupling interaction with one proton and, possibly, other weaker interactions too small to produce additional splitting of the signal [43]. Furthermore, the *g*-tensor values (g_x,g_y,g_z) found in the high-field EPR spectrum (Figure 2.3) were similar to those expected for a tyrosyl radical (even though the g_y, and g_z were slightly below the values reported in unmodified tyrosyl radicals) and, thus, an electronically modified tyrosyl-like radical was suggested [31]. Therefore, the hyperfine couplings contributing to the EPR signal come from the β-methylene hydrogens adjacent to the phenolic ring of a tyrosine containing the unpaired electron. These are known to produce an isotropic hyperfine coupling which was the case according to the principal splitting in the high-field EPR spectrum.

Twenty of the 21 tyrosine mutants in KatG exhibited the same narrow doublet in similar yields as in WT KatG when reacted with 8000-fold molar excess of H_2O_2, while KatG[Y229F] showed no signal in the $g = 2$ region (Figure 2.5) under such conditions.

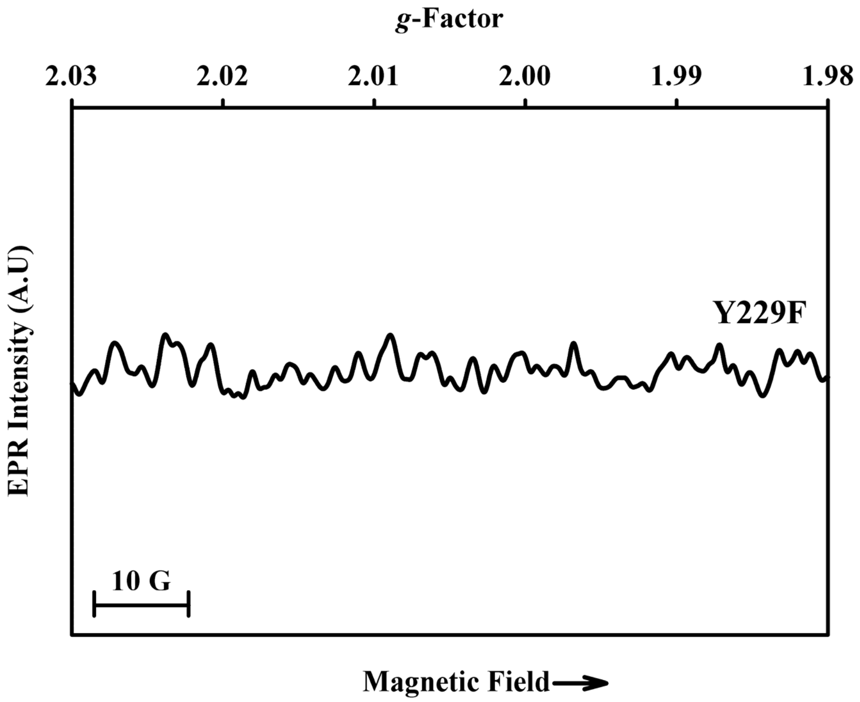

Figure 2.5. X-band RFQ-EPR spectrum of KatG[Y229F] (50 µM) treated with 8000-fold molar excess of H_2O_2 at pH 8.5 frozen manually within 1.5 sec after mixing. Experimental conditions: T = 77 K; microwave frequency = 9.45 GHz; microwave power = 0.1 mW; modulation amplitude = 1 G; average of 9 scans.

While the overall signal shape was nearly identical among all Tyr mutants and matched that of WT KatG, the intensity of the narrow doublet signal varied slightly from one mutant to another but this is expected under the manual mixing conditions as the signal is known to form after a few milliseconds and react quickly. Besides intensity, no significant difference was seen among the mutants in terms of hyperfine splitting (~11 Gauss) or linewidth (~17 Gauss) of the narrow doublet. Figure 2.S1 (Appendix B) shows the EPR spectra of the remaining 20 tyrosine mutants of *Mtb* KatG each mixed with 8000-fold molar excess H_2O_2 and frozen manually before EPR measurement.

So far, these results suggest that the narrow doublet signal arises from a radical located on Tyr229 (or that Tyr229 is required to form a radical on another Tyr).

2.5 __Isotopic-labeling of tyrosine in KatG.__

After the initial clues for assignment of the narrow doublet signal to Tyr229 based on the EPR results with mutant enzymes, it was of great interest to confirm that the observed narrow doublet signal comes from a radical located on Tyr229 in KatG. Therefore, the next step in the radical analysis was to use uniformly deuterotyrosine-labeled enzyme with isotopic labeling at the β-methylene group or in the tyrosine ring (Figure 2.6). The hypothesis was that if the radical is located on a tyrosine in KatG, changes in the linewidth of the EPR signal in a tyrosyl radical upon isotopic labeling at the β-methylene should be found due to the smaller magnetic moment of ^2H compared to ^1H [45]. Additionally, if the radical is located on Tyr229, isotopic labeling at the 3’ and 5’ positions of the tyrosine ring should not have an impact on the EPR signal because Tyr229 lacks hydrogen at these 2 positions (sites of covalent bonding to Met255 and Trp107).

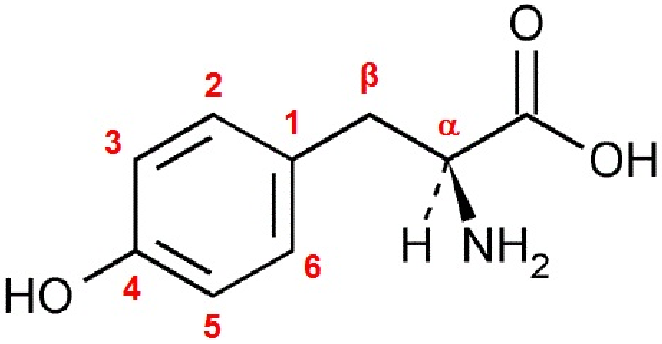

Figure 2.6. Structure of L-tyrosine.

In the first experiment, uniformly deuterotyrosine-labeled KatG with isotopic labeling at the β-methylene group was prepared. The EPR spectrum of the labeled enzyme mixed with H_2O_2 showed a singlet characterized by a linewidth of 10 Gauss and *g*-factor of 2.0040 (Figure 2.7, blue spectrum).

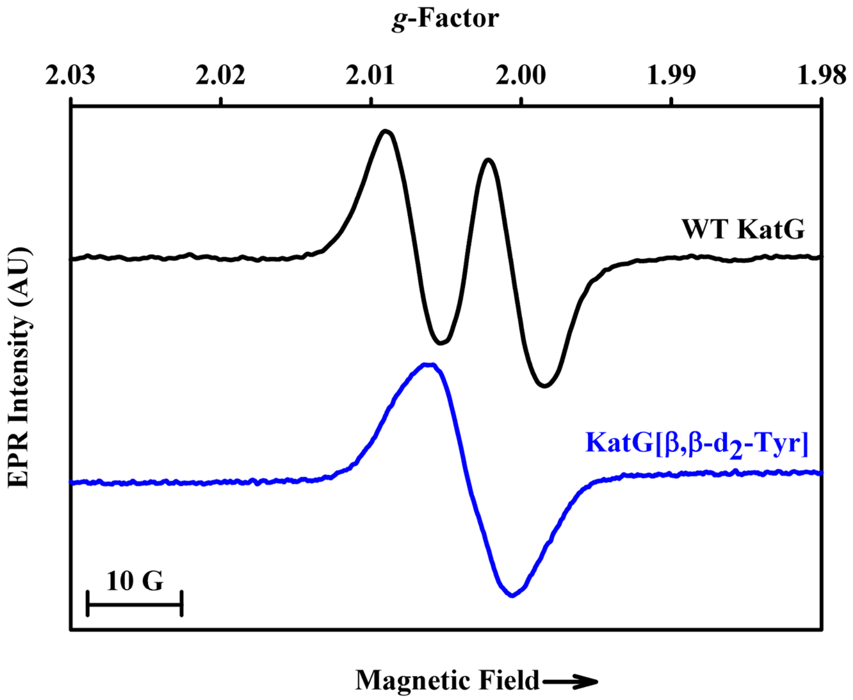

Figure 2.7. X-band RFQ-EPR spectra of WT KatG and KatG[β,β-d_2-Tyr] (50 μM) treated with 8000-fold molar excess of H_2O_2 at pH 8.5 frozen manually within 1.5 sec after mixing. Experimental conditions: T = 77 K; microwave frequency = 9.45 GHz; microwave power = 0.1 mW; modulation amplitude = 1 G; average of 9 scans.

Signal narrowing occurs, as mentioned before, because the magnetogyric ratio of ^2H is about 1/6 the value of ^1H, which reduces hyperfine couplings at the β-methylene in a tyrosyl radical, confirming the general assignment. This observation about signal narrowing was confirmed by simulating the EPR spectra shown in Figure 2.7. The narrow doublet was simulated using *g*-tensor values taken from the high-field EPR data [31] (Figure 2.8).

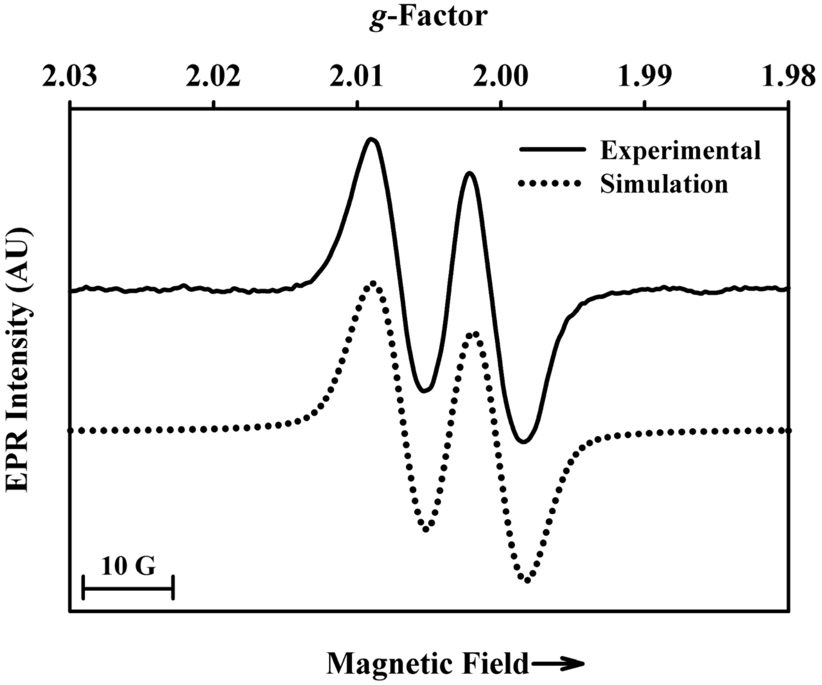

Figure 2.8. Simulation of the X-band RFQ-EPR spectrum of WT KatG (50 µM) treated with 8000-fold molar excess of H_2O_2 performed using *Simfonia* and *WinEPR* software (Bruker). Hyperfine couplings: $A_x = A_y = A_z =$ 11 G (β-$^1H_1$); $A_x = A_y = 2$ G, $A_z = 2.5$ G (β-$^1H_2$); $A_x = 1.55$ G, $A_y = 0.8$ G, $A_z = 1.2$ G (2',6'-^1H). Line broadening: X = Y = Z = 5 G. *g*-tensor values ($g_x = 2.0058$, $g_y = 2.0034$, $g_z = 2.0019$) were taken from the high-field EPR data [31].

Simulating the signal for KatG[β,β-d_2-Tyr] was begun by reducing the hyperfine interactions at the β-methylene by a factor of 6.51 which yielded a spectrum that was slightly narrower than the experimental one. This could be attributed to the presence of some population of unlabeled KatG in the deuterated enzyme sample resulting in some line broadening. *E. coli*, used as the overexpression system for KatG, can utilize glucose from the M9 minimal growth medium to synthesize 'proteo' tyrosine [46], and no analysis was performed to quantify the percent deuterium in tyrosines in the enzyme prepared in cultures containing commercial β,β-d_2-Tyr (98% isotopic purity). Another reason behind the observation that simple reduction of the β-methylene hydrogen coupling values for the deuterium-substituted enzyme does not produce a very good match between simulation and data for the singlet is that the M-Y-W adduct radical is not equivalent to an ordinary tyrosyl radical; the unpaired electron spin is delocalized to some extent into the tryptophan ring according to previous DFT calculations [31] and therefore, additional hydrogens and the indole nitrogen also contribute to the total hyperfine interactions in the radical. This suggestion was shown to be valid, as adding weak couplings for the Trp hydrogens and the indole nitrogen, along with 15% of simulated WT signal, resulted in a simulated spectrum closely matching the experimental one (Figure 2.9).

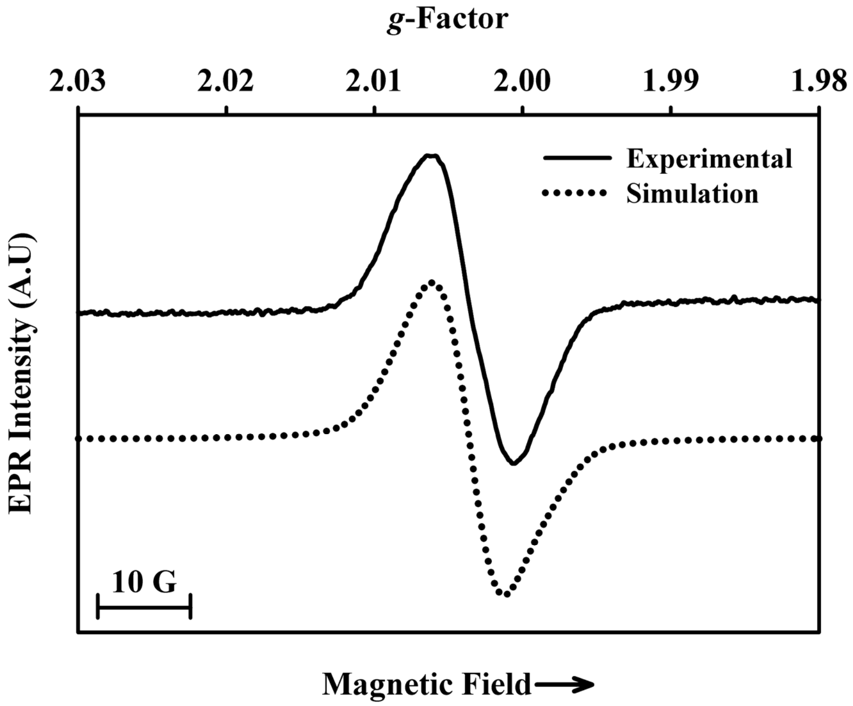

Figure 2.8. Simulation of the X-band RFQ-EPR spectrum of KatG[β,β-d_2-Tyr] (50 μM) treated with 8000-fold molar excess of H_2O_2 performed using *Simfonia* and *WinEPR* software (Bruker). Hyperfine couplings: $A_x = A_y = A_z = 1.6$ G (β-$^2H_1$); $A_x = A_y = 0.33$ G, $A_z = 0.42$ G (β-$^2H_2$); $A_x = 1.55$ G, $A_y = 0.8$ G, $A_z = 1.2$ G 2(2’,6’-^{1}H); $A_x = A_y = A_z = 3$ G (^{14}N). Line broadening: X = Y = Z = 5 G. *g*-tensor values ($g_x = 2.0058$, $g_y = 2.0034$, $g_z = 2.0019$) were taken from the high-field EPR data [31].

In a similar fashion, we used enzyme overexpressed in the presence of 3',5'-^{2}H-Tyr to examine changes in the EPR spectrum of the radical. It is important to state here that all tyrosines in KatG contain 3’ and 5’ ring hydrogens except Tyr229 due to the unique post-translational modification in the adduct structure where Tyr229 is covalently linked to Met255 and Trp107 at the 3’ and 5’ positions respectively. The EPR spectrum of the 3’,5’-d_2-tyrosine enzyme mixed with H_2O_2 exhibited a narrow doublet signal identical to that obtained from WT KatG (Figure 2.10, red spectrum).

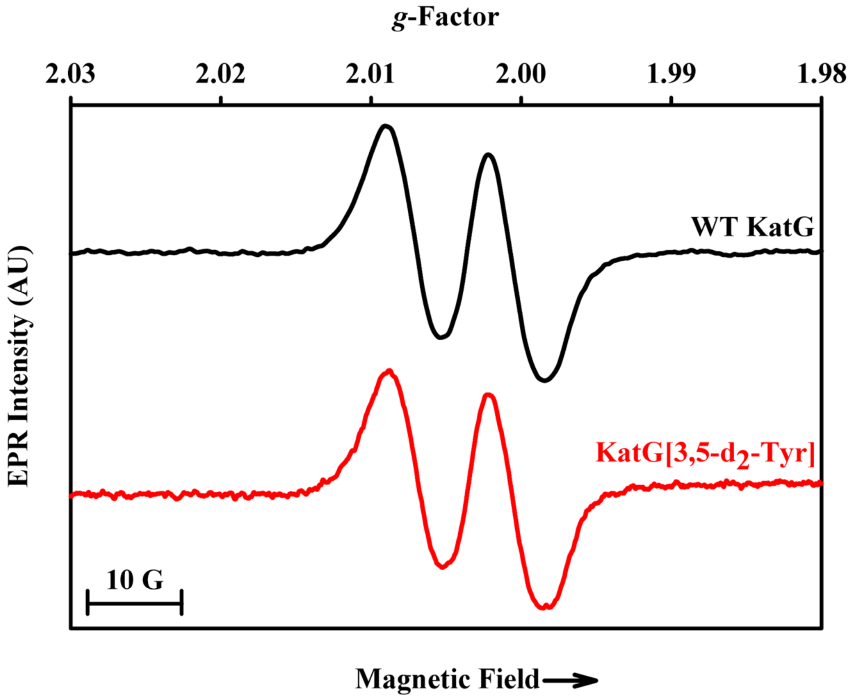

Figure 2.10. X-band RFQ-EPR spectra of WT KatG and KatG[3,5-d_2-Tyr] (50 µM) treated with 8000-fold molar excess of H_2O_2 at pH 8.5 frozen manually within 1.5 sec after mixing. Experimental conditions: T = 77 K; microwave frequency = 9.45 GHz; microwave power = 0.1 mW; modulation amplitude = 1 G; average of 9 scans.

The similarity in the EPR spectra between the 3’,5’-tyrosine-labeled and unlabeled KatG was an additional proof that Tyr229 of the adduct is part of the radical site in KatG responsible for the narrow doublet EPR signal since Tyr229 is the only tyrosine in KatG that lacks the 3’ and

5’ hydrogens and thus will not reveal any effects from the isotope labeling at these positions of the phenolic ring.

That the KatG used here was in fact labeled with 3’,5’-d_2-Tyr was demonstrated by taking advantage of the previous observations that in reactions of KatG with alkyl peroxides, tyrosyl (and tryptophanyl) radicals remote from the M-Y-W adduct are formed (more details about the remote radicals in Chapter 3). As shown in Figure 2.11, the linewidth of the singlet signal typical of WT KatG treated with peroxyacetic acid (PAA) and frozen 5 sec after mixing was reduced from 23 Gauss (Figure 2.11, black spectrum) to 19 Gauss for the 3’,5’-d_2-Tyr labeled enzyme (Figure 2.11, red spectrum). These findings prove that 3’,5’-d_2-Tyr was successfully incorporated into KatG.

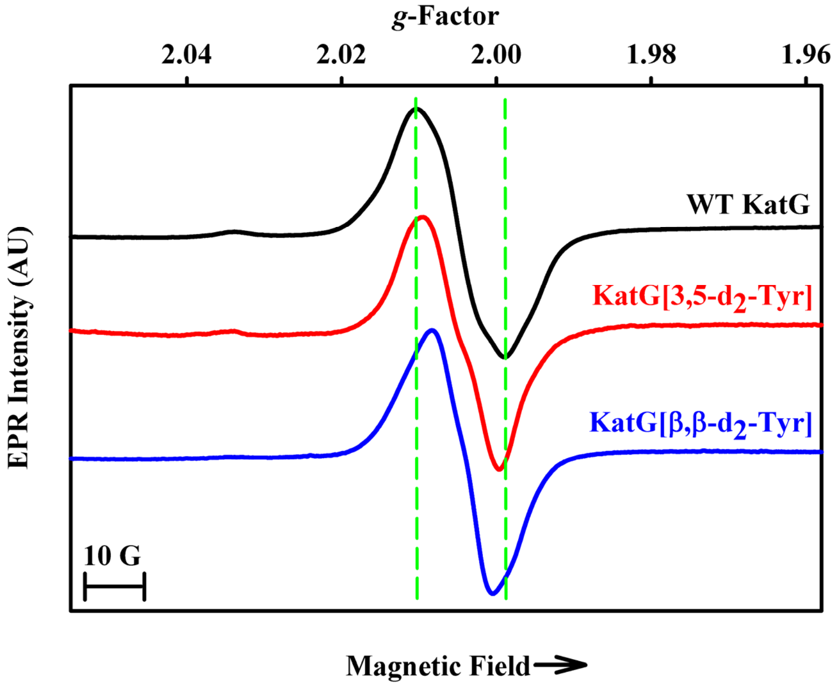

Figure 2.11. X-band RFQ-EPR spectra of WT KatG, KatG[3,5-d_2-Tyr], and KatG[β,β-d_2-Tyr] (50 μM) treated with 3-fold molar excess of PAA at pH 7.2 frozen 5 sec after mixing. Experimental conditions: T = 77 K; microwave frequency = 9.44 GHz; microwave power = 0.1 mW; modulation amplitude = 1 G; average of 9 scans.

For enzyme labeled with Tyr deuterated at the β-methylene sites, the linewidth was reduced from 23 Gauss to 14 Gauss (Figure 2.11, blue spectrum), again demonstrating that the majority species giving these EPR signals upon turnover with PAA is a tyrosyl radical and that the radical(s) formed using PAA is different from that formed during catalase turnover using excess H_2O_2 (Chapter 3).

2.6 Rapid freeze-quench EPR and quantitative analysis of the narrow doublet.

The robust catalase activity of *Mtb* KatG (turnover number ~5000 s^{-1}) is suitably measured in the presence of a large molar excess H_2O_2, which are conditions that allowed observation of only a low yield of radical with manual mixing/freezing. The application of RFQ-EPR spectroscopy to learn about the kinetics of the catalase reaction and to improve the radical yield (and possibly obtain a signal from KatG plus small excess H_2O_2) was carried out next. Also, complementary UV-Vis stopped-flow experiments were used to follow the consumption of H_2O_2 under the same conditions. RFQ-EPR sampling allows mixing of ferric KatG with H_2O_2 followed by rapid freeze-quenching of reactions in the millisecond time scale. The narrow doublet signal described above appears at the earliest time point accessible and was the only signal in the $g = 2$ region. Figures 2.12 and 2.13 show the EPR spectra recorded as a function of incubation time after mixing KatG with a 1000-fold molar excess of H_2O_2 at pH 7.2 and 8.5, respectively.

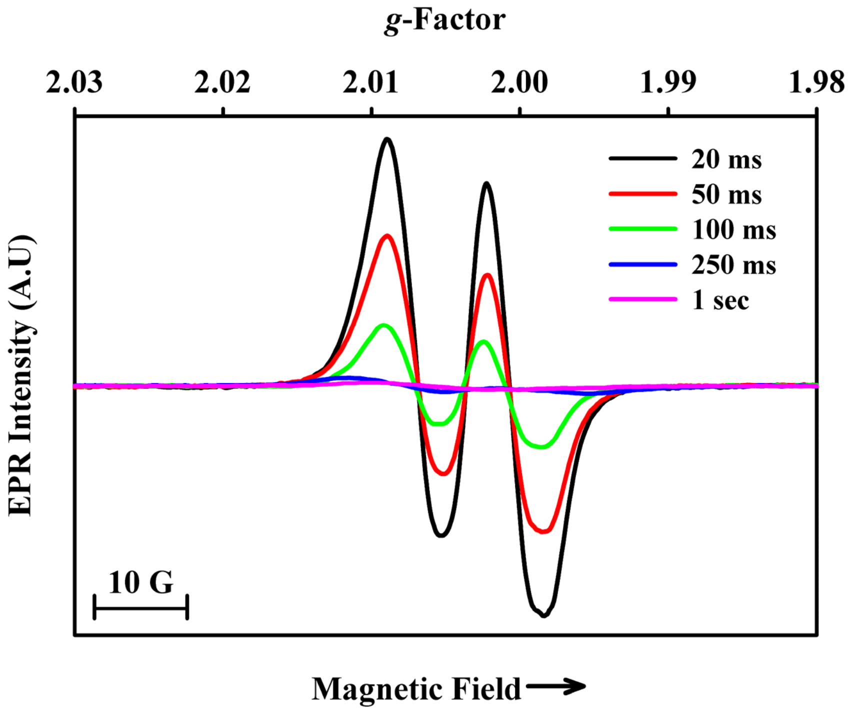

Figure 2.12. X-band RFQ-EPR spectra of WT KatG (50 µM) treated with 1000-fold molar excess of H_2O_2 at pH 7.2 frozen at the indicated times after mixing. Experimental conditions: T = 77 K; microwave frequency = 9.44 GHz; microwave power = 0.1 mW; modulation amplitude = 1 G; average of 9 scans.

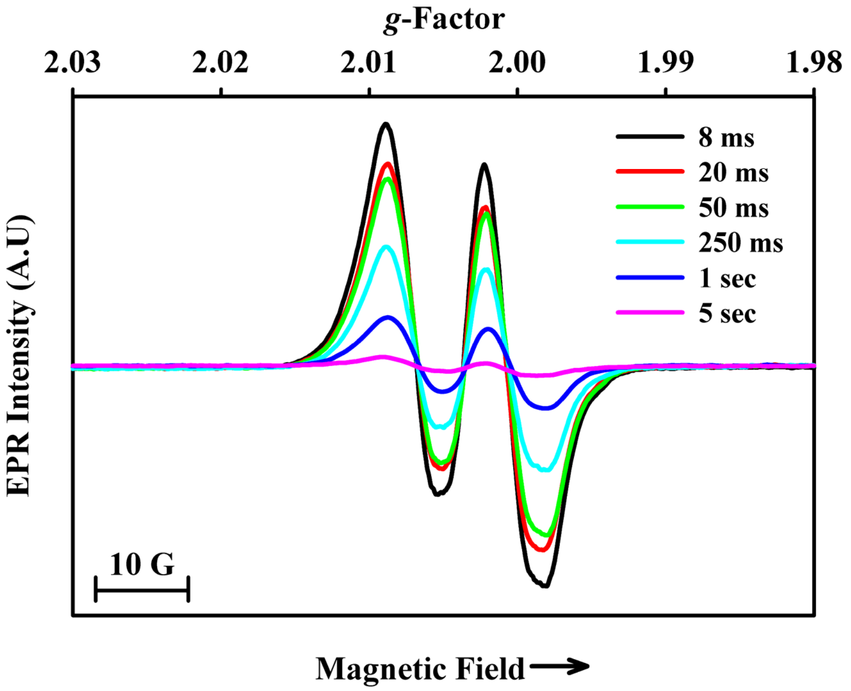

Figure 2.13. X-band RFQ-EPR spectra of WT KatG (50 µM) treated with 1000-fold molar excess of H_2O_2 at pH 8.5 frozen at the indicated times after mixing. Experimental conditions: T = 77 K; microwave frequency = 9.44 GHz; microwave power = 0.1 mW; modulation amplitude = 1 G; average of 9 scans.

The intensity of the signal, expressed as 'spins per heme', was maximal in the sample frozen at the earliest quench time (~0.28 spins/heme for the reaction run at pH 7.2 and frozen after 20 ms, and ~0.27 spins/heme for the reaction run at pH 8.5 and frozen after 8 ms) and the intensity went down thereafter until the signal was no longer detectable after ~1 sec for the pH 7.2 reaction and after ~5 sec for the pH 8.5 reaction (Figures 2.14 and 2.15).

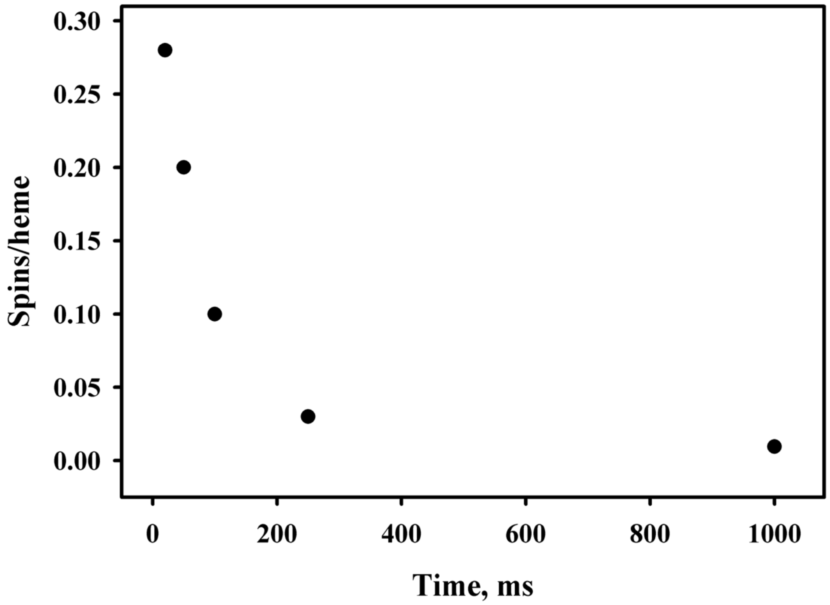

Figure 2.14. Intensity (spins/heme) of the narrow doublet EPR signal as a function of time in RFQ-EPR samples frozen after mixing WT KatG (50 µM) with 1000-fold excess of H_2O_2 at pH 7.2.

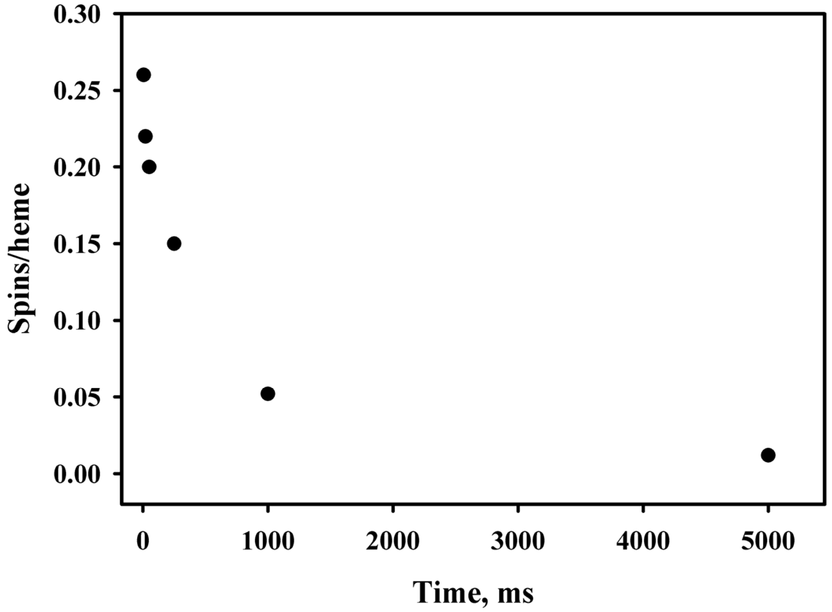

Figure 2.15. Intensity (spins/heme) of the narrow doublet EPR signal as a function of time in RFQ-EPR samples frozen after mixing WT KatG (50 µM) with 1000-fold excess of H_2O_2 at pH 8.5.

Here, it is also necessary to mention that the yields of the radical at later time points are not considered to be accurately calculated due to the dilution of the samples by oxygen gas evolution especially at pH 7.2 where it is estimated that ~200 µL of O_2 are produced from 100 mM H_2O_2 in mixtures similar to those used in the RFQ experiment. For this reason, the data points in Figures 2.14 and 2.15 were not fitted into any function.

At alkaline pH, the narrow doublet signal persisted more than 5 times longer than at neutral pH, corresponding reasonably well to the ~8-fold lower rate of the catalase reaction (~4000 units/mg at pH 7.2 and ~500 units/mg at pH 8.5). Due to the lower catalase activity and slower consumption of the radical at pH 8.5, some RFQ-EPR (and most manually-mixed) samples were prepared at this pH. The correlation between the catalase activity and the radical consumption suggests that the radical represents a kinetically-competent intermediate of the catalase reaction pathway. The relationship between the narrow doublet signal and the catalase activity in KatG is discussed in more detail later in this chapter. Optical (and UV) stopped-flow experiments were also carried out under the same conditions as the RFQ-EPR to directly follow the rate of consumption of hydrogen peroxide and compare it with the kinetics of the M-Y-W radical.

2.7 ***The intensity of the narrow doublet as a function of peroxide concentration.***

RFQ-EPR samples of KatG mixed with increasing molar excess of hydrogen peroxide were prepared to determine the maximum amount of unpaired spin that can be obtained per KatG molecule. The concentrations of H_2O_2 used were known from optical experiments not to cause damage to KatG.

Interestingly, the narrow doublet was detected with as little as 5-fold molar excess of H_2O_2 in a sample mixed at pH 8.5 and frozen 20 ms after mixing (Figure 2.16). Although the amount of radical was small (~0.02 spins/heme), this data could allow the assumption that the narrow doublet might be obtained and detected using a single molar equivalent of H_2O_2 per heme if sample were frozen faster. This is important toward probing the electronic structures of KatG intermediates because theoretically 1 molar equivalent of peroxide should be enough to form the adduct radical (Fe(IV)=O(W-Y-W)$^\bullet$), via the spontaneous reduction of the first hypervalent heme species in KatG (Fe(IV)=O(Por$^{\pi+\bullet}$)), the phenomenon that has not been observed experimentally yet.

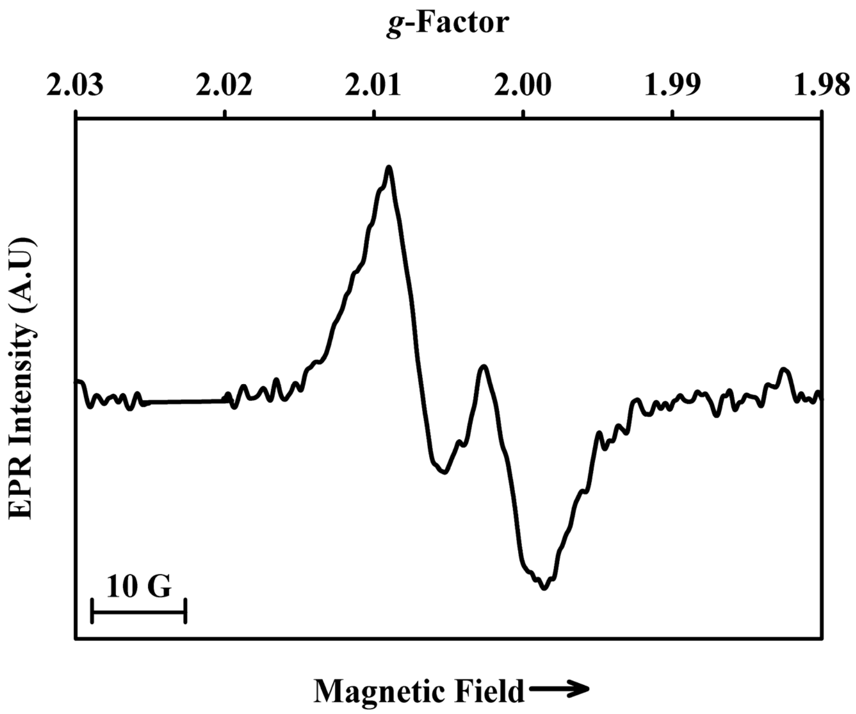

Figure 2.16. X-band RFQ-EPR spectrum of WT KatG (50 µM) treated with 5-fold molar excess H_2O_2 at pH 8.5 frozen 20 ms after mixing. Experimental conditions: T = 77 K; microwave frequency = 9.44 GHz; microwave power = 0.1 mW; modulation amplitude = 1 G; average of 9 scans.

For RFQ-EPR of samples mixed at pH 8.5 and frozen 20 ms after mixing in each case, the intensity of the narrow doublet signal was proportional to the initial H_2O_2 concentration (Figure 2.17). A maximum initial yield of radical (~0.40 spins/heme) was obtained using 100,000-fold molar excess of H_2O_2 (Figure 2.18).

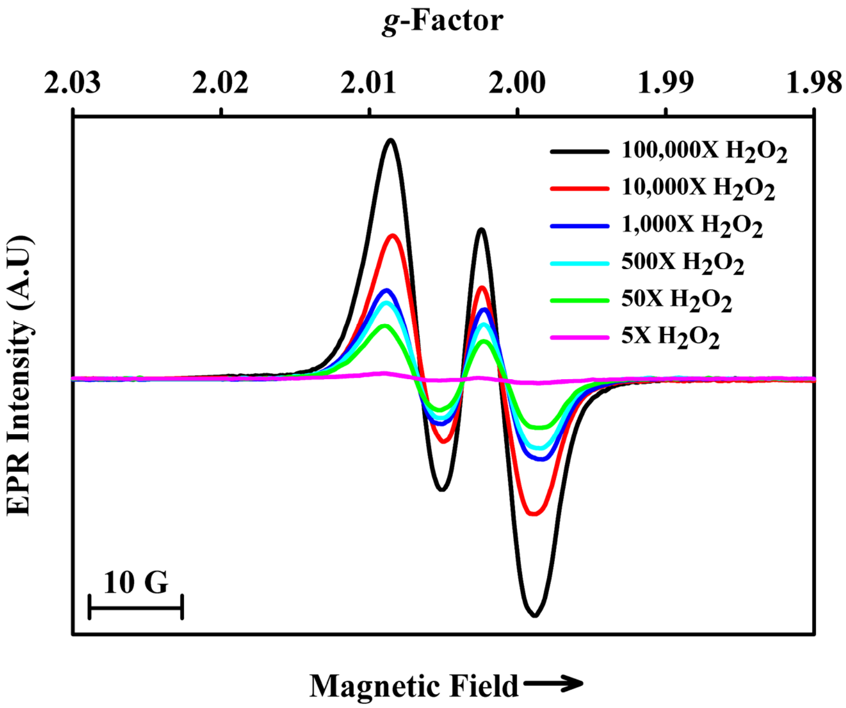

Figure 2.17. X-band RFQ-EPR spectra of WT KatG (50 μM) treated with the indicated molar excess of H_2O_2 at pH 8.5 frozen 20 ms after mixing. Experimental conditions: T = 77 K; microwave frequency = 9.44 GHz; microwave power = 0.1 mW; modulation amplitude = 1 G; average of 9 scans.

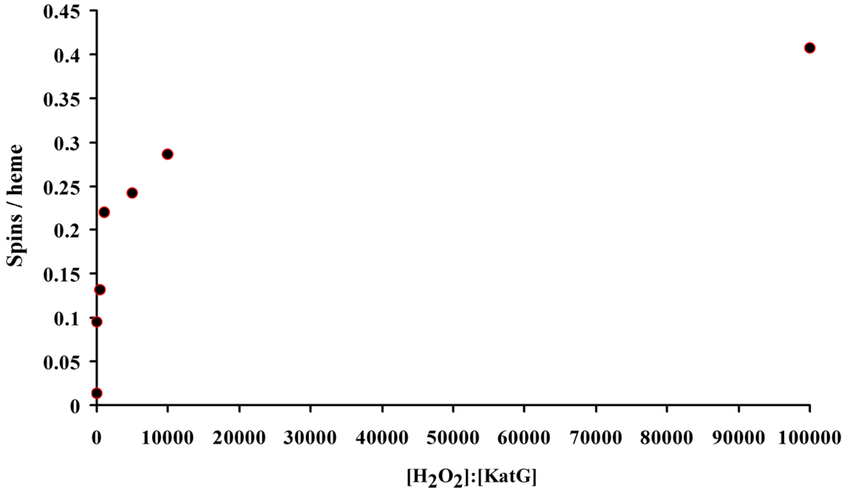

Figure 2.18. Intensity (spins/heme) of the narrow doublet EPR signal as a function of molar excess of peroxide relative to KatG (heme) in RFQ-EPR samples frozen 20 ms after mixing WT KatG with H_2O_2 at pH 8.5.

The data shown above are consistent with the formation of a catalytically-competent steady-state intermediate (not a radical formation and decay) evidenced by the non-linearity of data points shown in Figure 2.18 and the presence of a 'saturating' concentration of spins per heme regardless of H_2O_2 above a certain amount. Actually, the calculated spin per heme concentrations in KatG (based on the narrow doublet signal from the enzyme mixed with H_2O_2) has never exceeded a value of 0.5 in any RFQ experiment. While this phenomenon is not quite understood, it could possibly indicate that only half of the WT enzyme (1 monomer) is in the active form during H_2O_2 turnover and the M-Y-W radical is forming in 1 of the 2 subunits.

2.8 The M-Y-W radical does not form or accumulate when KatG reacts with alkyl peroxides.

Based upon earlier work, our group (and others [47]) suggested a novel pathway for a catalase-like reaction incorporating a radical and oxyferrous heme (Fe(II)-O_2(Por)) as catalytic intermediates in KatG [31]. RFQ-EPR experiments (Figures 2.12 and 2.13) showed that the M-Y-W radical species appears at its maximum intensity at the earliest time points accessible (a few ms). Theoretically, the same radical species should be present whether with H_2O_2 or alkyl peroxide assuming that an initial Fe(IV)=O(Por$^{\pi+\bullet}$) (typical Compound I) is formed in both cases, and that an internal electron transfer readily produces the M-Y-W radical next. Experimentally, the turnover of a small excess (3-fold) of PAA yields an EPR signal, labeled a 'wide doublet' (details in Chapter 3), in very low yield within milliseconds representing predominantly tyrosyl radical(s) along with some contribution from tryptophanyl radical(s). The EPR signal intensity grows during extended incubation reaching close to 1 spin per heme. During this interval (several seconds), optical changes in heme spectra are consistent with the slow return of the initial heme intermediate to ferric heme, reflecting the electron transfers giving the relatively stable amino acid radicals observed by EPR. The processes that are catalyzed by a small excess of alkyl peroxide (the low-yield radical signal and slow accumulation of unpaired spin) are not considered relevant to the catalase reaction in KatG.

The same wide doublet EPR signal observed using 3-fold excess of PAA is seen upon turnover of larger excesses (20- and 200-fold) of PAA (Figure 2.19), or using *meta*-chloroperoxybenzoic acid (CPBA) (not shown). Both peroxides had been carefully scrubbed of residual H_2O_2.

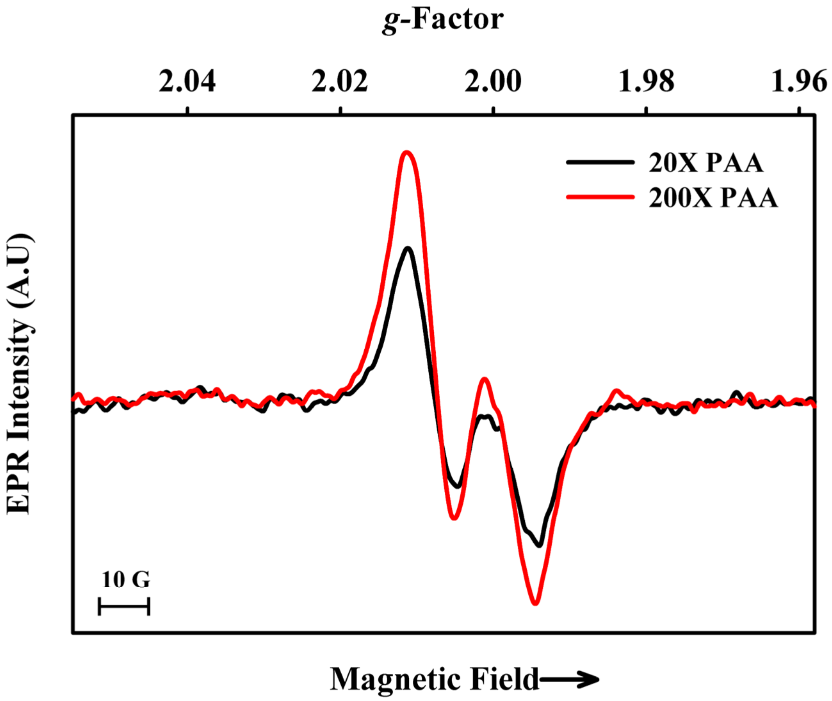

Figure 2.19. X-band RFQ-EPR spectra of WT KatG (50 µM) treated with 20- and 200-fold molar excesses of PAA at pH 7.2 frozen 100 ms after mixing. Experimental conditions: T = 77 K; microwave frequency = 9.44 GHz; microwave power = 0.1 mW; modulation amplitude = 1 G; average of 9 scans.

These experiments were crucial to defining a mechanism for the catalase reaction in KatG because they strongly suggested that the M-Y-W radical is not produced from an initial Fe(IV)=O($Por^{\pi+\bullet}$) which could form upon turnover of any of the different peroxides, and therefore suggests a reaction pathway involving H_2O_2 as a unique substrate for production of the M-Y-W radical.

*2.9 **Role of residues beyond the M-Y-W adduct in the catalase activity of KatG.***

The data presented so far in this chapter show that the radical located on the M-Y-W adduct giving the narrow doublet EPR signal is a unique intermediate the formation of which is required for the catalase activity in KatG. Mutation of any of the M-Y-W residues eliminates this radical and reduces catalase activity to less than one percent of the rate in WT KatG, but without compromising peroxidase activity [48-52]. These findings suggested that the M-Y-W adduct provided a catalase-specific intermediate required for efficient turnover of H_2O_2. Explaining the catalytic function of this unique cofactor and the operation of its radical in the catalase reaction particular to KatG is the goal of the study presented in the remaining parts of this chapter.

As the loss of catalase activity in certain mutant enzymes might arise from an absence of the M-Y-W adduct radical, clues about the catalase mechanism could come from other catalase-deficient mutants that have the M-Y-W adduct. It is known that residues beyond the M-Y-W adduct but near the heme are also required for high catalase activity in KatG. For example, when Arg418 is replaced with aliphatic amino acids, the catalase activity is severely reduced [53-54]. This residue was proposed to induce electronic steering effects on the heme because in one of its pH-dependent conformations, its side chain guanidiniuim group can interact with the phenolate oxygen of Tyr229 [53] (Figure 2.20).

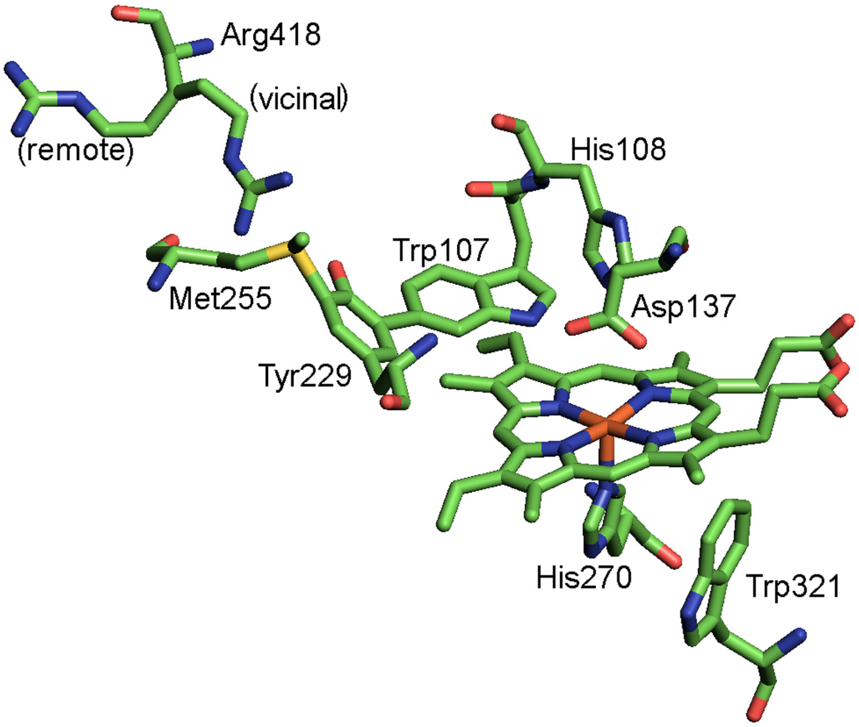

Figure 2.20. The active site and nearby amino acids of *Mtb* KatG. The side chains of Met255, Tyr229 and Trp107 are covalently linked forming a unique cofactor required for catalase activity. The side chain of residue Arg418 is shown in the two conformations, vicinal and remote (3.5 and 11.5 Å from Tyr229, respectively), found in the crystal structure. This figure was generated using PyMOL (The PyMOL Molecular Graphics System, version 1.2r3pre, Schrödinger, LLC.) based on published KatG crystal structure (2cca.pdb).

Another residue, Asp137 (Figure 2.20), is also essential for KatG catalase activity for reasons that are not completely defined [55]. Both KatG[R418L] and [D137S] mutations nearly eliminate the catalase activity. Investigating the role of Arg418 (and briefly that of Asp137) in the context of a potentially novel catalase reaction seemed warranted and was pursued for the study shown below.

One unusual feature in KatG is that an oxygenated form of heme (dioxyheme) accumulates and persists in the presence of excess H_2O_2. The term 'dioxyheme' designates the complex in which molecular oxygen is bound to heme iron, formally a ferrous heme-dioxygen (Fe(II)-O_2(Por)) or ferric heme-superoxy (Fe(III)-$O_2^{-\bullet}$(Por)) complex analogous to peroxidase Compound III [30-31]. In monofunctional catalases, very rapid dismutation steps prevent the accumulation of the single intermediate assumed to be Compound I. In most peroxidases, Compound III is generally a catalytically inert species slowly formed in the presence of excess H_2O_2 [28].

In the studies presented in the following sections, the focus is on gaining an understanding of two issues: 1) the formation and discharge of dioxyheme in KatG; and 2) the role of key remote residues (along with the M-Y-W adduct radical) in a catalase reaction mechanism specific to KatG.

A new perspective on features of the catalase reaction mechanism of KatG emerges from the kinetic data from optical and UV stopped-flow spectrometry (dioxyheme formation and H_2O_2 consumption) and RFQ-EPR experiments used to compare reactions in WT KatG and KatG[R418L] and [D137S] mutant enzymes. Supporting these experiments are optical spectrophotometry (CO inhibition), and oligomerization studies (both by Dr. X. Zhao), and DFT analysis (in collaboration with Dr. A. Jarzecki). The findings and discussions about the catalase reaction mechanism, presented in the sections below, are parts of a manuscript under review at the time of this writing.

2.10 <u>M-Y-W adduct radical in WT KatG, and KatG[R418L] and [D137S] mutant enzymes.</u>

In an earlier study, our group presented evidence that a radical on the M-Y-W adduct and dioxyheme were simultaneously present in KatG during catalase turnover at neutral pH [31]. In an attempt to explore the role of this radical in the catalase reaction, the behavior of the M-Y-W adduct radical was first characterized in WT KatG under various conditions for comparison with the catalase-deficient mutants KatG[R418L] and KatG[D137S]; these mutants exhibit catalase activities of only 2% and 0.5%, respectively, relative to that in WT KatG. The EPR experiments were performed near the pH optimum (7.2) for WT KatG catalase activity. KatG[R418L] has a flat pH-dependence for its very poor catalase reaction. The catalase-specific activity of KatG[D137S] does not change in the region of pH 5-8 [55].

Figure 2.21-A shows the narrow doublet EPR signal characteristic of the M-Y-W adduct radical recorded at an early time point (20 ms) for WT KatG, where a maximum intensity occurs corresponding to approximately 0.3 spin/heme. The radical signal is detected during a time period corresponding to the UV absorbance trace for H_2O_2 concentration under the same conditions (Figure 2.21-A, right panel). The linear slope is consistent with a low apparent K_M for H_2O_2 [30].

A narrow doublet EPR signal was found in yields similar to WT KatG for KatG[R418L] and KatG[D137S] (Figure 2.21-B,C). And, as with WT KatG, the persistence of the radical approximated the period required for H_2O_2 consumption detected optically (~30 sec for KatG[R418L] and ~50 sec for KatG[D137S]) (Figure 2.21-B,C, right panels).

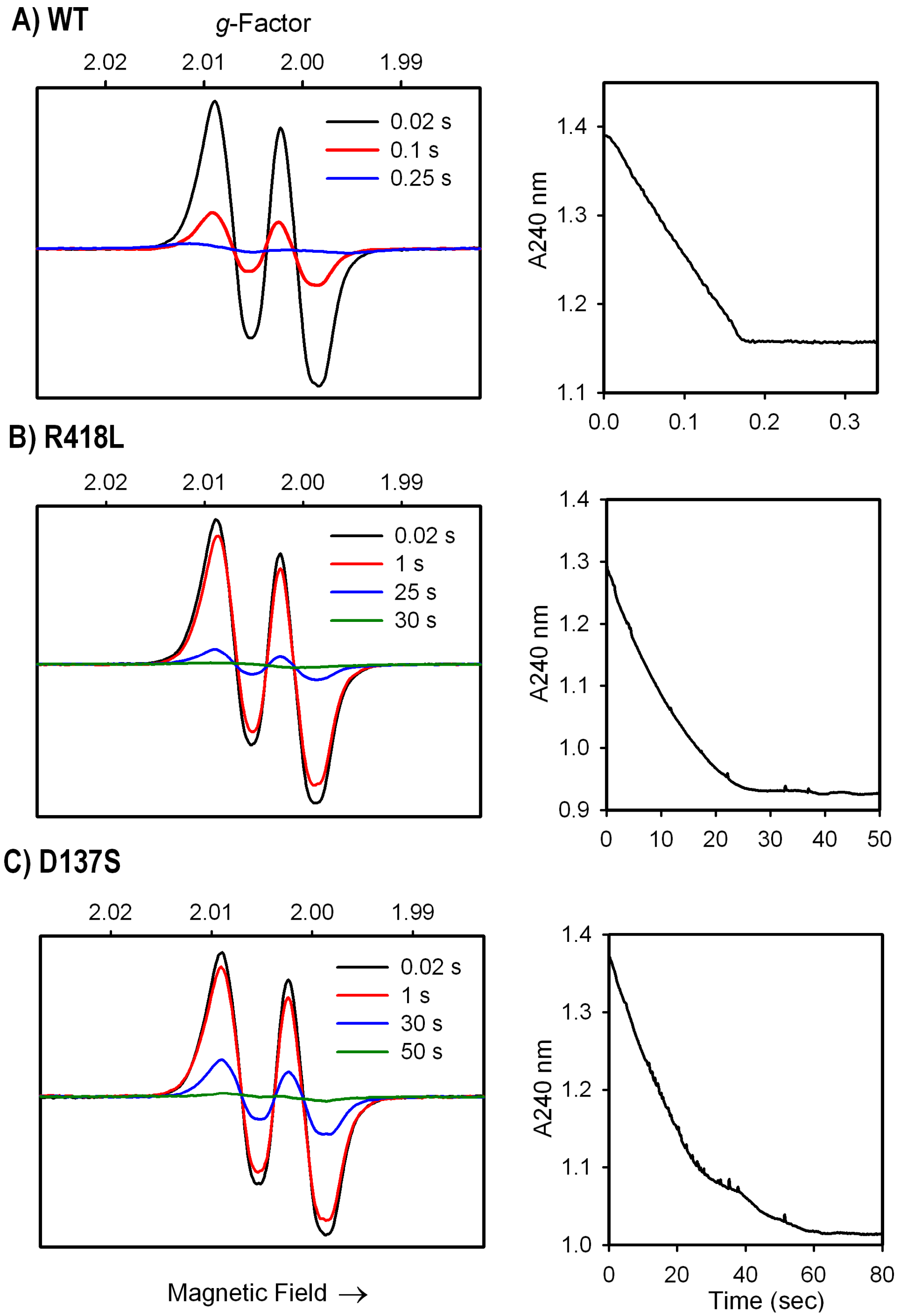

Figure 2.21. Radical formation and H_2O_2 consumption in WT KatG and KatG[R418L] and [D137S] mutants. Left panels: Rapid freeze quench X-band EPR spectra of enzymes (50 µM) reacted with 1000-fold molar excess of H_2O_2 at pH 7.2. Samples were frozen at the indicated times after mixing at room temp. Experimental conditions: T = 77 K; microwave frequency = 9.44 GHz; microwave power = 0.1 mW; modulation amplitude = 1 G; average of 9 scans. Spectra are plotted on the same signal intensity scales. Right panels: stopped-flow spectrophotometric time courses showing H_2O_2 consumption monitored at 240 nm under the same conditions used for the EPR experiments.

The above findings suggest that the poor catalase activity of these two mutant enzymes arises from some defect in radical utilization. Interestingly, the initial yield of M-Y-W adduct radical in both mutants was not significantly higher than for WT protein, nor did the radical persist significantly longer than the substrate H_2O_2. These observations suggest that an M-Y-W adduct radical 'escape' pathway may exist in the mutant enzymes, which limits accumulation despite poor utilization of the radical in a catalase reaction step. Evidence for such a pathway is shown from the enhanced formation in both mutants of enzyme cross-links involving amino acid radicals on the enzyme surface (Dr. X. Zhao, personal communication).

*2.11 **Dioxyheme formation in KatG.***

Dioxyheme and the narrow doublet signal are found at the same time during turnover of excess H_2O_2 by WT KatG [31, 56]. However, very rapid turnovers prevent evaluation of the kinetics of dioxyheme formation using typical optical stopped-flow methods. Since the KatG mutants defective in catalase activity still exhibit the narrow doublet signal, a lack of dioxyheme formation could be responsible for the absence of catalase activity. Furthermore, the KatG[R418L] mutant, which conserves all the catalytically essential heme pocket residues including the intact M-Y-W adduct [54] and its radical, provides a valuable tool for the study of dioxyheme formation thanks to its very slow catalase turnover.

As shown in Figure 2.22 (top), the formation of dioxyheme was complete within a few milliseconds of mixing using a 1000-fold molar excess of H_2O_2, evidenced by the shift of the Soret peak to 418 nm and the appearance of β and α bands at 542 and 580 nm [57]. Moreover, the dioxyheme species could be observed using as little as a 2-fold molar excess of peroxide

(Figure 2.22, top). In WT KatG, the only condition under which an intermediate can be observed spectrophotometrically involves the use of very large excesses of H_2O_2 because while an efficient and rapid pathway to dioxyheme must also be present, rapid subsequent turnovers consume this intermediate. These observations show that an efficient pathway for dioxyheme formation exists in KatG[R418L] but that catalase activity is blocked by a defect in dioxyheme consumption. This finding is related to an earlier one demonstrating that dioxyheme, when prepared through aerobic photolysis of carbonyl KatG (Fe(II)-CO) in the absence of H_2O_2 [56], is very stable because the M-Y-W adduct radical is not present under those conditions.

KatG[D137S] was reported several years ago to lack catalase activity [55], yet formation of the M-Y-W adduct radical in this mutant is unchanged (Figure 2.21-C). Optical spectra here show that only traces of dioxyheme are seen with excess H_2O_2 (500- or 5000-fold) with the state of heme in the remainder of the enzyme remaining uncharacterized (Figure 2.22, bottom). It is suggested that for the small fraction of mutant enzyme that forms dioxyheme, the WT catalase reaction pathway can operate, since the M-Y-W adduct radical and Arg418 are both available. The lost catalase activity is then suggested to arise simply from the lack of abundant dioxyheme. These observations indicate the importance of residue Asp137 in formation of dioxyheme and overall, the results are crucial to formulating key steps in the KatG catalase reaction mechanism.

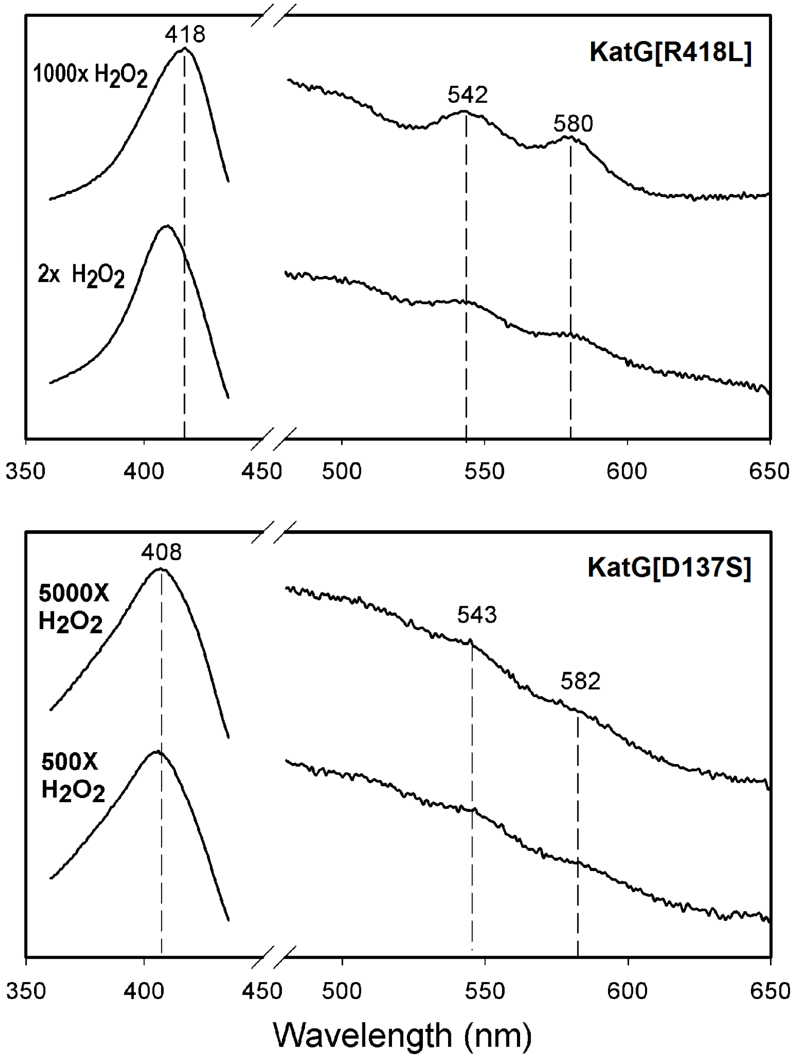

Figure 2.22. Optical stopped-flow spectra showing dioxyheme formation in KatG[R418L] and [D137S] upon mixing the enzymes (10 μM) with the indicated molar equivalents of H_2O_2 at room temperature and pH 7.2. The peaks in the visible wavelength region through which lines are drawn closely match those assigned to typical peroxidase Compound III [57], and indicate the dioxyheme component in both reactions.

2.12 <u>Summary of other findings associated with the catalase reaction mechanism in KatG.</u>

This section reports experimental and theoretical observations from work performed by colleagues in the laboratory and by collaborators at Brooklyn College related to the catalase reaction mechanism and the M-Y-W adduct radical.

A mechanistic insight into the catalase reaction came from the observation of inhibition of the catalase activity of WT KatG monitored under typical assay conditions, but in CO-saturated buffer (performed by Dr. X. Zhao). The assumption was if the dioxyheme intermediate exchanges oxygen gas, CO could inhibit the catalase reaction by binding tightly to ferrous heme iron, thereby removing enzyme from catalytic competence by trapping it in the stable carbonyl form. Results showed that at pH 6.0, the activity was ultimately inhibited around 95%. A similar level of inhibition was found at pH 8.5. Thus, under both acidic and basic conditions, either free ferrous heme or a dissociable form of dioxyheme must be present during catalase turnover.

It was interesting to know what happens to the M-Y-W radical as it decays in the 2 catalase-deficient mutants because the radical dissipates after certain time. So for further understanding of the catalase reaction mechanism in KatG and defects in the mutants as well as the behavior of radicals in KatG, oligomerization studies were carried out. The hypothesis was that the non-catalytic consumption of the M-Y-W adduct radical due to its inefficient utilization in the mutants, might allow for increased electron transfers that ultimately produce surface tyrosyl radicals and then dityrosine cross-links. Such oligomers are known to form in WT KatG in the presence of a slow flux of H_2O_2 (generated by glucose + glucose oxidase) [58]. Enhanced cross-linking of KatG[R418L] was observed upon decay of the catalytically-defective M-Y-W adduct radical in this mutant (Dr. X. Zhao, personal communication). The EPR results above, show that the concentration of M-Y-W adduct radical in KatG[R418L] does not exceed that in WT KatG. Radical decay can be enhanced in this mutant if Arg418 is required for a catalytic step in the reaction following the formation of Compound III (Scheme 2.1). This is likely to be the rapid recombination of unpaired electrons in Fe(III)-$O_2^{-\bullet}$(Por) and M-Y-W radical that restores the resting enzyme and releases O_2. A slower recombination favors escape of the adduct radical through pathways different from its direct reaction with dioxyheme. KatG[D137S], also, showed significant oligomer formation consistent with enhanced migration of the M-Y-W adduct radical as this mutant lacks the dioxyheme species required for a rapid adduct-radical quenching reaction.

Furthermore, DFT calculations were applied to evaluate energies for a series of models of the M-Y-W adduct radical:dioxyheme species to examine whether Arg418 influences its properties with the aim to provide insights into the behavior of the dioxyheme/M-Y-W adduct radical intermediate and to validate the radical recombination step of the catalase pathway (Scheme 2.1). The calculations showed that the side chain of residue Arg418 promotes discharge of the oxygen ligand and quenching of the adduct radical through electronic effects mediated by the guanidinium salt bridge to the phenolic oxygen of Tyr229 in the adduct radical (Dr. A. Jarzecki, personal communication).

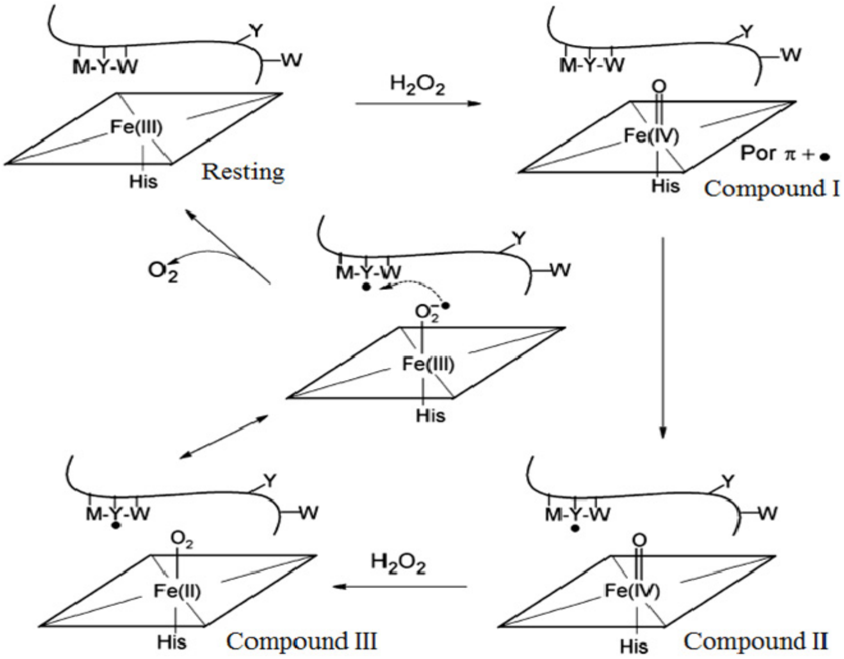

Scheme 2.1. Proposed catalase reaction mechanism in KatG. (Adapted from Suarez [31]).

2.13 ***Conclusions.***

In an attempt to explore the possible roles of specific tyrosine residues in radical formation and in the catalase mechanism in *Mtb* KatG, each of the 21 tyrosine residues in KatG monomer was mutated. As shown in Table 2.1 and the EPR spectra in Appendix B, except for KatG[Y229F], each Tyr mutant enzyme exhibited the narrow doublet EPR signal upon reaction with H_2O_2 and most of them had close to normal catalase activity. Do these observations directly confirm Tyr229 as the radical site? It is conceivable that this residue or an intact M-Y-W adduct is required for formation of a tyrosyl radical(s) on some other site or sites during catalase turnover. However, the observation of the same narrow doublet in each mutant would then mean that upon mutation of one of the residues other than Tyr229, yet another Tyr radical that exhibits the same EPR signal as the WT protein is formed. This is very unlikely. Furthermore, a scenario in which different tyrosyl residues beyond Tyr229 could be radical sites is unreasonable given the conserved catalase activities, since a catalytic function of the radical in the active site containing oxyferrous heme (dioxyheme, peroxidase Compound III) must be maintained in each functional mutant [30, 56].

The narrow doublet EPR signal was unchanged during catalase turnover in KatG labeled with ring-deuterated tyrosine (3’,5’-d_2-Tyr) relative to unlabeled enzyme. Taken together, the findings are then best explained by assigning the catalytic radical to Tyr229 of the M-Y-W adduct. The evidence for a radical associated with the M-Y-W adduct and catalase activity in KatG is supported by the observation that the EPR signal intensity can be as high as ~0.40 spins per heme in rapid freeze-quench samples frozen after a few milliseconds of reaction with excess H_2O_2.

According to previous DFT calculations, the majority of unpaired spin density is contained within the tyrosyl ring in this structure [31]. This adduct radical does not form or accumulate when KatG reacts with alkyl peroxides and therefore it may not evolve from a typical peroxidase Compound I in KatG. This means that KatG is most likely to begin a catalase reaction cycle when it encounters hydrogen peroxide, as it should, rather than form Compound I with turnover of H_2O_2 under conditions where it may not have a peroxidase substrate available.

Unlike other peroxidases, KatG readily forms dioxyheme upon reaction with excess H_2O_2 and rapidly turns over massive excesses of peroxide. In mutants such as KatG[M255A], [Y229F], and [W107F], the formation of a stable dioxyheme species requires only a very small excess of H_2O_2, and similar to the case of monofunctional peroxidases, no catalase turnover occurs [31, 56, 59]. The rapid catalase activity of KatG therefore depends on efficient recycling of dioxyheme. Consistent with this idea are earlier suggestions that a radical could participate in a reaction with dioxyheme, enabling dioxygen release and yielding ferric KatG [31, 56] as proposed by other groups [30]. Therefore, it is reasonable that the two unpaired electrons (superoxyl ligand and the adduct radical) present in the steady-state intermediate, recombine to release O_2 during catalase turnover by KatG.

The finding that the M-Y-W adduct radical is formed in 2 catalase deficient mutants demonstrates that residues Asp137 and Arg418 are responsible either for formation or discharge of dioxyheme in the proposed catalase reaction mechanism (Scheme 2.1). The very rapid formation of the M-Y-W adduct radical may proceed the same way in all three cases in a concerted turnover that bypasses a ‘free’ Compound I intermediate. Once the initial turnover has occurred, the most likely route to dioxyheme in the proposed mechanism is by rapid H_2O_2-reduction of ferryl heme in a reaction common to other peroxidases [60-61] including

KatG[Y229F] [50]. Residue Asp137 seems to be crucial for this conversion and may be responsible for an important proton transfer step that enhances the reactivity of ferryl heme [62]. This aspartate residue is absent from Type III peroxidases such as horseradish peroxidase, in which Compound III (dioxyheme) is only slowly formed in the presence of excess H_2O_2 [61]. Thus, facile formation of dioxyheme in KatG distinguishes this enzyme from monofunctional Class I and most other peroxidases and is obligatory in its catalase reaction mechanism.

Overall, the current results demonstrate that formation of the M-Y-W adduct radical is not sufficient for efficient catalase turnover by KatG; there must also be dioxyheme and a regulating remote influence (Arg418) on the electronic structure of the M-Y-W adduct radical for maximal activity. It seems clear that *Mtb* KatG is structured for very rapid formation of dioxyheme and robust catalase activity under a wide range of H_2O_2 concentrations, arguably important for the survival of an intracellular pathogen subjected to fluctuating oxidative stress from host cells.

To summarize this chapter and put the experimental findings together with the DFT calculations into a mechanism for the catalase reaction pathway in KatG, one can say that a key step requires a radical on the M-Y-W adduct (Tyr229) (Rxn. 1). The conversion of ferryl heme to dioxyheme by the second peroxide is facilitated by Asp137 (Rxn. 2). The recombination of unpaired electrons stored in the superoxyl ligand and the M-Y-W adduct radical, promoted by Arg418, restores the resting enzyme and releases O_2 bringing the catalase cycle to completion (Rxn. 3).

$$\mathrm{Fe(III)(Por)(MYW)} + \mathrm{H_2O_2} \rightarrow \mathrm{Fe(IV){=}O(Por^{\pi+\bullet})(MYW)} \rightarrow \mathrm{Fe(IV){=}O(Por)(MYW)^{\bullet}} \qquad (1)$$

$$\mathrm{Fe(IV){=}O(Por)(MYW)^{\bullet}} + \mathrm{H_2O_2} \rightarrow \mathrm{Fe(II)\text{-}O_2(Por)(MYW)^{\bullet}} \leftrightarrow \mathrm{Fe(III)\text{-}O_2^{-\bullet}(Por)(MYW)^{\bullet}} \qquad (2)$$

$$\mathrm{Fe(III)\text{-}O_2^{-\bullet}(Por)(MYW)^{\bullet}} \rightarrow \mathrm{Fe(III)(Por)(MYW)} + \mathrm{O_2} \qquad (3)$$

Chapter 3: Characterization of radicals not associated with the catalase reaction in *Mtb* KatG.

3.1 Introduction.

After gaining a considerable understanding of the catalase reaction mechanism in KatG and the role played by the M-Y-W adduct radical, the work presented in this section of the thesis is devoted to address the less-understood reactions occuring in KatG with alkyl peroxides and other conditions. As stated earlier, despite the high sequence homology between KatG and monofunctional peroxidases, KatG differs mechanistically most noticeably by the decay of its first hypervalent heme intermediate (Compound I) to the ferric resting state without the formation of the typical peroxidase Compound II. During this process, an extended slow formation of amino acid-based radicals, different from the M-Y-W adduct radical, takes place, resulting in a possible formation of a new radical intermediate(s) which might have a catalytic role [29-30] despite their detection under 'non-peroxidase' conditions in the absence of a reducing substrate. These radicals might be expected to form through a single-electron oxidation of tyrosine and/or tryptophan residues by Fe(IV)=O(Por$^{\pi+\bullet}$) (typical peroxidase Compound I, assuming the same species forms in KatG) when the enzyme is turned over with alkyl peroxides, but could also form after Fe(IV)=O(M-Y-W)$^{\bullet}$.

Understanding these reactions may be relevant to the activation of INH by KatG in *M. tuberculosis*. It has been proposed that INH becomes activated in a peroxidation reaction by KatG reactive intermediate considered by us to be Fe(IV)=O(Por$^{\pi+\bullet}$). In contrast to this however, was an earlier finding from our group based on quenching of a radical signal formed during turnover of peroxyacetic acid by INH [42]. These results suggested that in addition to reacting with heme intermediate(s), INH could be oxidized by amino acid radicals.

It is of great interest to confirm that radicals other than the M-Y-W adduct radical are involved in the catalytic function and INH activation by KatG under physiological conditions. Based on previous results from this laboratory [43, 63], it is expected that some redox-active residues in KatG such as Tyr229, Trp107 and Tyr353 could be sites of radical and, possibly, part of a pathway involving electron transfer in KatG. Tryptophan radicals on residues W135, W149, and W321 were suggested elsewhere to be involved in reaction with INH [33]. This was investigated here by carrying out RFQ-EPR experiments to follow the radicals formed upon turnover of WT KatG and several Tyr and Trp mutants with stoichiometric excess of PAA in the absence of peroxidase substrate.

Another important topic in KatG research that is still debated in the literature is the electronic structure of its first hypervalent heme species. While Fe(IV)=O(Por$^{+\bullet}$) is assumed to be the first intermediate that forms upon turnover of peroxide, this species has not been experimentally detected when the enzyme is mixed with H_2O_2. Instead, an amino acid-based radical species (the M-Y-W radical) was detected by EPR in the presense of hydrogen peroxide (Chapter 2). The work presented in this section attempts to verify whether Fe(IV)=O(Por$^{+\bullet}$) is indeed the only species that reacts with reducing substrates or another reactive species such as Fe(IV)=O(Trp$_{321}^{+\bullet}$) may also have a catalytic role upon turnover of alkyl peroxide, which would be analogous to cytochrome c peroxidase Compound I (Compound ES) [64]. For this reason, a considerable portion of this chapter is devoted to closely examine the intermediates that form in the KatG[W321F] mutant (Figure 3.1).

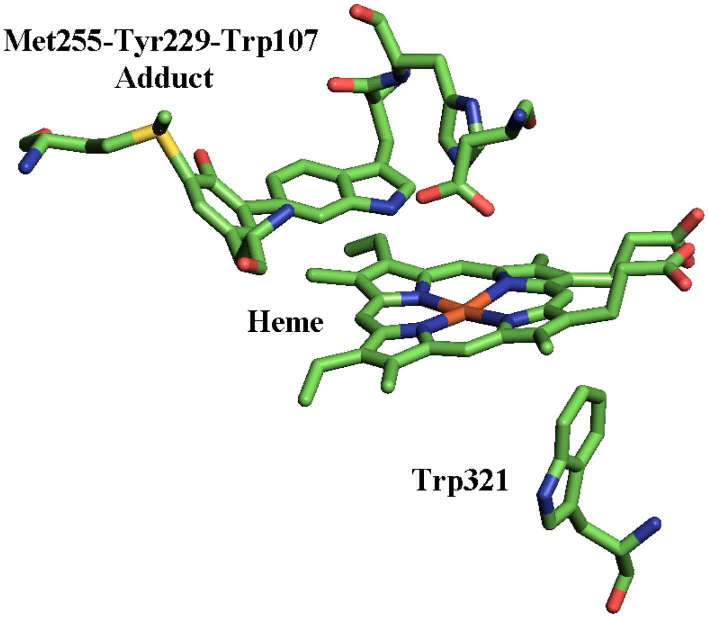

Figure 3.1. The active site of *M. tuberculosis* KatG showing tryptophan 321, the heme group, and the M-Y-W adduct. This figure was generated using PyMOL (The PyMOL Molecular Graphics System, version 1.2r3pre, Schrödinger, LLC.) based on published KatG crystal structure (2cca.pdb).

The initial turnover of peroxide and the events that follow have been investigated in the mutant enzyme and compared to WT KatG. Moreover, the KatG[W321F] section of this chapter is significant because many factors contribute to the assumption of an important catalytic role played by residue Trp321 in KatG. One assumption is based on the hypothesis that Trp321 could be a radical site giving rise to a species such as Fe(IV)=O($\text{Trp}_{321}{}^{+\bullet}$). This intermediate has been reported by another group [32]. Another reason suggesting the formation of a Trp321 radical arises from DFT calculations [65] that lead to the proposal that Compound I in KatG is actually a 'versatile' structure and there could be oxidizing equivalents distributed from the heme to the M-Y-W adduct to Trp321. It is worth mentioning that Trp 321 is conserved in all Class I peroxidases, and that no radical has been associated with this residue in ascorbate peroxidase or in *Synechocystis* KatG.

In addition to EPR, enzyme kinetics and INH-activation experiments were performed using KatG[W321F].

3.2 Formation of the 'wide doublet' EPR signal in KatG.

Prior to the experiments reported for this thesis, when WT KatG is treated with alkyl peroxides such as peroxyacetic acid (PAA) more than one type of radical species is observed; first a 'wide doublet' EPR signal characterized by *g*-factor of 2.0032 and linewidth of 28 Gauss (peak to trough) appears within milliseconds of incubation. This signal grows in intensity and becomes a singlet after ~1 sec (Figure 3.2) and the radical concentration reaches ~0.5 spins per heme 10 sec after mixing (Figure 3.3). The signal decays slowly during few seconds after that.

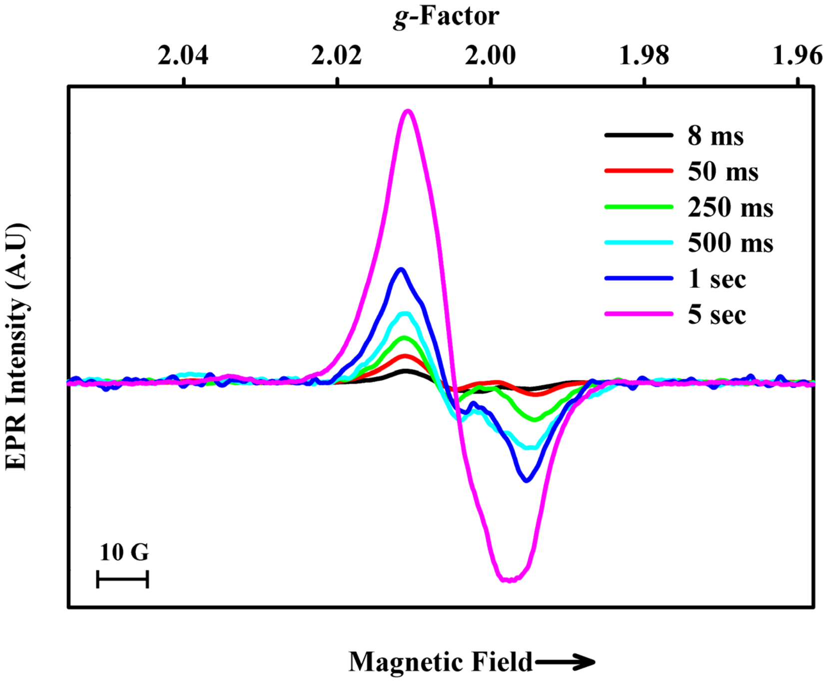

Figure 3.2. X-band RFQ-EPR spectra of WT KatG (50 µM) treated with 3-fold molar excess of PAA at pH 7.2 frozen at the indicated times after mixing. Experimental conditions: T = 77 K; microwave frequency = 9.44 GHz; microwave power = 0.1 mW; modulation amplitude = 1 G; average of 9 scans.

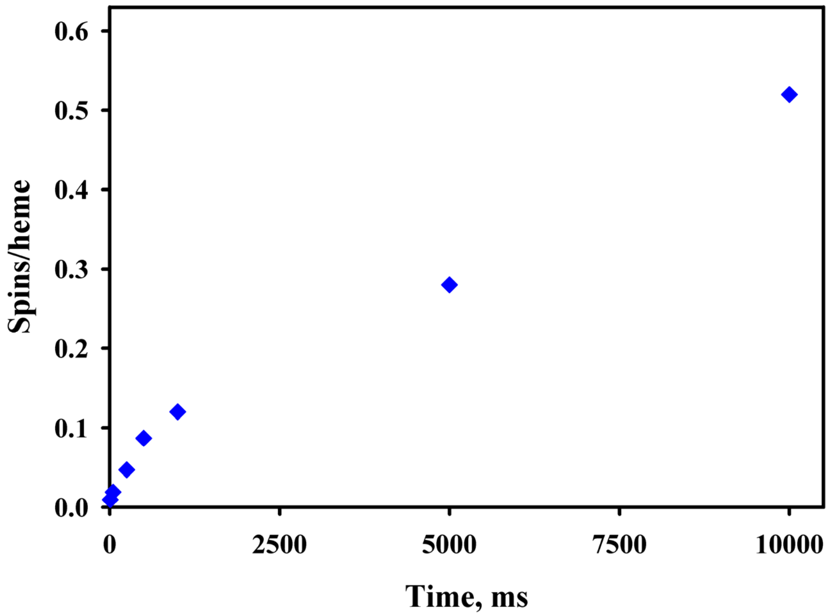

Figure 3.3. Intensity (spins/heme) of the wide doublet/singlet EPR signal as a function of time in RFQ-EPR samples frozen after mixing WT KatG (50 µM) with 3-fold excess of PAA at pH 7.2.

The doublet to singlet transition is assumed to be a product of the formation of amino acid-based radicals on several Tyr and/or Trp residues in KatG, or result of ring rotation that changes the hyperfine interaction of the aromatic radical with the β-methylene hydrogens. These radicals are likely to form after a turnover of alkyl peroxide that first produces a hypervalent heme:radical species (KatG Compound I) followed by a single-electron oxidation of Tyr and/or Trp residues by this reactive intermediate. Additional electron transfers occur that likely result in formation of radicals on the surface of the protein which can recombine and restore the resting enzyme.

The high-field RFQ-EPR spectrum detected upon turnover of PAA showed predominantly a tyrosyl radical along with some contribution from a tryptophanyl radical at ~800 ms after mixing [43]. Isotope labeling experiments confirmed that, the earliest radical species detected upon turnover of PAA is mostly tyrosyl radical [42].

Simulation of the wide doublet EPR signal (from the 250-ms sample) was attempted but results were not satisfactory as the simulated spectrum did not accurately match the experimental one (not shown). Using *g*-tensor values and ring proton nuclear hyperfine couplings similar to those reported elsewhere for tyrosyl radicals [42], and varying the β-methylene hydrogen coupling parameters did not achieve good simulation of data. This is most-likely because the observed doublet EPR signal contains other signals (tryptophanyl, peroxyl). A tryptophanyl radical can also give a doublet; the principal hyperfine splitting in both types of radical (Tyr and Trp) arises from the coupling of unpaired electron spin in the π-systems of phenol or indole rings with the β-methylene hydrogens [42]. These EPR simulation attempts supported the conclusion that a mixture of radicals forms in KatG upon turnover of PAA.

In an attempt to identify the sites responsible for giving the wide doublet signal upon turnover of PAA, RFQ-EPR samples were prepared from the available tyrosine mutants. Most of the mutant enzymes behaved the same as WT KatG. The RFQ-EPR spectra of KatG[Y28F], [Y64F], [Y95F], [Y197F], [Y210F], [Y337F], [Y339F], [Y390F], [Y413F], [Y426F], [Y608F], [Y638F], and [Y711F] each mixed with 3-fold molar excess PAA and frozen at the indicated times after incubation, are shown in Figure 3.S1 (Appendix B). The spectra of these mutants did not reveal a significant difference from that of WT KatG in terms of the *g*-factor, linewidth, spectral shape or the signal evolution (doublet to singlet transition). The remaining Tyr mutants (KatG[Y98F], [Y113F], [Y155S], [Y353F], and [Y304F], not shown), are known from prior experiments carried out in this laboratory to exhibit the wide doublet signal similar to WT KatG [66]. This leaves Tyr229, Tyr597, and Tyr678 as possible candidates for sites in KatG giving rise to the wide doublet EPR signal or sites required for its appearance.

Among the variants that showed alterations from WT was KatG[Y229F] which formed a radical having an EPR signal with $g_{//}$ ~2.038 and $g_{\perp}$ ~2.0040 (Figure 3.4), similar to that formed from a KatG-bound peroxyl radical characterized by $g_{//}$ ~2.035 and $g_{\perp}$ ~2.0050 (Figure 3S.2, Appendix B). Interestingly, the EPR signal intensity and shape remained essentially the same even for different incubation times, unlike the behavior observed in WT KatG. The results strongly suggested the involvement of Tyr229 (and/or the M-Y-W adduct), either solely or partially, in the reaction giving rise to a radical species responsible for the wide doublet signal observed in WT KatG. KatG[Y597F] also exhibited an EPR signal typical of peroxyl radical with $g_{//}$ at ~2.038 and $g_{\perp}$ at ~2.0050 (Figures 3.4), which remained unchanged in shape and only decreased in intensity as a function of freezing time after mixing. KatG[Y678S] also formed a peroxyl radical ($g_{//}$ ~2.038 and $g_{\perp}$ ~2.0040, Figure 3.4). As in KatG[Y229F], the signal here did not change in terms of line shape in the sample frozen 2 sec after mixing although the signal intensity dropped by a factor of ~2 compared to the early time point.

Are all these Tyr residues sites of the wide doublet signal in WT KatG? It would be understandable that Tyr229 is a radical locus due to its proximity to the heme active site. However, Tyr597 and Tyr678 are further away toward the protein surface. A more reasonable scenario would be that the absence of the wide doublet signal in these mutants is not because they are all sites of formation, but rather sites leading to its 'actual' location. This location could be Tyr597 or Tyr678, or possibly other aromatic residue near the protein surface.

Since the high-field EPR spectrum of the WT radical formed upon turnover of PAA revealed the presence of a tryptophanyl radical, preparation and characterization of some Trp mutants of KatG were carried out. Upon turnover of PAA, each of the following Trp variants

(KatG[W90F], [W135F], and [W149F]) produced an EPR spectrum with $g_{//}$ at ~2.038 and $g_{\perp}$ at ~2.0033 (Figure 3.4, right panels) characteristic of peroxyl radical.

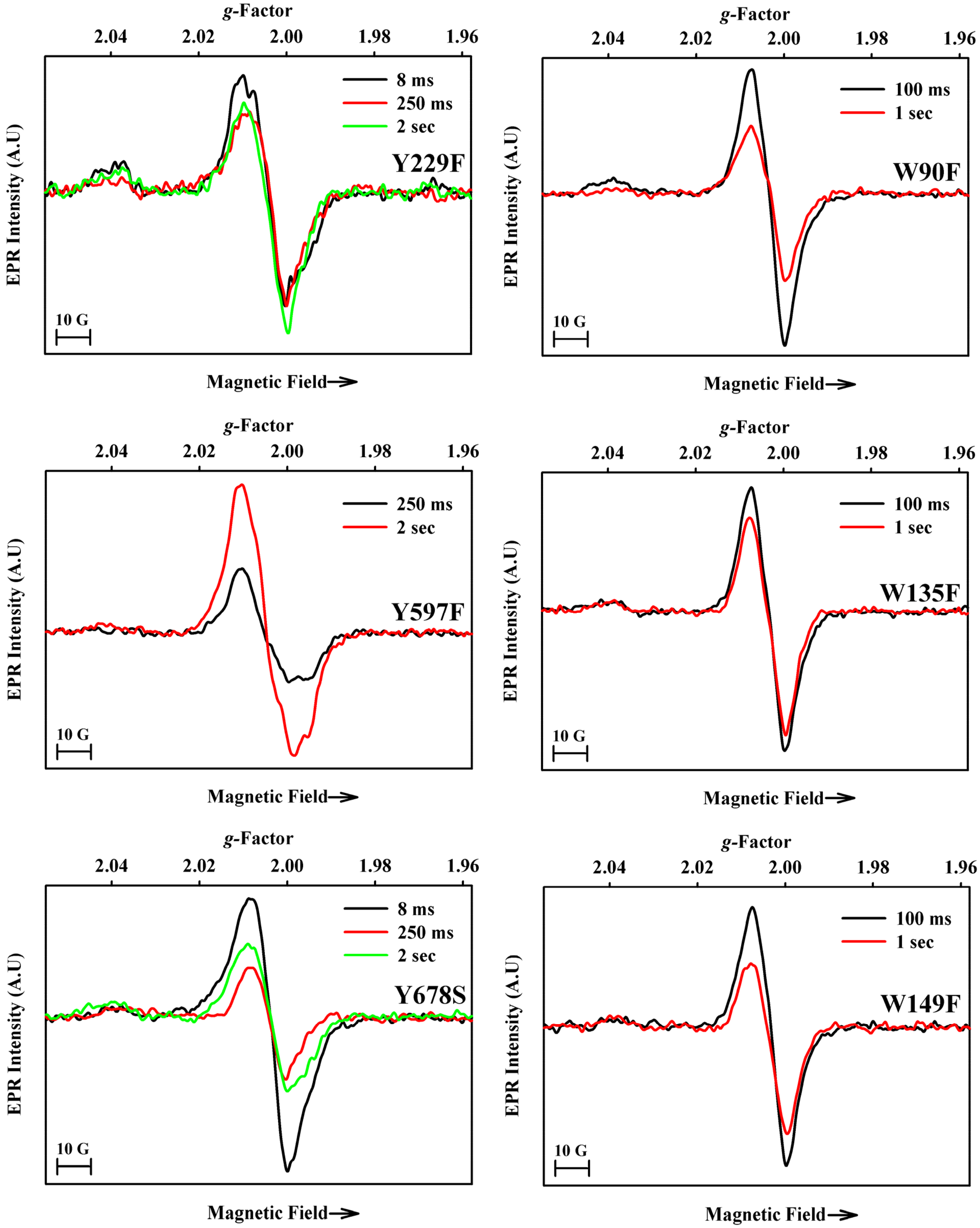

Figure 3.4. X-band RFQ-EPR spectra of KatG[Y229F], [Y597F], [Y678S], [W90F], [W135F], and [W149F] (50 µM) each treated with 3-fold molar excess of PAA at pH 7.2 frozen at the indicated times after mixing. Experimental conditions: T = 77 K; microwave frequency = 9.44 GHz; microwave power = 0.1 mW; modulation amplitude = 1 G; average of 6 scans.

It is worth mentioning that KatG[W90F] and KatG[W135F] exhibited close to normal catalase and peroxidase activities (2260 unit/mg catalase and 0.52 unit/mg peroxidase for KatG[W90F], and 2250 unit/mg catalase and 0.59 unit/mg peroxidase for KatG[W135F]), while KatG [W149F] exhibited about 10% of WT activity (325 unit/mg catalase and 0.14 unit/mg peroxidase). Also, all 3 Trp mutants exhibited the narrow doublet EPR signal of the M-Y-W adduct radical upon turnover of excess H_2O_2 (Figure 3.S3, Appendix B).

Further characterization of the peroxyl species is not possible because the X-band EPR data does not allow for the identification of the type of peroxyl radical since all radicals of the form $R_2COO^{\bullet}$ have similar *g*-values; however, a feature at 2.038 is closer to the $g_{//}$ value for Trp-$OO^{\bullet}$ (2.0379) rather than that of Tyr-$OO^{\bullet}$ (2.0356) reported according to high-field EPR measurements [67-68]. The evaluation of *g*-factors using the Bruker ElexSys spectrometer system should be accurate to at least 3 decimal places since the frequency is measured to 7 and the field to 6 significant figures. Therefore, the peroxyl radical observed in the mutants described above is most likely located on tryptophan.

Importantly, the concentration of peroxyl radical in spectra of the Tyr and Trp mutants shown above was always less than 0.01 spin per heme (< 2% of the unpaired spin in WT KatG under the same conditions). Therefore, due to low radical yield, no further characterizations of the peroxyl signal was attempted. PAA (CH_3CO_3H) could also be the source of peroxyl radical formation through a single-electron oxidation by hypervalent species in KatG but a search of the literature did not turn up an example of the EPR spectrum of peroxyacetic acid radical. Peroxyl radicals have been found in heme enzymes during reactions initiated by hydrogen peroxide or alkyl peroxides when molecular oxygen is present in the medium, as O_2 acts as a natural spin trap for radicals that form on Trp and less often Tyr sites. These amino acid-based peroxyl species are very reactive and can oxidize neighboring residues resulting in a chain-like intermolecular radical transfer [69].

Based upon information about peroxyl radical in heme enzymes [69], and with a previous knowledge that residues in KatG such as Tyr229 and Trp107 are required for significant yields of radicals upon turnover of PAA, while surface residue Tyr353 is a site of radical [43, 63], it might be reasonable to hypothesize the presence of an electron transfer pathway involving several redox-active residues in KatG (including the 3 Tyr and 3 Trp outlined earlier) upon turnover of a small excess of PAA. This would likely happen after the formation of the first hypervalent species in KatG in a pathway that, likely, starts near the heme active site and terminates at the surface of protein exposed to solvent. Interruption of this pathway at any one of the Tyr and Trp residues can interfere with the appearance of a radical at some final site giving the wide doublet EPR signal, which still remains unidentified. For each mutant to give only peroxyl it could mean that a Trp near the heme (early in the pathway) loses its immediate and rapid reacting partner that would otherwise continue the transfer to the residue giving the wide doublet, and since it cannot oxidize its nearby partner rapidly, it has time to react with oxygen instead to form a peroxyl.

Another Trp residue that could be a part of the suggested electron transfer pathway is the proximal W321 (Figure 3.1) based upon results shown later in this chapter. As stated in the introduction, due to the important role played by this residue in catalysis and radical formation in another Class I peroxidase such as CCP, it was studied in a more comprehensive manner through experiments carried out on the KatG[W321F] mutant enzyme.

*3.3 **Radical production in KatG[W321F].***

Purified KatG[W321F] enzyme showed a normal optical purity ratio (A_{405}/A_{280}= 0.50) within the range expected for WT KatG (0.55). The spectroscopic features are consistent with a mixture of 5- and 6-coordinate high-spin ferric heme in the resting enzyme much like that in WT KatG. The catalase-specific activity of KatG[W321F] was normal compared to WT KatG (3700 *vs.* 4000 unit/mg), while the peroxidase activity was slightly lower than that of WT (0.74 *vs.* 1.1 unit/mg).

Evaluation of the rate of formation of the first hypervalent heme species detected is among our approaches to characterize catalytic function of KatG enzymes. The optical spectrum formed upon turnover of ferric KatG[W321F] with small excesses of PAA was similar to that reported for WT KatG and showed ~30% hypochromicity and red shift to 413 nm in the Soret region and peaks at 550 and 590 nm, together with shoulders at 350 and 665 nm (Figure 3.5, red spectrum) similar to other reports in which the species was identified as 'ferryl-like' [30, 44].

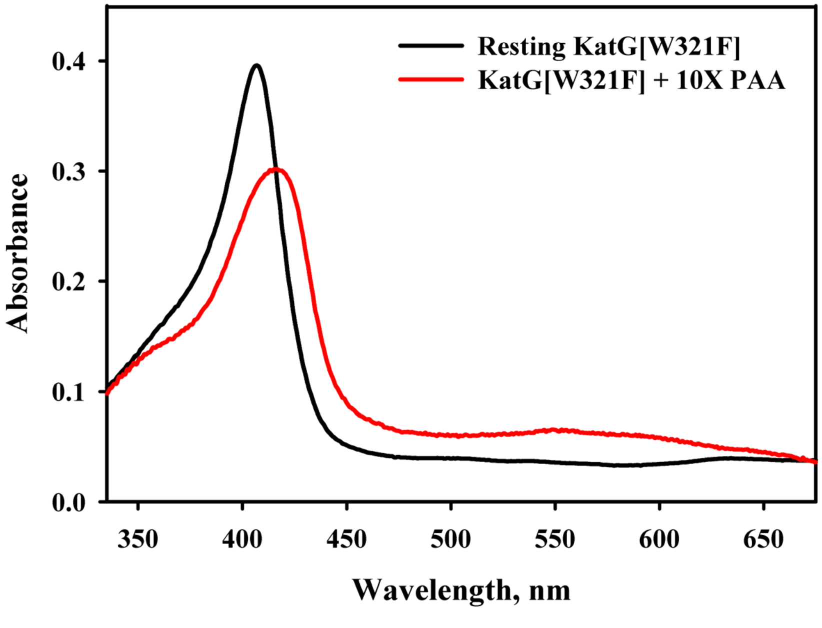

Figure 3.5. UV-Vis spectra of resting KatG[W321F] and its Compound I. Optical absorption spectra of 5 µM KatG[W321F] (black spectrum), and 5 µM KatG[W321F] mixed with 50 µM PAA (final concentrations) in stopped-flow experiment (red spectrum), in 20 mM potassium phosphate buffer, pH 7.2, at 25 °C.

The second order rate constant for the conversion of ferric enzyme with PAA was determined from the linear plot of the k_{obs} values as a function of the concentration of peroxide (Figure 3.6). This value of 9.9×10^3 $M^{-1}.s^{-1}$ was very close to that obtained for WT KatG (1.2×10^4 $M^{-1}.s^{-1}$) under the same conditions. This suggests that the first intermediate is the same in WT and this mutants, and is formed without any requirement for Trp321.

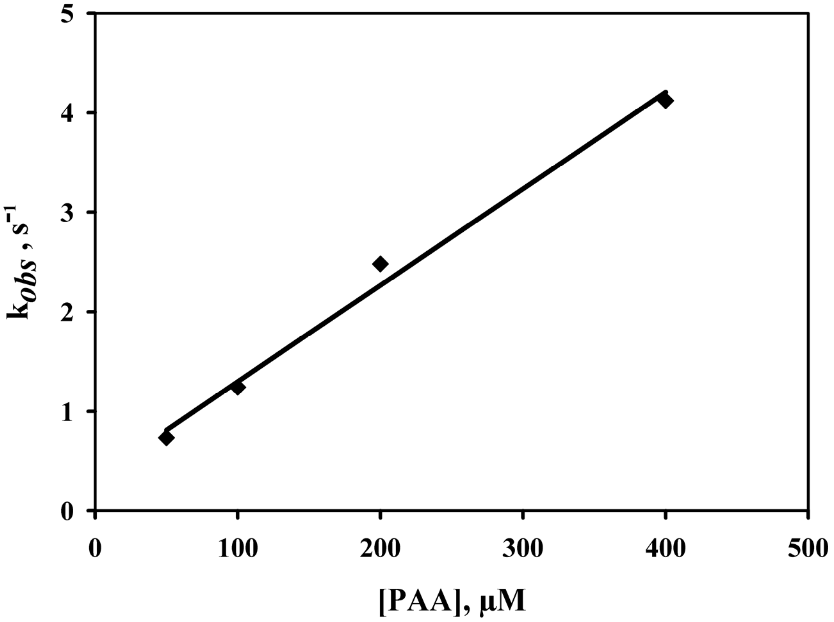

Figure 3.6. Linear dependence of the observed rates of Compound I formation in KatG[W321F] as a function of PAA concentration. Linear best-fit gives a second order rate constant equal to 9.9×10^3 $M^{-1}.s^{-1}$.

The spontaneous return to the resting enzyme after formation of the first intermediate is of great interest because this process involves producing the amino acid-based radicals described above for the experiments using PAA [42-43, 70]. Interestingly, the decay period of 'Compound I' was ~2 times longer in KatG[W321F] compared with WT KatG. The rate was estimated from the time the enzyme took to return back to resting state (increase in absorbance *vs.* time at 407 nm) after turnover of KatG[W321F] with a small excess of PAA. Spectra in Figure 3.7 show that when reacted with 3-fold excess PAA, KatG[W321F] returns to the resting state after ~100 sec *vs.* ~50 sec for WT KatG. This slower return is the first clue that hints to a possible involvement of Trp321 in the electron transfer processes following the formation of 'Compound I' in KatG. More clues came from spectrophotometric studies of the reaction of the KatG[W321F] 'Compound I' with a reducing substrate under more peroxidase-relevant conditions, and from EPR data (below).

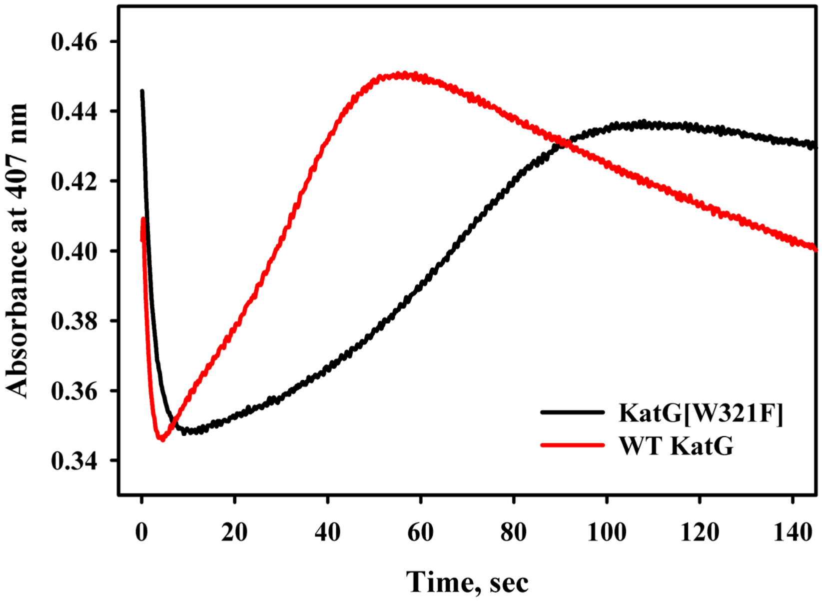

Figure 3.7. Formation and decay of Compound I in KatG[W321F] and WT KatG. Extended time traces (at 407 nm) recorded after mixing 5 µM resting KatG[W321F] or WT KatG with 15 µM PAA (final concentrations) in 20 mM potassium phosphate buffer, pH 7.2, in stopped-flow experiments at 25 °C. The initial rapid decrease is followed by the slow return to the starting absorbance value.

3.4 INH activation by KatG[W321F].

Although the physiological peroxidase substrate of KatG has not been identified yet, a more insight into the 'peroxidase-like' reaction of the KatG[W321F] mutant after formation of Compound I could be gained by using a reducing organic substrate such as INH. Double mixing optical stopped flow experiments were performed according to a previously published protocol [59] to test for some loss of function in KatG[W321F] after formation of Compound I and to directly examine the catalytic competence for INH activation by this mutant. The hypervalent heme intermediate, preformed by the reaction of KatG[W321F] with 10-fold molar excess PAA, was reacted after a 2-sec delay with increasing concentrations of INH (20-, 40-, 100-, and 200-fold molar excess), after which the absorbance changes at 407 nm were followed. As observed in WT KatG [59], after formation of Compound I, INH accelerated the return to the ferric enzyme (Figure 3.8).

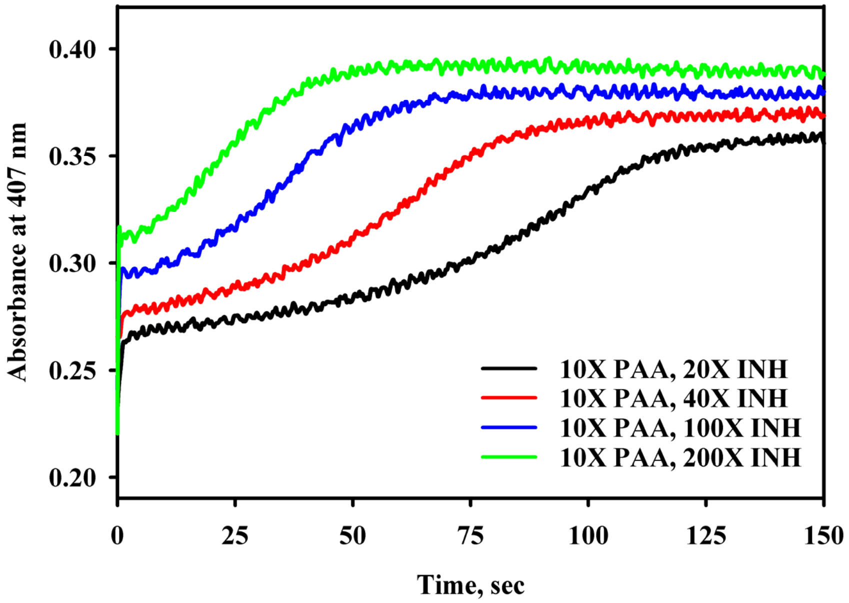

Figure 3.8. Reaction of KatG[W321F] Compound I with INH. Absorbance *versus* time traces at 407 for double mixing stopped-flow experiments are shown. Resting enzyme was prereacted with PAA to form Compound I, followed by the addition of increasing concentrations of INH. The final concentrations of enzyme and PAA were 5 and 50 µM, respectively; the final concentrations of INH are as labeled in the figure for each time trace.

Interestingly, the rate of return after the second mixing step was ~2.5-fold slower in KatG[W321F] than that in WT KatG (for each INH concentration). These results directly demonstrate the deficient turnover of the drug by the mutant enzyme. This could mean that either Trp321 is needed (as a radical) to react with INH, or the deficiency in INH oxidation is due to poor binding caused by structural modification by the replacement of the tryptophan residue on the heme proximal side.

3.5 *IN-NAD adduct formation catalyzed by KatG[W321F].*

As stated in Chapter 1, it is widely accepted that an isonicotinic acyl radical (IN$^\bullet$) formed upon oxidation of INH by KatG peroxidase function reacts with NAD$^+$ at the C-4 position of the nicotinamide ring to form an IN-NAD adduct [15-17, 21, 71-73] (Figure 3.9).

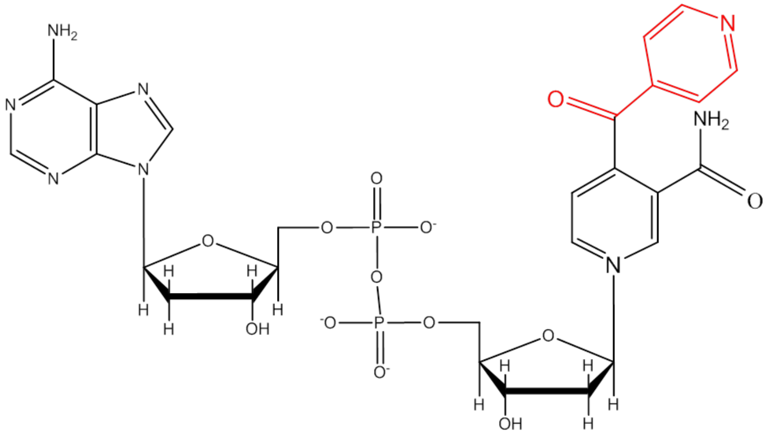

Figure 3.9. Structure of the IN-NAD adduct. (Adapted from Rozwarski [15]).

Since NAD$^+$ does not bind to KatG (known based upon the lack of signal in isothermal titration calorimetry (ITC) experiments), nor is it a peroxidation substrate, the rate of formation of the IN-NAD adduct depends completely on the rate of formation of the isonicotinyl acyl radical that can react non-enzymatically with NAD$^+$ [21]. WT KatG was previously shown to be capable of catalyzing the formation of the IN-NAD adduct in a physiologically-relevant biomimetic reaction system while KatG from clinical INH-resistant strains such as KatG[S315T] and [S315G] showed much less efficiency [21, 74]. In that approach, the IN-NAD adduct formation was evaluated using a biomimetic method in which continuous low-concentration H_2O_2 produced enzymatically using glucose plus glucose oxidase, initiates peroxidase activity. Using WT KatG, the rate of appearance of IN-NAD depended on the concentration of INH up to a saturating amount reached at 500 μM INH under conditions in which H_2O_2 was generated at 2 μM/min [21].

In the case of KatG[W321F] under the same conditions, INH concentration up to ~2 mM was required to produce the IN-NAD adduct at the same rate (0.4 µM/min) as WT KatG, with a maximum rate of formation (0.45 µM adduct/min) reached at about 3 mM INH, in the presence of 50 µM NAD$^+$ (Figure 3.10).

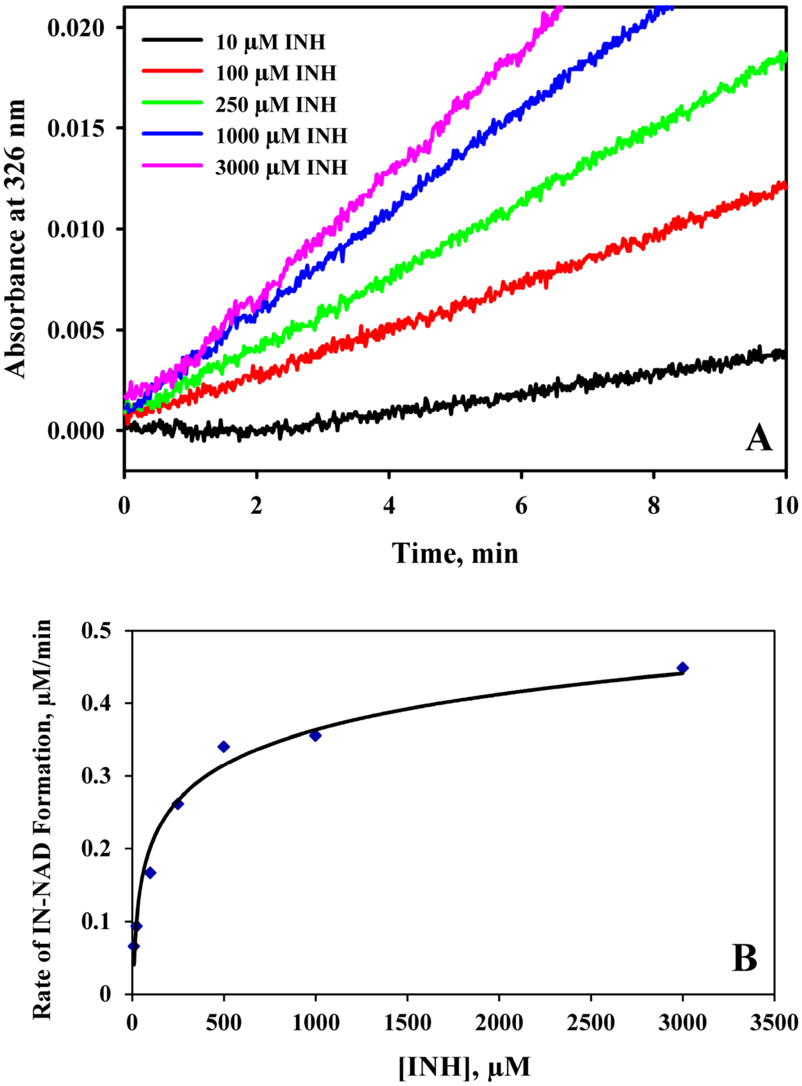

Figure 3.10. Effect of INH concentration on the rate of production of the IN-NAD adduct. A: IN-NAD adduct formation was followed at 326 nm [16]. KatG[W321F] (0.5 µM), NAD$^+$ (50 µM), and H_2O_2 (2 µM/min generated enzymatically using glucose/glucose oxidase), were incubated with varying concentrations of INH. B: rates of IN-NAD adduct formation as a function of INH concentration.

These observations are in agreement with the double mixing stopped-flow kinetics results (above), in which it was shown that INH was an apparently poorer substrate of KatG[W321F] compared with WT KatG. Overall, the results are consistent with significant loss in INH activation by the mutant enzyme and could correspond to considerable levels of resistance *in vivo* in mutants in which W321 is replaced with another amino acid. While KatG[W321F] is not a known drug resistant mutant, KatG[W321G] is [75]. And since the Trp to Gly replacement gave us an unstable mutant enzyme, the Trp to Phe replacement was amenable to these studies and provides a clue that mutations at this position have an impact on peroxidase turnover and INH activation. This could be due to a change in enzyme structure at a crucial locus within the active site (proximal side) and could be related to changes in an INH-binding site near the heme edge. Such a site has been proposed based on the 3-dimensional crystal structure of a CCP-INH complex [76] but confirmation of a binding site in KatG awaits further study.

3.6 <u>Catalase function in KatG[W321F].</u>

Chapter 2 addressed the M-Y-W adduct radical and its role in the catalase reaction mechanism in KatG. Even though KatG[W321F] has the same catalase activity as WT KatG, we wanted to examine a possible role for Trp321 in the catalase reaction and on the behavior of the adduct radical. This is important because a species labeled 'versatile Compound I' reported by another group [65], was said to share oxidizing equivalents among the M-Y-W adduct, the porphryin, and the proximal Trp321 residue in KatG. Therefore, RFQ-EPR experiments were undertaken to compare the narrow doublet signal intensity and radical utilization during the catalase reaction in KatG[W321F] with those in WT KatG.

The X-band RFQ-EPR spectra of KatG[W321F] mixed with a 1000-fold molar excess of H_2O_2 at pH 8.5 recorded at 77 K as a function of incubation time showed the usual WT narrow doublet signal characterized by *g*-factor of 2.0036, linewidth of 17 Gauss (peak to trough), and a principal hyperfine splitting of 11 Gauss as the only signal in the *g* = 2 region (Figure 3.11).

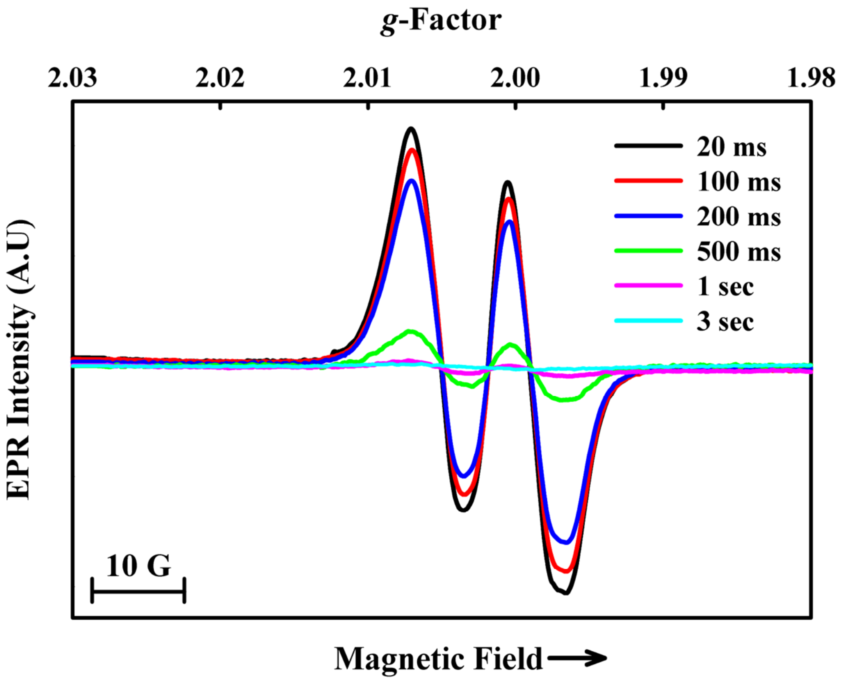

Figure 3.11. X-band RFQ-EPR spectra of KatG[W321F] (50 µM) treated with 1000-fold molar excess of H_2O_2 at pH 8.5 frozen at the indicated times after mixing. Experimental conditions: T = 77 K; microwave frequency = 9.44 GHz; microwave power = 0.1 mW; modulation amplitude = 1 G; average of 9 scans.

As observed in WT KatG, the intensity of the signal was maximal at the earliest time point accessible and in the sample frozen after 20 ms the spin per heme concentration was 0.20 for KatG[W321F], compared to 0.22 spin per heme for WT KatG under the same experimental conditions. The radical species was consumed during the catalase reaction and the narrow doublet signal became no longer detectable after ~1.5 sec at pH 8.5 (Figure 3.11), and ~700 ms at pH 7.2 (Figure 3.12).

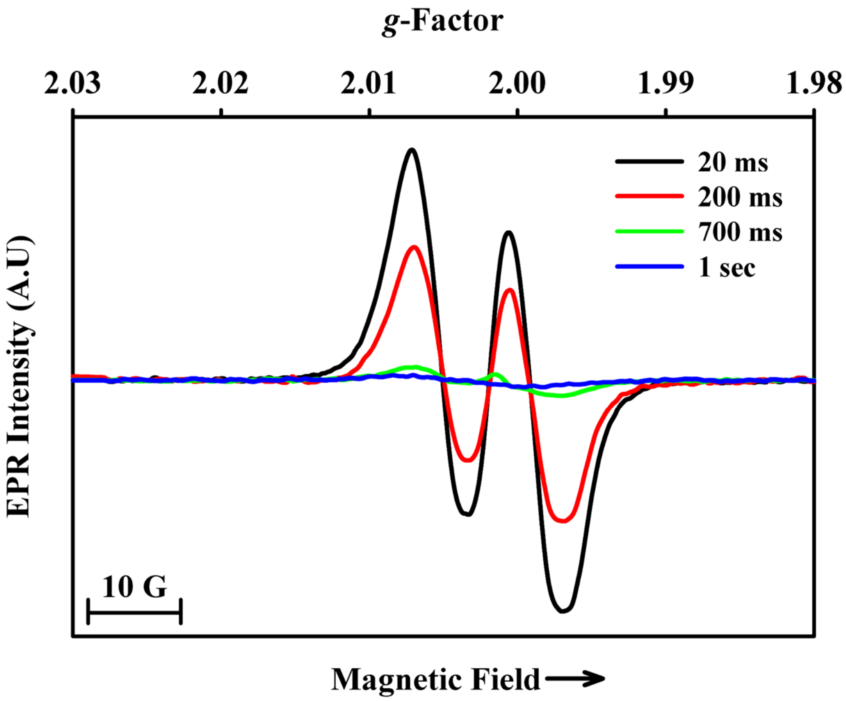

Figure 3.12. X-band RFQ-EPR spectra of KatG[W321F] (50 µM) treated with 1000-fold molar excess of H_2O_2 at pH 7.2 frozen at the indicated times after mixing. Experimental conditions: T = 77 K; microwave frequency = 9.44 GHz; microwave power = 0.1 mW; modulation amplitude = 1 G; average of 9 scans.

The catalase-specific activity of KatG[W321F] (~3700 unit/mg at pH 7.2 and ~650 unit/mg at pH 8.5) allows estimation that a 1000-fold excess of H_2O_2 should be completely consumed within ~0.3 sec at pH 7.2 and after ~1.5 sec at pH 8.5. These time intervals, particularly the second, correspond reasonably well to the interval during which the M-Y-W radical is present, confirming once again that it represents a kinetically-competent intermediate of the catalase reaction pathway and ruling out any significant involvement of Trp321 in M-Y-W adduct radical formation and utilization.

3.7 __Stopped-flow spectrometry for the reaction of KatG[W321F] with H_2O_2.__

The above correlation between the persistence of the narrow doublet signal and the estimated time required for complete turnover of H_2O_2 was experimentally demonstrated, under the same conditions, using stopped-flow spectrophotometery. Figure 3.13-A,B shows the time course for the consumption of H_2O_2 upon mixing with KatG[W321F] at pH 7.2 and 8.5 with the reaction monitored at 240 nm. Note that the slight difference between radical kinetics and H_2O_2 consumption in the EPR and UV spectra arises from the difference in enzyme and peroxide concentrations used in each method due to instrumental limitation, although the molar ratio was kept constant (50 μM KatG and 50 mM H_2O_2 in EPR, 25 μM KatG and 25 mM H_2O_2 in stopped-flow).

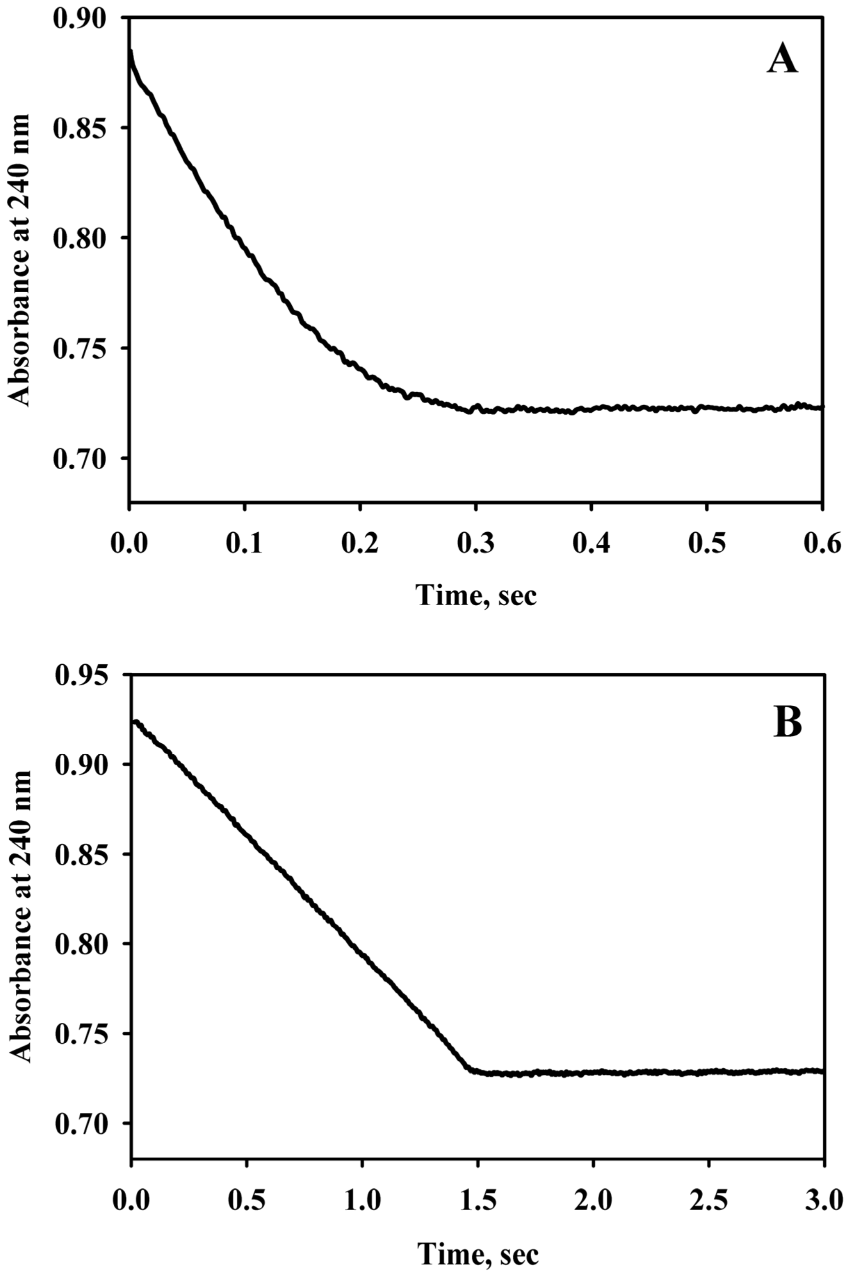

Figure 3.13. Time course for the consumption of H_2O_2 upon mixing with KatG[W321F]. Enzyme (25µM final concentration) was mixed with 1000-fold excess peroxide at pH 7.2 (A), and 8.5 (B), and reaction was monitored at 240 nm using stopped-flow spectrophotometry.

Similar behavior was observed when WT KatG was mixed with H_2O_2 under the same conditions (Figure 3.14-A,B) and was also similar for other mutants (Chapter 2), suggesting that the narrow doublet signal represents a kinetically-competent intermediate of the catalase reaction pathway and demonstrating that no significant change was caused by the replacement of Trp321 in terms of the behavior of the radical.

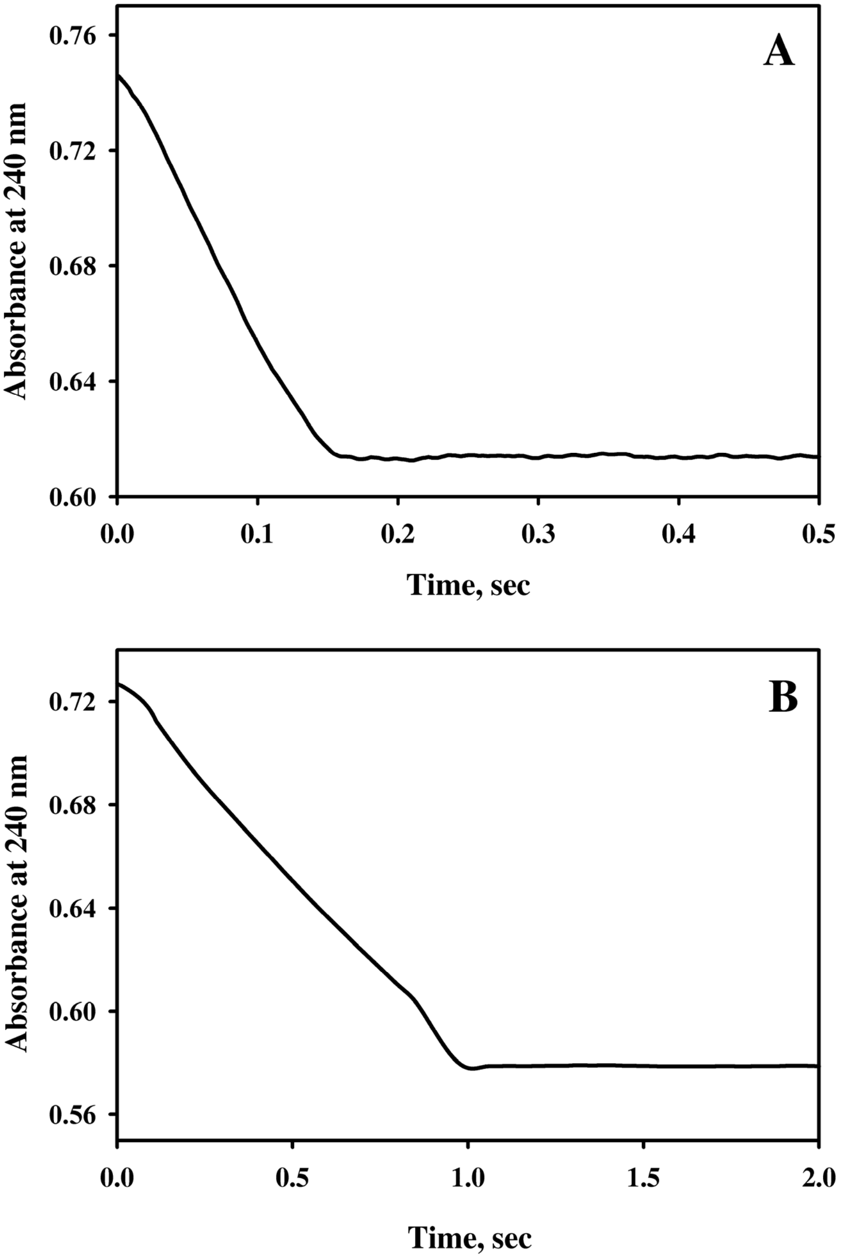

Figure 3.14. Time course for the consumption of H_2O_2 upon mixing with WT KatG. Enzyme (25µM final concentration) was mixed with 1000-fold excess peroxide at pH 7.2 (A), and 8.5 (B), and reaction was monitored at 240 nm using stopped-flow spectrophotometry.

Examination of the UV-Visible spectrum of KatG[W321F] upon mixing with 1000-fold excess H_2O_2 and comparison with the spectrum of the resting enzyme revealed a shift in the Soret peak (originally at ~407 nm) and the presence of other weak peaks at ~545 and ~585 nm and a shoulder at ~508 nm (Figure 3.15, arrows). These features are known to be characteristic of either six-coordinate low spin ferric heme or oxyferrous heme (peroxidase Compound III [57]), and are also observed in WT KatG when mixed with excess H_2O_2 [31]. Thus, the heme in KatG[W321F] is converted to the same intermediate as in WT KatG during the catalase turnover (see Figure 3 in [31] for example of WT).

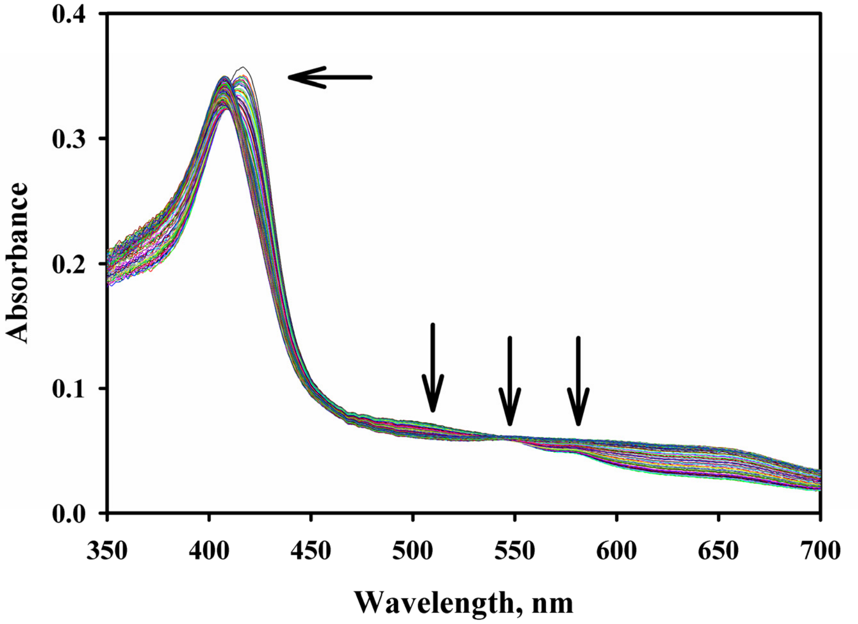

Figure 3.15. UV-Visible spectra of KatG[W321F] upon mixing with H_2O_2. Enzyme (5 μM) was mixed with 1000-fold excess peroxide at pH 7.2 and wavelength spectra were recorded for 4 sec using stopped-flow spectrophotometer.

3.8 Rapid freeze-quench EPR experiments and the wide doublet in KatG[W321F].

It was shown earlier in this chapter that when the WT KatG was treated with alkyl peroxide such as PAA, more than one type of radical species was detected; first a low-intensity wide doublet EPR signal appeared within milliseconds of mixing and then the signal grew in intensity and became a singlet after ~1 sec of incubation (Figure 3.2). This transition was assumed to be a product of the formation of a series of amino acid-based radicals on tyrosine and/or tryptophan residues in KatG (or because of aromatic ring rotation and change in hyperfine interactions of β-methylene hydrogens with the radical).

To check for the involvement of Trp321 in the radical species giving rise to the wide doublet signal, RFQ-EPR samples of KatG[W321F] mixed with 3-fold excess PAA were prepared. The EPR spectra revealed a complex signal, different from WT KatG, consisting of a mixture of, mostly, peroxyl radical with $g_{//}$ at ~2.038 and $g_{\perp}$ at ~2.0050 that overlapped and nearly masked an amino acid-based radical signal (Figure 3.16).

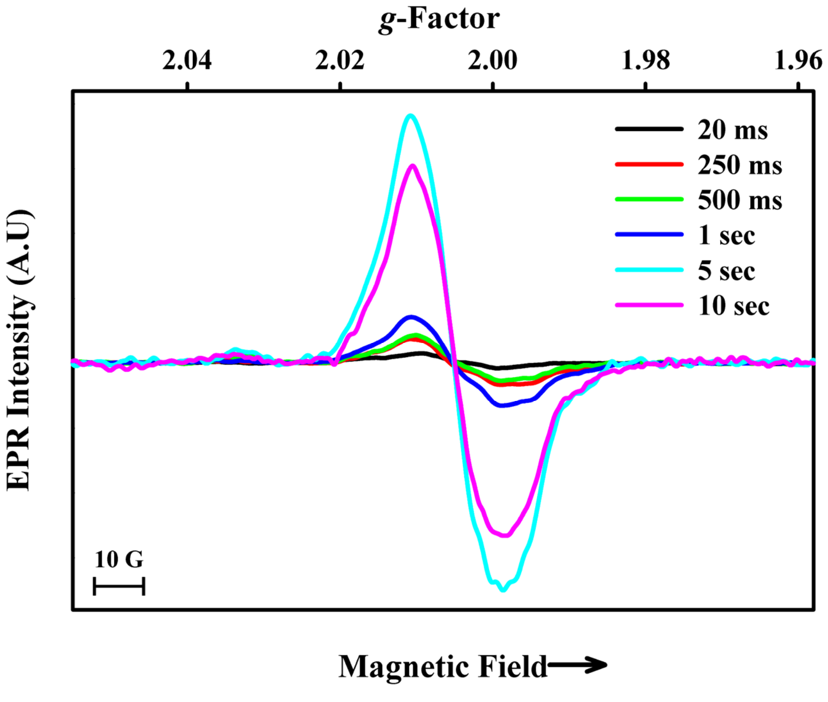

Figure 3.16. X-band RFQ-EPR spectra of KatG[W321F] (50 µM) treated with 3-fold molar excess of PAA at pH 7.2 frozen at the indicated times after mixing. Experimental conditions: T = 77 K; microwave frequency = 9.44 GHz; microwave power = 0.1 mW; modulation amplitude = 1 G; average of 9 scans.

Interestingly, the EPR signal in KatG[W321F] was unstable and changed upon aging, while samples were stored frozen at 77 K all the time, as the $R_2COO^{\bullet}$ slowly decayed and the wide doublet features became more evident. Spectral subtraction of a 'pure' peroxyl radical, previously generated from another mutant forming this species in high abundance (KatG[S315G], Figure 3.S2), from the 'fresh' signal obtained for KatG[W321F] resulted in the usual wide doublet centered at g = 2.0032 with linewidth of ~28 Gauss (Figure 3.17), similar to that obtained from WT KatG incubated with PAA under the same experimental conditions.

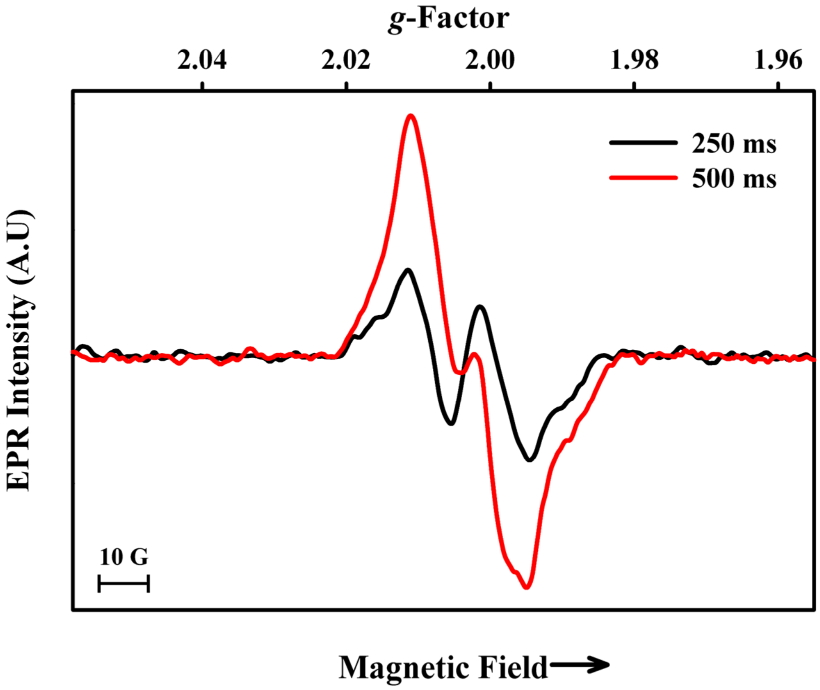

Figure 3.17. EPR spectral deconvolution resulting from subtracting the peroxyl radical signal from the signals obtained for KatG[W321F] (50 µM) treated with 3-fold molar excess of PAA at pH 7.2 at the indicated time points of reaction.

Comparison between the mutant enzyme and wild type in terms of the spin per heme concentration of the wide doublet signal alone showed that KatG[W321F] had always about 30% of the unpaired spin concentration found in WT KatG (0.014 *vs.* 0.047 spins/heme at 250 ms, and 0.040 *vs.* 0.12 spins/heme at 1 sec). The formation of significant yield of peroxyl radical (along with the WT wide doublet) in the mutant enzyme could be because Trp321 is required for the efficient formation of the radical giving the wide doublet signal. However it is unlikely that

Trp321 is itself, the site of radical giving rise to the wide doublet signal since 30% of the WT signal was seen in the mutant enzyme. Whether these observations mean that Trp321 is a site for radical hopping in WT KatG remains to be proven since it is also possible that a structural change on the proximal side alters the radical formation pathway elsewhere.

*3.9 **Low-temperature EPR spectra of WT KatG and KatG[W321F] mixed with PAA.***

Manual mixing of KatG with 15-fold molar excess PAA followed by freezing the samples and recording the EPR spectra at low temperature (4.8 K) revealed some differences between WT KatG and KatG[W321F]. As seen in Figure 3.18 (black spectrum), WT KatG exhibited a signal centered at $g = 2.0021$ with broad asymmetric high- and low-field 'wings' (~550 Gauss total linewidth) indicative of at least one organic radical (S = 1/2) in magnetic interaction with the heme iron (S = 1) similar (but not identical) to that found in monofunctional peroxidases such as horseradish peroxidase [77] and turnip peroxidase [38]. The EPR spectrum of KatG[W321F] mutant mixed with PAA under the same conditions (Figure 3.18, red spectrum) showed a narrower signal (~180 Gauss linewidth), similar to a previously published spectrum for the same mutant in KatG [32], where the 'wings' flanking the $g = 2$ region, seen in the WT spectrum were essentially missing. A similar observation (the loss of the wings) has been reported for CCP, when the analogous Trp residue (W191) was replaced by Phe [78]. The difference between the EPR spectra for WT KatG and the mutant enzyme is attributed to the difference in the strength of the spin coupling interaction between the organic radical (S = 1/2) and the iron center (S = 1). Therefore, this could be an evidence for Trp321 being the site for formation of the exchange-coupled radical intermediate ($\mathrm{Trp}^{\pi+\bullet}$, S = 1/2) in WT KatG (giving the broad signal) although these experimental conditions are known, from previous observations to produce multiple turnovers of the enzyme, and lead to heme degradation and enzyme cross-linking (Dr. J. Suarez, personal communication). Therefore, after a few seconds of incubation with a large excess of PAA (manual mixing conditions) what is being observed in the low-temperature EPR spectrum is probably a protein-based radical, not the first hypervalent heme species (Compound I) given that at 77 K the EPR results show appearance and growth of a signal resembling that seen in WT KatG.

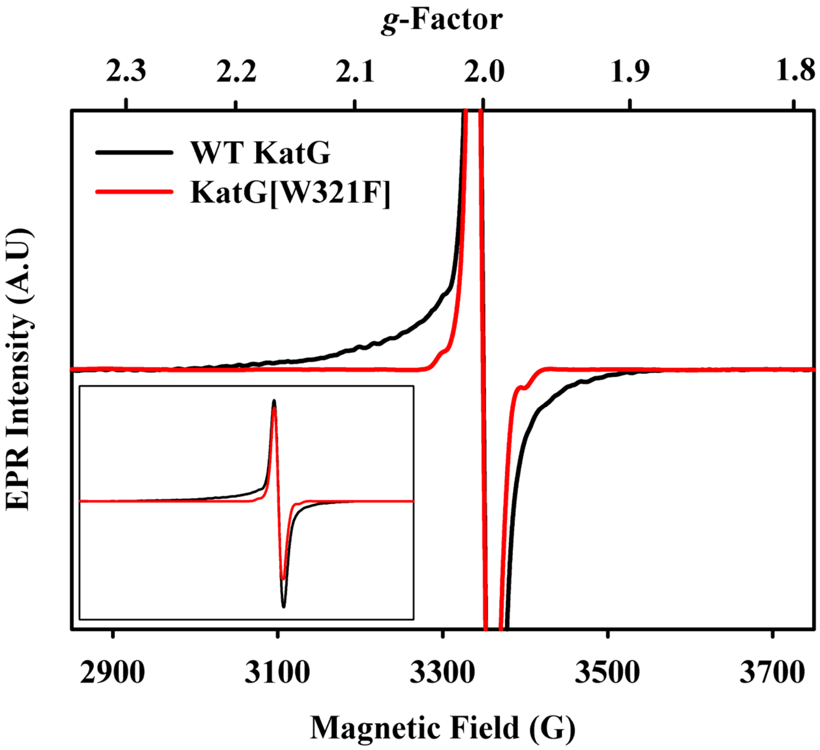

Figure 3.18. Low-temperature EPR spectra of KatG[321F] and WT KatG reacted with PAA. 200-µM samples of KatG[321F] (black spectrum) and WT KatG (red spectrum) were manually-mixed with 15-fold excess PAA at pH 7.2. EPR spectra (single scan) were recorded using the following conditions: T = 4.8 K, microwave frequency = 9.39 GHz; microwave power = 1 mW; modulation amplitude = 4 G.

3.10 <u>Conclusions.</u>

The studies shown in this chapter attempt to examine the poorly-understood function of KatG in the presence or absence of a peroxidase reducing substrate. A radical giving a wide doublet EPR signal forms on tyrosine (and tryptophan) residues in WT KatG upon turnover of alkyl peroxides that has not been assigned to a specific site(s). Mutagenesis and RFQ-EPR experiments reveal involvement of Tyr229, Tyr597, Tyr678, Trp90, Trp135, and Trp149 as mutating KatG at each of these positions eliminates formation of the wide doublet. These observations suggest that a radical 'hopping' network consisting of the above aromatic residues exists in KatG and awaits further work to be confirmed. Whether one or more of these radicals can be responsible for the activation of INH by KatG remains an important issue.

Identifying the electronic structure of KatG Compound I, or the hypervalent heme species formed in the first turnover by peroxide, is another important topic that has been an ongoing research goal for the past years and is still of great interest toward understanding the catalytic reaction mechanisms in KatG. This species has been labeled (by other groups) as a 'versatile' composite structure according to hybrid DFT QM/MM calculations, such that the ferryl heme:porphyrin π-cation radical shares an oxidizing equivalent with the M-Y-W adduct and the proximal Trp321 residue, with the distribution of unpaired spin on these three sites being pH dependent [65].

In Chapter 2 of this thesis, EPR data shows that the yield of M-Y-W adduct radical in WT KatG is nearly equal at pH values near 7.2 and at 8.5, which argues against the composite structure suggested by those calculations. Moreover, EPR results presented in this chapter show that the M-Y-W adduct radical is produced in the mutant KatG[W321F] in yields similar to WT under typical RFQ-EPR conditions. This is consistent with the nearly normal catalase activity of KatG[W321F] and also argues against the Trp321 residue sharing oxidizing equivalents from the heme during catalase turnover. This proximal Trp residue in *Mtb* and *B. pseudomallei* KatG but not in *Synechocystis* KatG was assigned as a site for formation of a π-cation radical coupled to ferryl heme [32] in an intermediate analogous to CCP Compound I, but formed in the presence of excess alkyl peroxide [65] in KatGs. One possible reason for a divergence of radical forming pathways upon turnover of the different peroxides is that a concerted formation of the M-Y-W adduct radical in the initial turnover with H_2O_2 could prevent reactions in which a fully formed Fe(IV)=O(Por$^{\pi+\bullet}$) generated by alkyl peroxide would be available to produce other amino acid radicals (such as on Trp321).

While KatG[W321F] shows a normal rate of formation of the hypervalent heme intermediate (Compound I, detected optically) relative to WT KatG, the EPR, optical, and kinetic stopped-flow data shown in this chapter indicate that Trp321 is involved in secondary radical formation. This is best evidenced by the slower spontaneous decay of the hypervalent heme species back to the ferric resting state of the enzyme, the different low-temperature EPR signal obtained upon turning the enzyme over with PAA, the deficiency in INH activation, and the less efficient catalysis of IN-NAD adduct all observed in the KatG[W321F] mutant. While most of these observations might be traced to the dependence of the reaction on a radical that forms on Trp321 in WT KatG, the lower INH-activation by KatG[W321F] could also be attributed to structural changes; i.e. the active site in the mutant enzyme is possibly changed and this affects INH binding. Trp321, however, does not seem to affect the initial step leading to the formation of the M-Y-W adduct radical during the catalytic turnover of H_2O_2, evidenced by the fact that the spin concentration of the narrow doublet at the early time point in the mutant is similar to that in WT. Trp321, therefore, has no significant effect on the catalase reaction mechanism in KatG discussed in the previous chapter.

However, the RFQ-EPR spectra show that Trp321 seems to play a role in the formation of other (Tyr or Trp) radicals when KatG is turned over with alkyl peroxide evidenced by the multiple-signal EPR spectrum obtained upon reaction of the mutant enzyme with PAA which contains a high contribution from a peroxyl radical. Nevertheless, Trp321 is unlikely to be the sole requirement for the radical giving rise to the wide doublet signal in WT KatG as a small amount of this signal is found in KatG[W321F] mutant. Thus, unlike the EPR observations for some Tyr and Trp mutants studied in this chapter where $R_2COO^{\bullet}$ is the only species detected while the wide doublet signal is completely absent, the EPR spectrum of KatG[W321F] mixed with PAA shows that Trp321 could be part of a radical network but the radical can find an alternative path to bypass the broken step caused by the replacement at the Trp321 position.

When KatG is turned over with H_2O_2, the M-Y-W adduct radical is the catalytically competent species that develops immediately from the first oxidized heme species and stays around during the reaction cycle as a function of the hydrogen peroxide availability. Upon turnover of alkyl peroxides such as PAA, optical results show that $Fe(IV)=O(Por^{\pi+\bullet})$ is likely to be the first oxidized heme species that forms in KatG which, then, oxidizes a neighboring tyrosine or tryptophan residue and initiates a ‘slow’ radical transfer process that involves a number of Tyr and Trp residues leading to the site giving the wide doublet signal. Yet, optical and EPR (RFQ and low temperature) data shown in this chapter did not completely rule out the possibility of coexistence of some $Fe(IV)=O(Trp_{321}{}^{+\bullet})$ species (analogous to CCP Compound I) along with $Fe(IV)=O(Por^{\pi+\bullet})$ as the hypervalent heme species formed during the turnover of PAA under certain conditions, as suggested by others [65].

At the end of Part I of this thesis, from the experimental results obtained using EPR and optical methods shown in this chapter, and based on previous results, the peroxidase reaction mechanism in KatG can be proposed to occur via the formation of a ferryl heme:porphyrin π-cation radical species upon oxidation of resting enzyme by alkyl peroxide (Rxn. 1, below). This is followed by oxidation of a redox-active residue in the vicinity of the heme group (Rxn. 2) different from the M-Y-W adduct. In the absence of an electron donor (peroxidase substrate), a slow step involving the oxidation of several Tyr and Trp residues starts and leads to accumulation of radicals (Rxn. 3). When the radical reaches the surface of the protein, recombination can take place, destroying the native enzyme structure by forming cross-links and bringing the peroxidase cycle to completion (Rxn. 4).

$$\mathrm{Fe(III)(Por)} + \mathrm{ROOH} \rightarrow \mathrm{Fe(IV){=}O(Por^{\pi+\bullet})(TyrX,TrpX)} + \mathrm{ROH} \tag{1}$$

$$\mathrm{Fe(IV){=}O(Por^{\pi+\bullet})(TyrX,TrpX)} \rightarrow \mathrm{Fe(IV){=}O(Por)(TyrX/TrpX)^{\bullet}} \tag{2}$$

$$\mathrm{Fe(IV){=}O(Por)(TyrX,TrpX)^{\bullet}} \rightarrow \mathrm{Fe(III)(Por)(TyrX/TrpX)^{\bullet}(TyrY/TrpY)^{\bullet}} \tag{3}$$

$$\mathrm{Fe(III)(Por)(TyrZ/TrpZ)^{\bullet}} + \mathrm{Fe(III)(Por)(TyrZ/TrpZ)^{\bullet}} \rightarrow \mathrm{(KatG)Tyr{-}Tyr(KatG)} \tag{4}$$

While most of the steps shown in the above scheme are based upon experimental evidence combining EPR, optical and stopped-flow, DFT, and oligomerization observations, some of them (EPR spectrum of $\mathrm{Fe(IV){=}O(Por^{\pi+\bullet})}$) have not been experimentally confirmed yet. Therefore, the peroxidase reaction mechanism in KatG awaits further experiments and new approaches in order to be validated.

PART II

Application of EPR and optical spectroscopy to study the chemical and paramagnetic properties of melanin in the melanized fungus *Cryptococcus neoformans* in response to high-dose ionizing radiation.

Chapter 4: The paramagnetic and chemical properties of melanin in the fungus *Cryptococcus neoformans* are resistant to major modification by radiation-induced radicals.

The second part of this thesis describes work done in collaboration with medical scientists at the Albert Einstein College of Medicine (AECOM, Bronx, NY), concerning the properties of the important biological molecule, melanin, whose structure contains a stable radical, and its potential as a radioprotective material for medical and other uses.

EPR and optical spectroscopy were used to obtain experimental evidence showing, for the first time, that melanin in live fungal cells exhibits remarkable chemical and structural stabilities towards lethal doses of ionizing radiation and works as a protecting barrier for cells from radiation-induced hydroxyl radicals.

The results and data presented in this chapter are reproduced, with permission, from the article: "Protection of Melanized *Cryptococcus Neoformans* from Lethal Dose Gamma Irradiation Involves Changes in Melanin's Chemical Structure and Paramagnetism." Khajo, A., Bryan, R. A., Friedman, M., Burger, R. M., Levitsky, Y., Casadevall, A., Magliozzo, R. S., and Dadachova, E. (2011) *PLoS ONE* 6(9), e25092. Copyright © 2011 Public Library of Science [79].

All the chemical analyses, optical experiments and EPR measurements presented in this chapter were performed by the author at Brooklyn College, and the cell-based experiments and irradiation were done at AECOM.

4.1 Introduction to melanin radicals.

Melanins are complex polymers, formed by oxidation of various precursors, including tyrosine, tryptophan, and L-3,4-dihydroxyphenylalanine (L-DOPA). They are pigments ubiquitous in nature, found in most organisms from all biological kingdoms. The most common form of biological melanin is eumelanin, a brown-black polymer of dihydroxyindole carboxylic acids, and their reduced forms. Figure 4.1 shows an accepted structure for the subunits of eumelanin produced from L-DOPA [80].

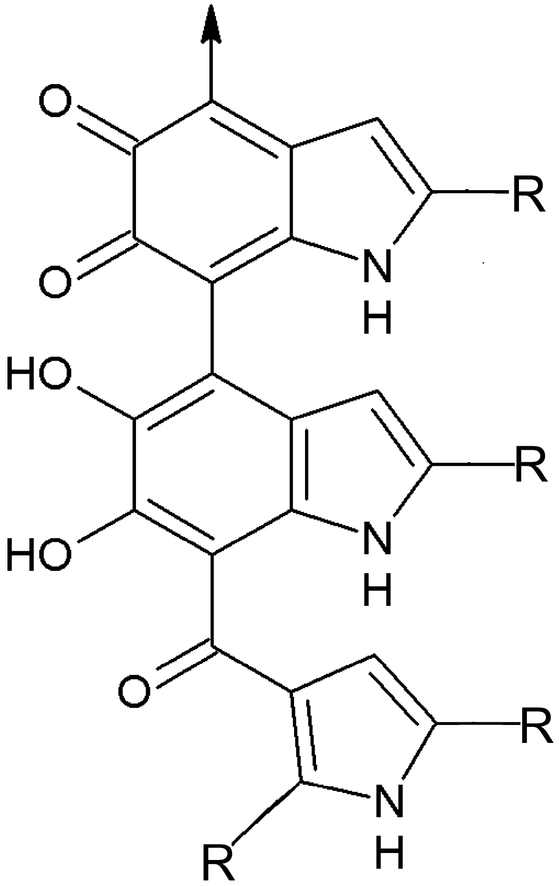

Figure 4.1. Structure of eumelanin oligomer. (Adapted from Wakamatsu [80]). R = H, COOH, or other subunits.

Chemical studies on melanins have been exceptionally difficult due to their insolubility and resistance to hydrolysis, and further complicated by their irregularity. However, the photochemical properties of melanins make them excellent photoprotectants. This is because they efficiently absorb harmful UV-radiation and transform the energy into heat. This occurs by means of a process called ‘ultrafast internal conversion’ which enables melanin to dissipate more than 99.9% of the absorbed UV radiation as heat [81]. This prevents the DNA damage that is responsible for the formation of melanoma and other skin cancers. In addition to protection from damage by UVC light [82-83], melanins reduce oxidative stress in microorganisms [84], and participates in energy transduction and electron transfer processes [85-88]. Recent evidence suggested that melanins in live *Cryptococcus neoformans* (*C. neoformans*) cells can function both in energy transduction [89] and as radioprotectants [90]. Melanized microbial species are found in highly radioactive environments such as the cooling pools of nuclear reactors, in the stratosphere, in space stations, and inside the damaged nuclear reactor at Chernobyl [91]. The physics of interaction of ionizing radiation with synthetic eumelanins and pheomelanins (sulfur-containing) was described based on a variety of physico-chemical techniques including EPR spectroscopy [80, 90-91]. Dry melanins were reported to be resistant to high-dose (300 Gy), high-energy (^{137}Cs, 661.6 keV) irradiation because of an unchanged EPR signal characteristic of stable melanin radicals [92]. Other studies have reported that ionizing radiation could damage melanin [93-94], but no specific chemical analyses were presented, and this is among the gaps in knowledge the study presented in this chapter aimed to address.

Although the initial goal when this research started was to use EPR as the main tool to probe the structural integrity of eumelanin (by means of its radical stability) in fungi in response to high-dose ionizing radiation and prove its protective role in cells, eventual findings (especially chemical analyses) showed that, while the main assumption about protection was essentially valid, melanin was not completely inert to high radiation doses.

Since this study presented below is only about one form of melanin, eumelanin, the term ‘melanin’ used throughout this chapter refers to this species.

In this chapter, the effects of lethal doses of ionizing radiation on viable fungal cells were investigated under aerobic aqueous conditions. But which properties of melanin are the most meaningful to probe to demonstrate resistance to, or damage from, the effects of ionizing radiation? While radicals in melanin are among the intriguing features of its structure, the relationship between these radicals and functional properties of the polymer in living cells is not clearly understood. The radical population is known to depend on the position of the equilibrium between reduced and oxidized quinoid groups (Eq. 1),

$$Q + H_2Q \rightleftharpoons 2HQ^{-\bullet} \qquad \text{(Eq. 1)}$$

which shifts in response to pH, temperature, light, and other effectors [95-96] (Q denotes *o*-quinone, H_2Q is *o*-hydroquinone (quinol), and $HQ^{-\bullet}$ is an EPR detectable *o*-semiquinone radical). Melanin also interacts with metal ions, which can bind to *o*-semiquinone moieties in the polymer and shift the equilibrium [97] though the specific relevance of this property, and that of other effectors, to fungal physiology have not been established.

While much is unknown about the relationship between melanin's properties and its cellular function(s), there is convincing evidence that it serves as a radioprotective agent [90]. Therefore, it was considered important to investigate the effects of ionizing radiation on cellular melanin in aqueous environments.

In the present work, EPR, optical spectroscopy, and chemical analysis techniques were used to study the response of melanized *C. neoformans* cells to γ radiation. Among the key findings is that chemical modification of melanin could be detected in samples that showed an actual increase in melanin radical population after γ-irradiation. Thiobarbituric acid (TBA)-reactive aldehydes were released due to hydroxyl radical-induced modification of melanin. This novel observation may have implications in the physiology of melanized fungi like *C. neoformans* and even the physiology of other cell types.

4.2 EPR spectroscopy of C. neoformans cells.

All melanins contain a small population of semiquinone radicals within their structure and exhibit a characteristic EPR signal. Melanized *C. neoformans* cells collected from cultures grown in the presence of L-DOPA are black and exhibit an apparent singlet X-band EPR signal (77 K) at $g = 2.0030$ with a linewidth (peak to trough) of 5 Gauss (Figure 4.2) similar to that of synthetic eumelanin [97-98].

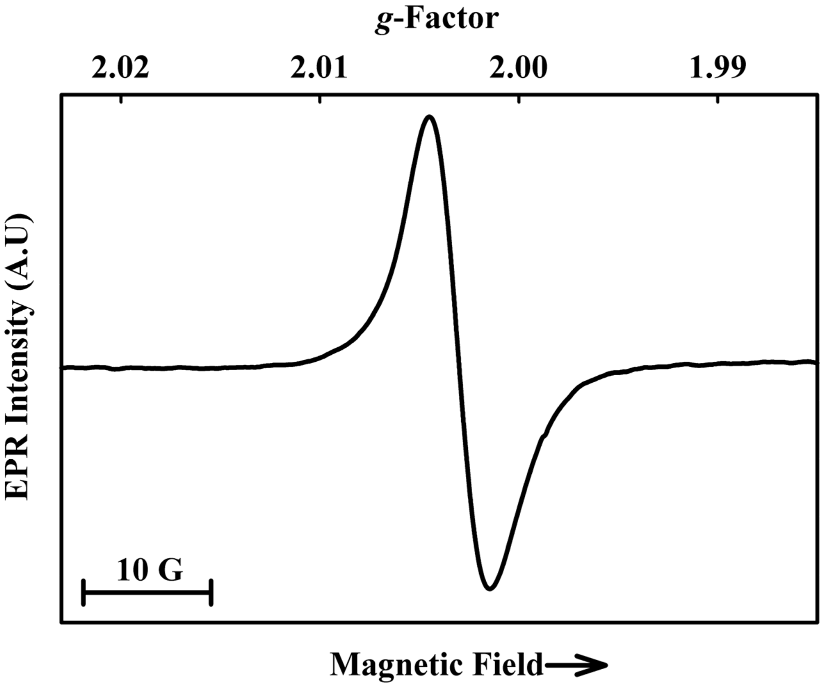

Figure 4.2. X-band EPR spectrum of melanized *C. neoformans* cells (1.9×10^9 cells/mL). Experimental conditions: T = 77 K; microwave frequency = 9.49 GHz; microwave power = 0.1 mW; modulation amplitude = 1 G; average of 3 scans.

Comparison of the signal intensity to that from a suspension of melanized-cell ghosts (shells prepared from *C. neoformans* cells composed of essentially only melanin) suggests a melanin concentration of ~3.0 mg/mL in typical cell samples. The radical concentration in melanins is known to respond to effectors including pH, temperature, and light, which alter the equilibrium between reduced and oxidized quinoid species [95-96].

To investigate the properties of melanin in the cells and for later experiments in which the effects of γ-irradiation were monitored, the EPR signal from cell suspensions was recorded before and after illumination with high intensity light from a Xe lamp. This approach provides a probe of the integrity of melanin subunit structure, as it depends on the formation of new semiquinone radicals different from the intrinsic radicals.

Illumination of cells at room temperature caused an increase in EPR signal intensity (measured at 77 K) in a dose-dependent manner, reaching a maximum of 2.5-fold after ~60 min (Figure 4.3).

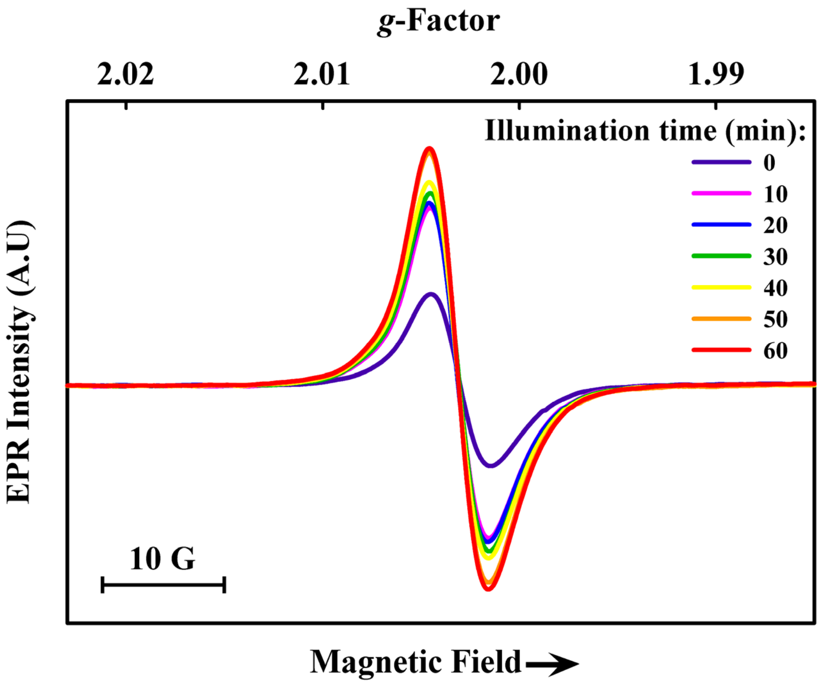

Figure 4.3. X-band EPR spectra of melanized *C. neoformans* cells after room temperature illumination with Xe-lamp for the time periods indicated. Experimental conditions: T = 77 K; microwave frequency = 9.49 GHz; microwave power = 0.1 mW; modulation amplitude = 1 G; average of 3 scans.

Illumination of frozen cell suspensions produced a 10-fold maximum increase in intensity after ~60 min (Figure 4.4).

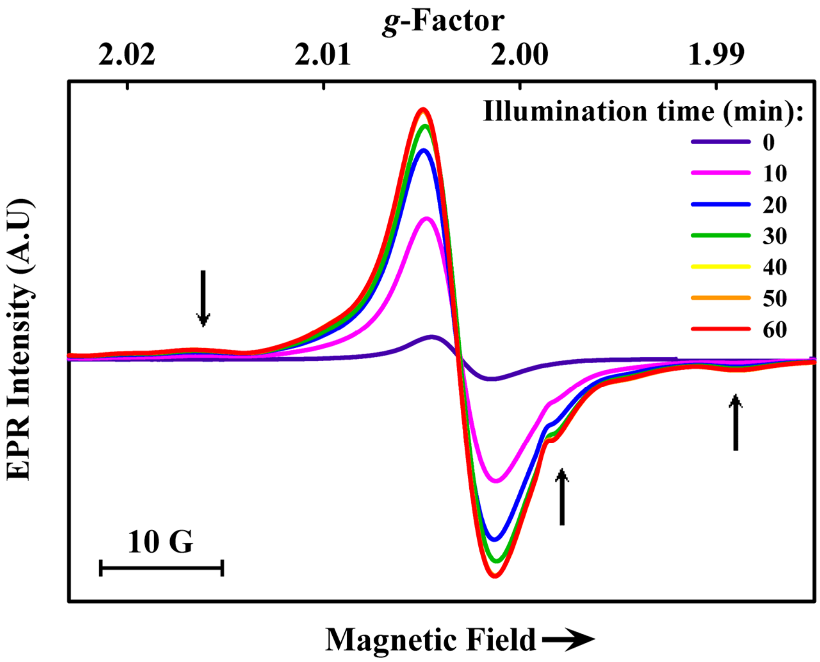

Figure 4.4. X-band EPR spectra of melanized *C. neoformans* cells after illumination with Xe-lamp at 77 K for the time periods indicated. Experimental conditions: T = 77 K; microwave frequency = 9.49 GHz; microwave power = 0.1 mW; modulation amplitude = 1 G; average of 3 scans.

Samples stored in the dark at 77 K retained the increased intensity for at least several days after illumination (not shown). In general, the response to light is consistent with the formation of semiquinones that persist briefly after illumination at room temperature, but which are trapped at 77 K. A small broadening of the signal (less than 1 Gauss) was also noted as previously reported [99] suggesting that the new radical sites are structurally distinct from the intrinsic radical sites. Non-melanized cell samples, which were pale in color, did not exhibit an EPR signal related to the typical melanin signal before or after Xe-lamp illumination (not shown).

In addition to the melanin radicals produced photochemically, illumination at 77 K produced other dilute paramagnetic species (arrows, Figure 4.4) in samples of both melanized and non-melanized cells. These features arise from photo-induced cellular radicals and paramagnetic centers in illuminated quartz (shoulder at *g* = 1.999) [100]. No difference was observed between melanized and non-melanized cells in these background signals.

The above survey of melanin radical behavior in whole *C. neoformans* cells provided the basis for interpretation of the effects of γ-irradiation.

*4.3 **EPR spectroscopy of gamma-irradiated C. neoformans cells.***

To examine the impact of ionizing radiation on the properties of melanin in *C. neoformans* cells, cell suspensions were irradiated at room temperature with 2 different doses of γ rays (10 and 30 min, ~120 and 360 Gy total, capable of killing about 50 and 80% of cells, respectively [91]) followed by freezing in liquid nitrogen within 1 min of removal from the beam. These radiation doses are in a range known from prior work to demonstrate significant protection of melanized *C. neoformans* cells relative to non-melanized cells [91]. Here, the γ-irradiation caused a 30% increase in melanin radical signal intensity measured at 77 K for the higher dose (Figure 4.5).

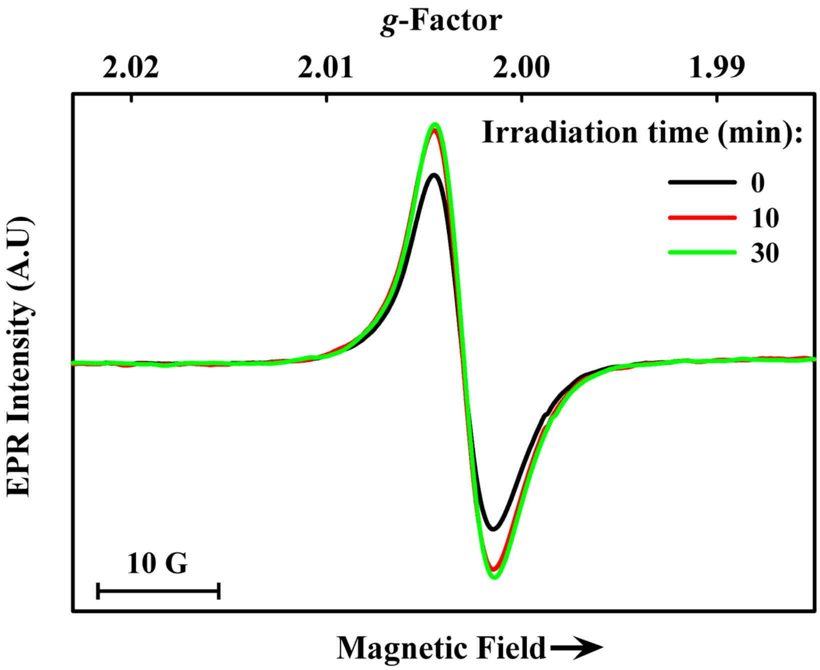

Figure 4.5. X-band EPR spectra of melanized *C. neoformans* cells after γ-irradiation at room temperature (11.94 Gy/min) for the time periods indicated. Experimental conditions: T = 77 K; microwave frequency = 9.49 GHz; microwave power = 0.1 mW; modulation amplitude = 1 G; average of 3 scans.

This gain in intensity, which could arise from a number of different processes, was reversed upon thawing and incubating the samples at room temperature (not shown) and was not explored further. The observations may be related to the previously reported enhancement in the ability of irradiated melanin to participate in electron transfer processes *in vitro* [89]. In non-melanized cell samples, no EPR signal related to the typical melanin signal was detected after γ-irradiation (not shown).

To probe for changes in the photoresponse of melanin, γ-irradiated melanized cell samples were subjected to illumination at 77 K as above. The EPR signal intensity again increased approximately 10-fold (Figure 4.6) compared to the intensity increase before irradiation (Figure 4.4) suggesting that melanin radical centers and the photoresponse processes that enhance radical population were not damaged during γ-irradiation at room temperature.

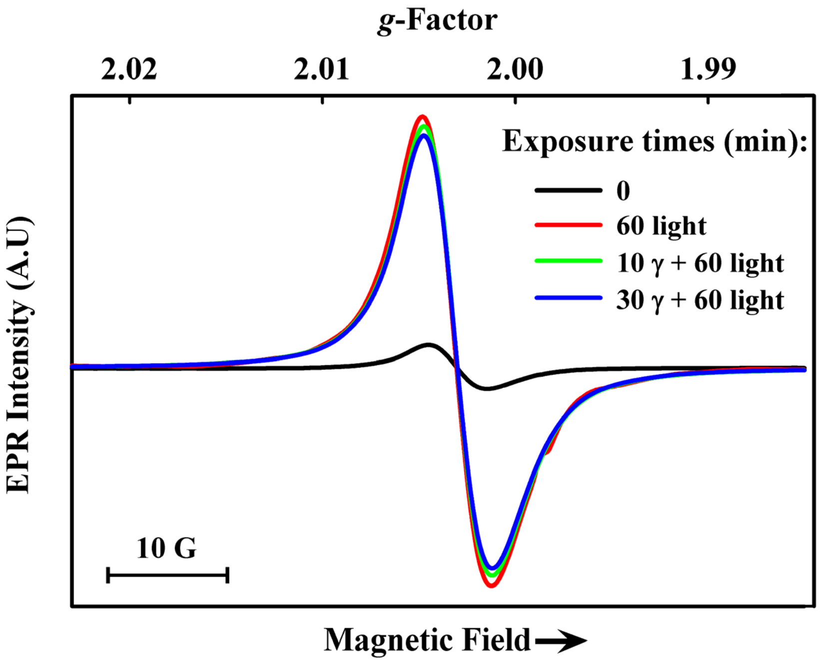

Figure 4.6. X-band EPR spectra of melanized *C. neoformans* cells after γ-irradiation at room temperature (11.94 Gy/min) for the indicated time periods followed by illumination with Xe-lamp after freezing at 77 K. Experimental conditions: T = 77 K; microwave frequency = 9.49 GHz; microwave power = 0.1 mW; modulation amplitude = 1 G; average of 3 scans.

To test for rapidly reversible changes occurring at room temperature that escaped detection in the EPR samples described above (which were frozen after removal from the radiation beam), melanized cells were γ-irradiated at 77 K. The observations here were complicated by new EPR signals that overlapped with and nearly completely masked the melanin radical signal, which is indicated by the arrow in Figure 4.7.

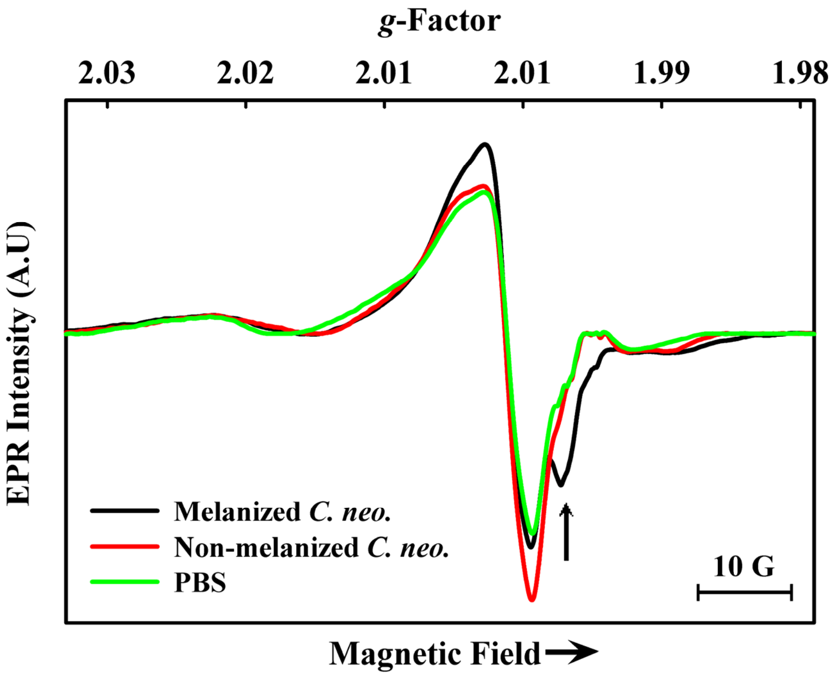

Figure 4.7. X-band EPR spectra of melanized *C. neoformans* cells, non-melanized *C. neoformans* cells, and PBS after 30-min γ-irradiation at 77 K (11.94 Gy/min). Experimental conditions: T = 77 K; microwave frequency = 9.49 GHz; microwave power = 0.1 mW; modulation amplitude = 1 G; average of 3 scans.

The broad new signals arise from hydroxyl and hydroperoxyl radicals produced in γ-irradiated ice, consistent with water radiolysis as their principal source [101-104]. Peroxyl radicals are formed by secondary processes following the decay of hydroxyl radicals, via the formation and build up of hydrogen peroxide or through the reaction of $^{\bullet}OH$ with H_2O [103]. These signals, which slowly decay by radical recombination [103] upon storage at 77 K or quickly decay at room temperature, were also seen with nearly equal intensities for γ-irradiated non-melanized cell suspensions and frozen PBS. Any of these new radicals for which EPR signals were detected, as well as other short-lived species produced during radiolysis of water such as e^{-}_{aq}, $CO_2^{-\bullet}$, $O_2^{-\bullet}$, $H^{\bullet}$ [93, 102] could contribute to damage to cells and melanin in our experiments and in environments where ionizing radiation is present.

In order to examine melanin radical signals in the samples that had been γ-irradiated, the non-melanin signals were allowed to decay by thawing the sample for 1 hr. The EPR spectrum after refreezing showed an intensity of the melanin radical signal was approximately 80% of its value before γ-irradiation (not shown).

Under anaerobic conditions, similar γ-irradiation experiments performed on melanized cells did not show any significant differences from the aerobic samples in either signal intensity or line shape. This observation rules out participation of oxygen in the processes occurring in these protocols.

To extend the analysis, Xe-lamp illumination was applied; a lower photoresponse was observed for the two γ-irradiated samples, compared with the 10-fold increase for the non-irradiated sample (Figure 4.8).

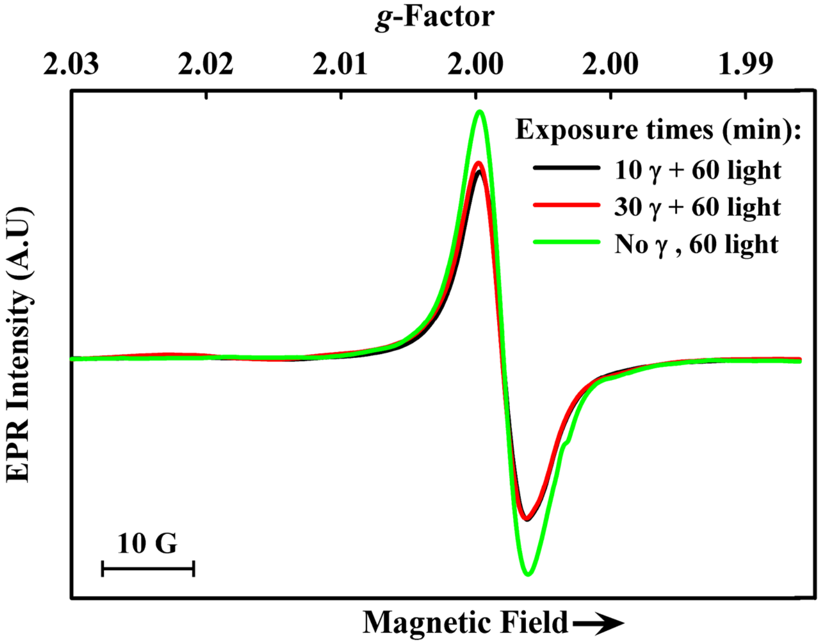

Figure 4.8. X-band EPR spectra of melanized *C. neoformans* cells γ-irradiated at 77 K (11.94 Gy/min) for the indicated time periods, stored frozen for 2 weeks, then illuminated with Xe-lamp at 77 K for 60 min. Experimental conditions: T = 77 K; microwave frequency = 9.49 GHz; microwave power = 0.1 mW; modulation amplitude = 1 G; average of 3 scans.

The small losses in the intrinsic radical population and in the photoresponse suggest that some damage had occurred to melanin, which may also have occurred in the room temperature protocol but was not detected by EPR. Therefore, a search for small molecule products was undertaken.

4.4 ***Soluble products released from γ-irradiated C. neoformans cells, melanized-cell ghosts, and synthetic melanin.***

An earlier report showed that radiolysis of melanin caused small changes in its broad and featureless optical absorption spectrum, but those observations did not provide specific structural insights [93]. If γ-irradiation causes chemical changes in melanin, soluble products might be found post irradiation. In fact, supernatants collected from γ-irradiated melanized (and non-melanized) *C. neoformans* cells, melanized-cell ghosts, and synthetic melanin all contained products exhibiting an absorption maximum near 263 nm (Figure 4.9).

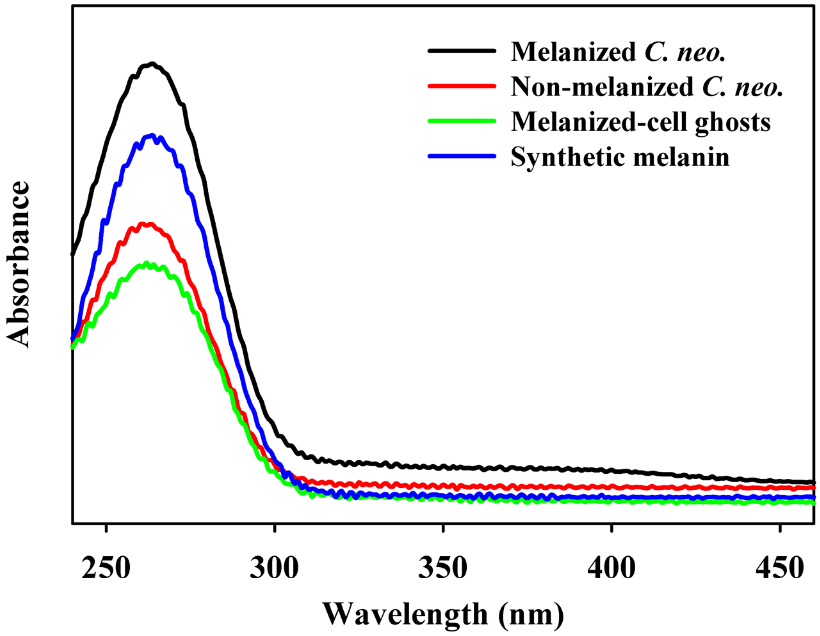

Figure 4.9. Optical spectra of supernatants collected from γ-irradiated samples of melanized *C. neoformans* cells, non-melanized *C. neoformans* cells, melanized-cell ghosts, and synthetic melanin, irradiated for 30 min at room temperature in PBS.

This observation provided evidence that damage to melanin had occurred and the soluble products have a UV-absorbing functional group in common with other cellular breakdown products.

Given that the γ-irradiated samples contained peroxyl radical detected by EPR and that melanin is digested by hydrogen peroxide, the soluble products in supernatants might have included the known principal peroxidation products, pyrrole-2,3-dicarboxylic acid (PDCA) and pyrrole-2,3,5-tricarboxylic acid (PTCA) [92]. However, the optical spectra of the supernatants were different from those of authentic PTCA and PDCA (Figure 4.10), and also different from ghost or synthetic melanin peroxidation products (which were most consistent with PDCA) (Figure 4.11) [105].

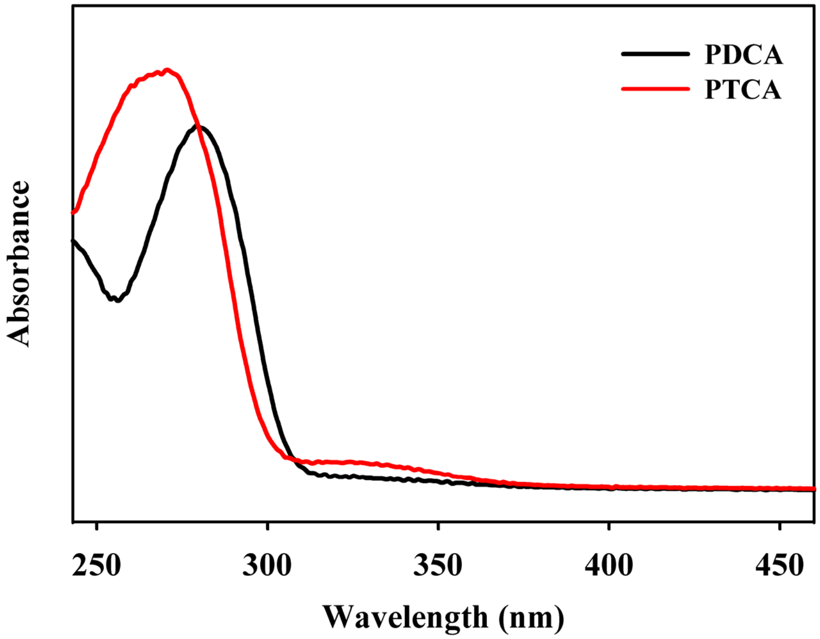

Figure 4.10. Optical spectra of PDCA and PTCA synthesized from indole precursors, according to [92].

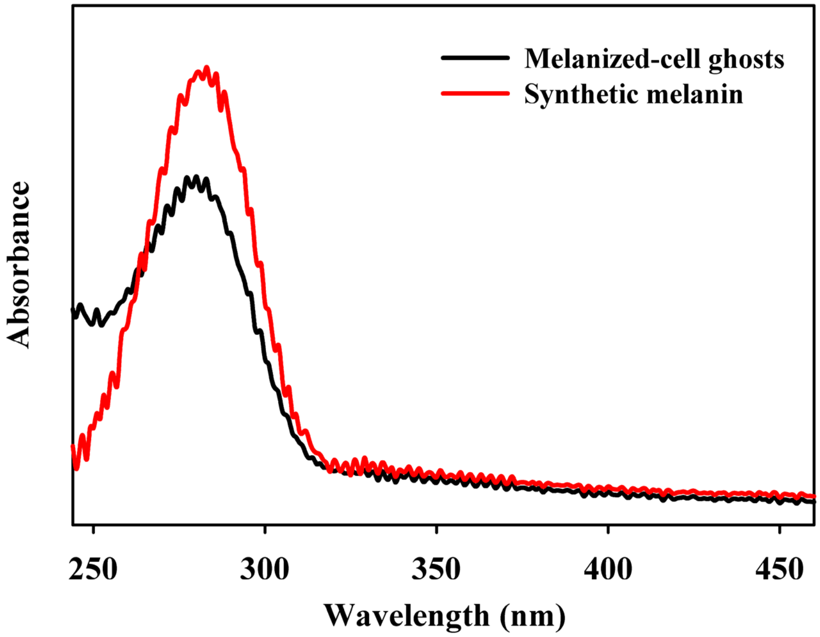

Figure 4.11. Optical spectra of supernatants collected from peroxide-treated melanized-cell ghosts and synthetic melanin.

Thin layer chromatography of supernatants collected from γ-irradiated melanized cells did not reveal detectable amounts of PDCA or PTCA (not shown).

Hydroxyl radical is among the abundant and potentially damaging species to which γ-irradiated cells were exposed. Therefore, an attempt to generate the soluble products described above was made using Fenton reaction chemistry ($Fe(II) + H_2O_2 \rightarrow Fe(III) + OH^- + {}^{\bullet}OH$, (Eq. 2)). Melanized and non-melanized cells and two sources of cell-free melanin were briefly incubated with Fenton reagents. The spectra of UV-absorbing material in supernatants collected from these samples (Figure 4.12) were similar to those from γ-irradiated samples, having λ_{max}~263 nm (Figure 4.9).

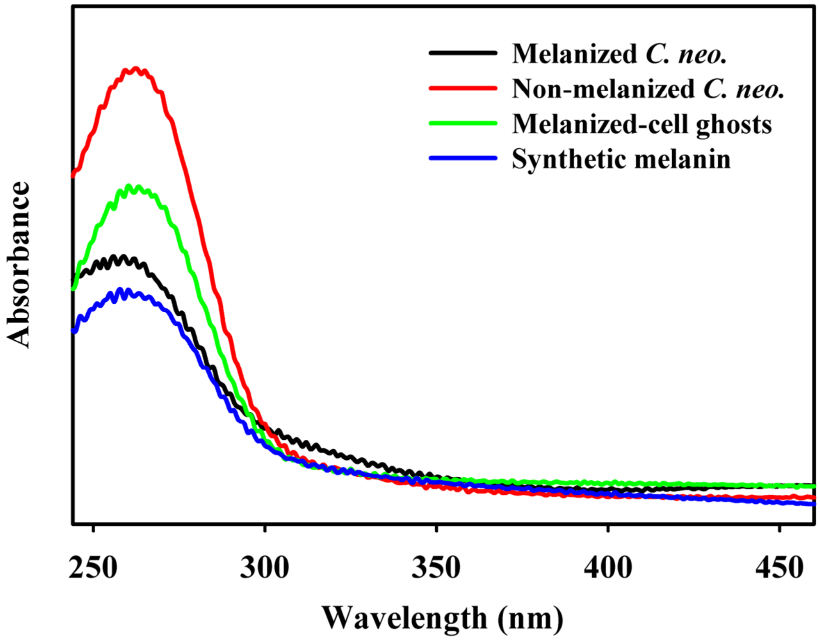

Figure 4.12. Optical spectra of supernatants collected from Fenton reagent-treated samples of melanized *C. neoformans* cells, non-melanized *C. neoformans* cells, melanized-cell ghosts, and synthetic melanin, incubated with Fe(II) and H_2O_2.

The yields increased with increasing concentration of iron and hydrogen peroxide (not shown). These results strongly suggest that the soluble products generated by γ-irradiation of melanized cells include some from hydroxyl radical damage to melanin, since •OH is the reactive species common to both the γ-irradiation and the Fenton reagent protocols.

4.5 ***Characterization of UV-absorbing products.***

Malondialdehyde (MDA) is among the expected soluble products from γ-irradiation of cells along with other 2-thiobarbituric acid (TBA)-reactive substances arising from damage to biomolecules [106-108]. No report of such products coming from melanin, however, could be found. Supernatants from each γ-irradiated and Fenton-reagent treated sample were tested for TBA reactivity, which is a widely-used method for determination of small molecule aldehydes [106-107]. A yellow chromophore (λ_{max}= 450 nm) was detected in all cases along with varying yields of another species with a λ_{max}= 532 nm typical of the MDA-TBA chromophore [106] (Figure 4.13). The chromophore with a λ_{max}= 450 nm has been reported for TBA adducts of saturated and unsaturated aldehydes [108-111].

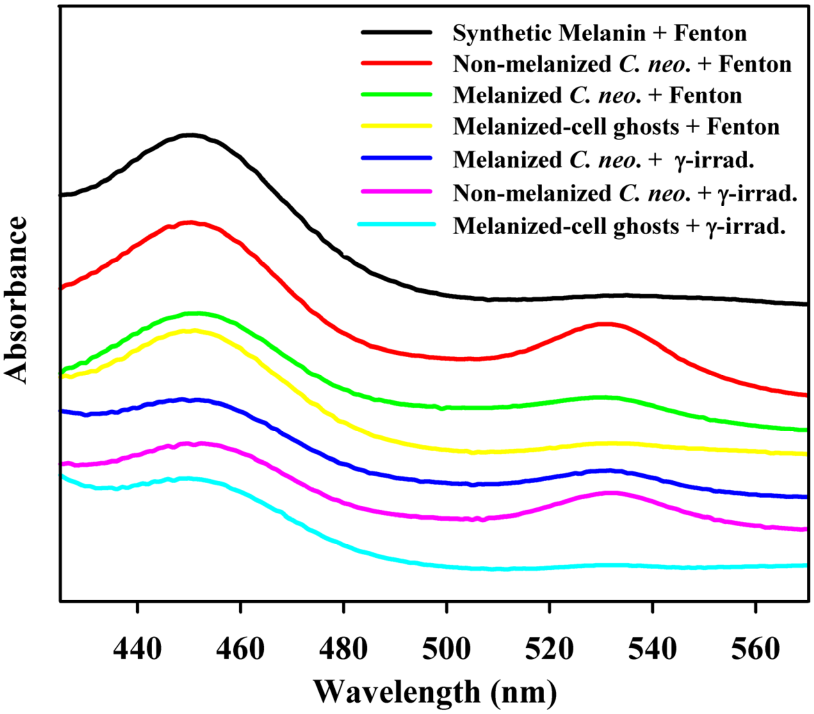

Figure 4.13. Optical spectra of TBA-adducts produced from supernatants collected from γ-irradiated samples. Spectra are offset for presentation.

The TBA-adducts produced from supernatants collected from γ-irradiated and Fenton-treated melanized-cell samples were very similar (Figure 4.13). For example, assuming that these adducts only produce TBA chromophores absorbing at 450 nm and/or 532 nm, a ratio of absorbances at these wavelengths should be constant for a similar aldehyde product profile. The A_{450}/A_{532} was approximately 3.5 for melanized cells exposed to radiation or Fenton reagents. A lower ratio (2.4) for the non-melanized cell products is consistent with an absence of melanin-derived aldehydes. Interestingly, the chromophores generated using supernatants from Fenton reagent-treated cell-free melanins had optical ratios of 12 or 16, for ghosts or synthetic melanin respectively. These observations confirm that the aldehydes derived from melanin decomposition principally produce a TBA-adduct chromophore with a λ_{max}= 450 nm.

4.6 ***Conclusion.***

The nature of the interaction of ionizing radiation with melanin is a relatively new area of research that has been poorly understood and rarely addressed in the literature. As melanin has potential usefulness for the design of new, nature-inspired radioprotective materials for a wide range of applications – from treatment and protection of cancer patients during radiation therapy to nuclear energy technology and space exploration – the analysis shown in this chapter provides important new insights.

A recent work reported on the remarkable stability of dry melanins towards ionizing radiation doses of 300 Gy [92]. To explain this phenomenon, it was suggested that the melanin polymer, studied in the form of dry *C. neoformans* cell ghosts, provides unique scattering and radical-scavenging properties due to its multiple stacked aromatic ring structures giving a complex conjugated π-electron system and offering protection from high energy radiation if a Compton recoil electron is not ejected from the solid phase but rather gradually loses energy while trapped in the π-electron system of the pigment, until it can recombine with an intrinsic radical. This process does not produce a net change in the melanin radical population upon re-equilibration of the reduced and oxidized sites (below) and would provide a mechanism for preventing direct damage to the chemical structure of melanin by γ-rays. Melanin damage by radicals in solution however, has not been explored in detail. Therefore, an investigation of the EPR properties and photoresponse of *C. neoformans* melanin in viable cells, including its response to γ-irradiation, was pursued here. Importantly, the high radiation doses applied are known to be more lethal to non-melanized cells, and thus explaining the role of melanin in protection of fungi was worthwhile investigating in more detail.

The results shown is this chapter demonstrated that EPR was useful to reveal alteration in melanin structure only under conditions where damage was enhanced while irradiated cells were frozen in the presence of the radicals produced during irradiation. The intrinsic radical population in melanized *C. neoformans* cells under resting conditions is governed by Eq. 1 [95-96], yet only a very small fraction of the melanin subunits exist in the semiquinone form. For example, quantitative EPR of a variety of melanins shows that the concentration of radicals (approximately 10^{18} spins/g) is accounted for by < 0.1% of the subunits bearing a semiquinone [92]. The photoinduction process, while it increases radical population according to the reactions in Eq. 3, still reports on the properties of a small fraction of melanin. Charge transfer reactions between hydroquinone and quinone in the triplet state of illuminated melanin yield two semiquinone radicals ($HQ^{-\bullet}$) by comproportionation [112].

$$Q\cdots H_2Q + h\nu \rightarrow [Q\cdots H_2Q]^S \rightarrow [Q\cdots H_2Q]^T \rightarrow 2HQ^{-\bullet} \qquad \text{(Eq. 3)}$$

Results show that a chemical analysis was more informative than EPR spectroscopy even when combined with illumination to probe melanin integrity, at least in the case of the physiologically relevant room temperature irradiations. More extensive analyses are required for a complete description of the phenomena and to reveal any mechanistic coupling between radical behavior and chemical reactivity. It is very clear that hydroxyl radical attack on susceptible sites in melanin subunits leads to C-C bond cleavage and the release of low molecular weight aldehydes.

Since melanized cells are not impervious to the effects of ionizing radiation in solution, a new question arises: Is melanin a sacrificial component of the cell surface architecture? The avirulent, acapsular *C. neoformans* cells used here lack an exterior polysaccharide coat but have an intact cell wall and cell membranes and, when melanized, contain an array of melanin particles in porous concentric layers within the cell wall [113]. A dense arrangement of these particles near the cell surface affords a protective physical barrier and was proposed to provide radiation protection by a combination of Compton scattering, energy attenuation of photons, and quenching of free electrons and free radicals generated by radiolysis of water [89, 92]. Most importantly, modifications of melanin structure can be metabolically repaired in viable fungal cells [113]. This supports the idea that melanin is a protective yet partially sacrificial cell wall component that may be damaged but still prevent cell death.

It is now clear that ionizing radiation leads to partial melanin damage/fragmentation in aqueous environments, which produces TBA-reactive substances related to those produced from other cellular components. A thorough understanding of the chemistry of melanin interactions with hydroxyl radical would help explain radiation resistance as a biological function of melanin. Sacrificial degradation of melanin should be included as a factor contributing to its radioprotective properties in cells.

Appendix A

Experimental procedures

Chapter 2

Chemicals and reagents. H_2O_2, PAA, CPBA, INH, *o*-dianisidine, and all the other chemicals were purchased from Sigma and were of the highest purity available. INH was recrystallized from methanol and stored at 4 °C. PAA (32%) was diluted to 10 mM in potassium phosphate buffer pH 7.2 and was incubated with 780 units/mL bovine liver catalase (BLC, Roche Applied Science) for 4 h at 37 °C, followed by removal of the enzyme by ultrafiltration, to remove hydrogen peroxide that interfered with the EPR and optical experiments. In some PAA treatments, KatG itself was used to remove H_2O_2 because it is more robust than BLC. After these preparations, PAA was stored at -80 °C in small aliquots. H_2O_2 was removed from *m*-CPBA by washing the crystals several times with 20 mM sodium borate buffer pH 8.5 and deionized water, using gravity filtration to collect the crystals. Solutions of *m*-CPBA for EPR experiments were prepared by dissolving the solid in 30% acetone in deionized water.

Construction, expression, and purification of wild-type and mutant KatG enzymes. The plasmid pKAT II was used as an overexpression vector for KatG as well as a mutagenesis template. *Escherichia coli* strain UM262 was used for overexpression as published previously [44]. UM262 and pKAT II were both gifts from Stewart Cole (Institut Pasteur, Paris). Mutagenesis was performed using the QuickChange II site-directed mutagenesis kit from Stratagene (La Jolla, CA). The pairs of complementary primers (synthesized and purified by Operon Biotechnologies, Inc.) were designed to introduce the desired mutations. Mutagenesis was performed according to the manufacturer's protocol and the reaction products were transformed into the *E. coli* XL1-Blue strain for selection purposes. The presence of the mutated codons in the *katG* gene was confirmed by DNA sequencing (Gene Wiz, Inc.) and the mutated plasmid was electroporated into *E. coli* strain UM262 for protein overexpression. The heme precursor δ-aminolevulinic acid was added to culture media to promote formation of holoenzyme [43]. Recombinant WT KatG and mutants were purified in potassium phosphate buffer, pH 7.2. The purified enzymes had an optical purity ratio (A_{405}/A_{280}) of ~0.45–0.50. Mutagenesis experiments were carried out according to published protocol [44] for which the author acknowledges the contributions from Dr. X. Zhao and Dr. J. Suarez.

Catalase- and peroxidase-specific activities of KatG. Catalase and peroxidase activities of KatG were determined at 25 °C in 20 mM potassium phosphate buffer, pH 7.2 (catalase), and 50 mM sodium acetate buffer, pH 5.5 (peroxidase). Catalase activity was assayed spectrophotometrically following the decrease in absorbance at 240 nm [44]. One unit of catalase activity is defined as the amount of enzyme catalyzing the decomposition of 1 μmol of H_2O_2 per min at 25 °C. Peroxidase activity was also measured spectrophotometrically using tert-butyl hydroperoxide and *o*-dianisidine, following color development at 460 nm [44]. One unit of peroxidase activity is defined as the amount of enzyme that catalyzes the oxidation of 1 μmol of *o*-dianisidine per min at 25 °C. Spectrophotometric measurements were obtained using an NT14 UV-Vis spectrophotometer interfaced to a personal computer (Aviv Associates, Lakewood, NJ).

Isotope-labeling of tyrosine residues in KatG. Isotopically labeled KatG enzymes were over-expressed in *E. coli* BL21, grown in M9 minimal medium supplemented with $MnSO_4 \bullet H_2O$ (0.1

mg/L), $ZnCl_2$ (0.5 mg/L), and $FeCl_2 \bullet 4H_2O$ (10 mg/L). Deuterated tyrosine (β-d_2-Tyr, or 3,5-d_2-Tyr, 98% isotopic purity) purchased from Cambridge Isotope Laboratories, Inc. (Cambridge, MA) was added to the culture (47.6 mg/L) 2 hours before induction. The isotope-labeling work was performed by Dr. X. Zhao according to published procedure [43]. The subsequent purification of deuterated KatG followed the same procedure employed for unlabeled enzymes.

Electron paramagnetic resonance spectroscopy. EPR spectra were recorded on a Bruker E500 ElexSys EPR spectrometer operating at X-band using an ER4122SHQE resonator cavity. Data acquisition and manipulation was performed using *XeprView* and *WinEPR* software (Bruker). EPR simulations were performed using *Simfonia* software (Bruker). Spectra were recorded at 77 K using an immersion quartz finger Dewar held in the resonator cavity. Experimental parameters used to acquire the EPR spectra were as follows: modulation amplitude, 1 G; microwave power, 0.1 mW; modulation frequency, 100 kHz; microwave frequency, 9.445 $\pm$ 0.05 GHz; sweep time, 327 s; conversion time, 335 ms; time constant, 1310 ms; number of scans, 9 (or 6). For quantitative EPR analysis, signal intensity was calculated by double integration of first-derivative EPR signals and spin concentration was based on the intensity of standards prepared from TEMPOL (4-hydroxy-2,2,6,6-tetramethylpiperidine-N-oxyl) dissolved in ethanol:acetone (24:1,vol:vol), or $CuSO_4$ prepared from solid 99% purity copper sulfate pentahydrate dissolved in $HCl/NaClO_4$. These two standards in frozen solutions gave values within 5% of one another for spectra collected at 77 K. The TEMPOL radical concentration was determined from its optical absorbance using $\varepsilon_{428\ nm}= 13.2\ M^{-1}\cdot cm^{-1}$ [114].

Rapid freeze-quench methods. The RFQ-EPR samples were prepared using an Update Instrument, Inc. Model 1000 chemical freeze-quench apparatus. The RFQ-EPR methodology has been published elsewhere [42-43, 63]. Briefly, the enzyme and peroxide solutions were mixed at room temperature in a 1:1 volume ratio, and the mixture was incubated for the indicated time periods determined by the length of the reactor tubes, or for longer periods by programming a delay interval and then sprayed into a funnel attached to an EPR tube submerged in an isopentane bath held at approximately -130 °C. The frozen powder was packed into precision bore EPR tubes, and the packed sample, which retains isopentane, was frozen in liquid nitrogen. For the reaction of KatG with hydrogen peroxide, samples were prepared in 20 mM potassium phosphate buffer, pH 7.2, or in 20 mM sodium borate buffer, pH 8.5, by mixing protein solution (~100 μM in heme) with 1000-fold (or other amount) molar excess (over heme) of H_2O_2. For the reaction of KatG with peroxyacetic acid, samples were prepared in 20 mM potassium phosphate buffer, pH 7.2, by mixing protein solution (~100 μM) with the desired molar excess of PAA. PAA solutions were freshly prepared before each experiment from H_2O_2-free stock solutions stored at -80 °C. The estimation of spin concentration in rapid freeze-quenched samples included application of a packing factor of ~0.35 to account for sample dilution by isopentane. This was determined by using the RFQ method to mix equal volumes of the EPR standard (TEMPOL or $CuSO_4$) of known concentration, followed by freezing and packing the sample under the same experimental conditions and recording the EPR spectrum. By comparing the intensity (double integration) of the EPR spectra from the RFQ and manually-frozen samples, the above isopentane dilution factor was obtained.

The foaming of solutions because of the rapid evolution of oxygen gas in some samples of KatG mixed with H_2O_2 leads to further dilution by an additional amount, but no correction of EPR signal intensity was made for this factor.

Kinetic measurements of H_2O_2 consumption. The experiments for evaluating the kinetics of H_2O_2 consumption were performed (by the author and Dr. X. Zhao) on the stopped-flow spectrophotometer (HiTech Scientific model SF-61DX2) using final enzyme and H_2O_2 concentrations of 50 μM and 50 mM, respectively. The absorbance of H_2O_2 at 240 nm was monitored for the desired time period. Due to strong absorbance caused by the high concentrations of enzyme and peroxide present in these samples, a 1.5-mm light path flow-cell was used.

Chapter 3

Enzyme kinetics measurements. Data acquisition and analyses were performed using the Kinet-Studio software package along with the HiTech Scientific model SF-61DX2 stopped-flow apparatus. All reactions were carried out at 25 °C in 20 mM potassium phosphate buffer, pH 7.2, or in 20 mM sodium borate buffer, pH 8.5. For calculation of second order rates for conversion of resting enzyme into the first intermediate characteristic of ferryl heme, the change in absorbance in the Soret region upon reaction with varying concentrations of PAA was followed for 2 sec, and data were fit to a single exponential decay function. Observed rates (k_{obs}) were used to calculate second order rate constants from the plot of k_{obs} *vs.* PAA concentration.

Double mixing stopped-flow experiments were performed as previously reported [59] to follow the reaction of the first hypervalent heme species, after it was pre-formed with a small excess of PAA, with INH as reducing substrate added in the second mixing step after a 2-sec delay.

IN-NAD adduct formation. The rate of IN-NAD adduct generation catalyzed by KatG[W321F] was examined in a spectrophotometric assay as a function of INH concentration according to a previously published method [21]. In this method, KatG (0.5 μM), NAD^+ (50 μM), glucose (5 mM), and glucose oxidase (10 milliunits/mL) were incubated in the presence of varying amounts of INH (10, 25, 100, 250, 500, 1000, and 3000 μM), and the increase in absorbance at 326 nm due to IN-NAD adduct formation ($\varepsilon_{326\ nm}$= 6900 $M^{-1}.cm^{-1}$) [43] was recorded for 10 min. The reference cuvette contained all components except NAD^+ to correct for the background.

Low-temperature EPR spectroscopy. EPR spectra were recorded at temperatures ~4.8 K on a Bruker E500 ElexSys EPR spectrometer operating at X-band using an Oxford Spectrostat continuous flow cryostat and ITC503 temperature controller. Data acquisition and manipulation were performed using *XeprView* and *WinEPR* software (Bruker). EPR samples of WT KatG and KatG[W321F] were prepared by mixing equal volumes of 200 μM enzyme solution in 20 mM potassium phosphate buffer at pH 7.2 and 3 mM PAA manually in a test tube followed by transferring the mixture immediately into 4 mm (3 mm i.d) precision bore quartz EPR tubes and immersion freezing in liquid nitrogen. Experimental parameters were as follows: modulation amplitude, 4 G; microwave power, 1mW; modulation frequency, 100 kHz; microwave frequency, 9.39 GHz; scan rate, 14.9 G/s; conversion time, 327 ms; time constant, 1310 ms.

Spectra from WT KatG and KatG[W321F] samples were obtained under identical instrumental conditions.

Chapter 4

***Cryptococcus neoformans* cell growth**. The strain used for these experiments was cap67, an acapsular, avirulent strain of *C. neoformans* derived from the serotype D strain B3501 [115]. This strain was used because it is safe to handle and because γ radiation would remove capsular material from wild-type cells [116] and thereby confound the analyses. The cells were grown and collected in collaborators' laboratory at Albert Einstein College of Medicine according to published procedure [117] for 20 days in minimal medium (29.4 mM KH_2PO_4, 10 mM $MgSO_4$, 13 mM glycine, 15 mM D-glucose, and 3 μM thiamine) supplemented or not with 1 mM L-DOPA, in the dark at room temperature (23 °C), shaking at 150 rpm. Only those cells grown in the presence of L-DOPA become melanized; thus, cells grown in the absence of L-DOPA provide minimally perturbed control cells. The cells were harvested by diluting the cultures with phosphate-buffered saline (PBS) pH 5.9 to improve pelleting, followed by centrifugation at 1300 × g for 10 min, then washing twice with PBS. The cells were resuspended in PBS and the cell concentration was adjusted to approximately 2×10^9 per mL. Melanized-cell ghosts, which are shells composed of essentially only melanin, were prepared from melanized *C. neoformans* cells as previously described [118].

Electron paramagnetic resonance spectroscopy of *C. neoformans* cells. Suspensions of freshly harvested *C. neoformans* cells (1.9×10^9 melanized cells per mL or 1.2×10^9 non-melanized cells per mL) were placed in 4 mm precision-bore quartz EPR tubes and were frozen by immersion in liquid nitrogen immediately after filling the tubes. EPR spectra were recorded at 77 K using a Bruker E500 ElexSys EPR spectrometer operating at X-band with an ER4122SHQE resonator cavity in which samples were held in a quartz immersion finger Dewar filled with liquid nitrogen. Data acquisition and manipulation was performed using *XeprView* and *WinEPR* software (Bruker). Experimental parameters used to acquire the EPR spectra were as follows: modulation amplitude, 1 G; microwave power, 0.1 mW; modulation frequency, 100 kHz; microwave frequency, 9.485 ± 0.005 GHz; scan rate, 1.2 G/s; conversion time, 163 ms; time constant, 1310 ms; number of scans averaged, 3. All spectra were obtained under identical instrumental conditions.

Xenon-lamp illumination of *C. neoformans* cells. Illumination of cell suspensions was carried out using a 75-watt xenon lamp (L2194-02, Hamamatsu Photonics, Japan). Light was focused on the samples in quartz EPR tubes (~0.8 cm^2 cross-section) at room temperature. Each sample received ~7 microeinsteins per second for the desired illumination times. For 77 K illumination, frozen samples in quartz EPR tubes were held in a liquid nitrogen-filled quartz finger Dewar.

Gamma-irradiation and Fenton-reagent treatment of *C. neoformans* cells and cell-free melanins. Cell suspensions (6.5×10^9 melanized cells/mL and 5.5×10^9 non-melanized cells/mL), melanized-cell ghosts (2 mg/mL), and L-DOPA synthetic melanin (2 mg/mL), each in PBS, were γ-irradiated at room temperature in microcentrifuge tubes; frozen cell samples were irradiated in quartz EPR tubes suspended in liquid nitrogen. The radiation dose was 11.94

Gy/min, delivered from a cesium-137 source in a Mark I irradiator (JL Shepherd and Associates, San Fernando, CA). The doses delivered for 10 and 30 minutes, ~120 and 360 Gy, respectively, are in a range lethal to 50-80% of the cell population [90]. Samples irradiated at room temperature were transferred to quartz EPR tubes and immediately frozen in liquid nitrogen. For control samples, microcentrifuge tubes or EPR tubes, filled with PBS alone, were similarly irradiated at room temperature or at 77 K. Gamma-irradiation of quartz EPR tubes generates paramagnetic centers [100, 119] and the background EPR spectrum (a narrow singlet with linewidth of ~3.5 Gauss at $g = 2.0004$) recorded from a tube filled with PBS and irradiated along with cell samples was subtracted from data where appropriate.

The Fenton reagent reactions were carried out using $Fe(NH_4)_2(SO_4)_2 \bullet 6H_2O$ and H_2O_2 in deionized water added to 800 μL of *C. neoformans* cells, melanized cell ghosts, or synthetic melanin each suspended in PBS at the concentrations given above, to give final Fe(II) and H_2O_2 concentrations of 5 mM and 10 mM respectively. Peroxide was added immediately after iron. Incubations were carried out at room temperature for 15 min, followed by centrifugation and recovery of supernatants.

Absorption spectroscopy of supernatants. Supernatants were collected from γ-irradiated cells and other samples by centrifugation to remove suspended material and were diluted 10-fold with PBS. Spectra were recorded using an NT14 UV-Vis spectrophotometer (Aviv Associates, Lakewood, NJ) interfaced to a personal computer. Spectra of supernatants from cells were normalized to correct for differences in cell concentration. Gamma-irradiated water or PBS collected from microcentrifuge tubes did not contain any detectable UV-absorbing material.

Peroxidation methods. Peroxide digestion of cell-free melanins was carried out as in [92] and [120] by suspending 1 mg of melanized-cell ghosts or synthetic melanin in 1.0 mL of deionized water. K_2CO_3 and H_2O_2 were added to give final concentrations of 0.1 M and 0.12%, followed by incubation at 100 °C for 20 min. After cooling of the reaction mixture, residual H_2O_2 was decomposed by adding 200 μL of 10% Na_2SO_3. The mixture was then acidified with 1.0 mL of dilute HCl. The resulting solution was centrifuged and the supernatant was used for optical measurements.

Pyrrole-2,3-dicarboxylic acid (PDCA) and pyrrole-2,3,5-tricarboxylic acid (PTCA) were synthesized from 5-hydroxyindole and 5-hydroxyindole-2-carboxylic acid, respectively, as in [92] and [120]. For optical spectra, 100 μg/mL PDCA and PTCA were dissolved in deionized water.

2-thiobarbituric acid-reaction methods. The TBA reactions were performed according to [121] using 200 μL of supernatants recovered from irradiated samples or Fenton reagent-treated samples, added to 800 μL of 31 mM TBA solution containing 1 mM Na_2EDTA in water, followed by incubation at 90 °C for 20 min. PBS was similarly treated with TBA/EDTA solution to establish a blank spectrum for subtraction from that of TBA adducts formed from the irradiated samples. For background correction in the case of Fenton reagent-treated samples, a TBA-reaction blank was prepared using 200 μL of a mixture containing 5 mM Fe(II) and 10 mM H_2O_2 in PBS that had been incubated for one hour, centrifuged to remove precipitated iron, and then treated as above with 800 μL of 31 mM TBA containing 5 mM EDTA. Optical spectra of the colored TBA adducts were recorded immediately after the samples had cooled to room temperature. Malondialdehyde (MDA) used as a standard was prepared from commercial malonaldehyde bis(dimethylacetal) (Fisher) according to [106].

Appendix B

Supplementary figures

Chapter 2

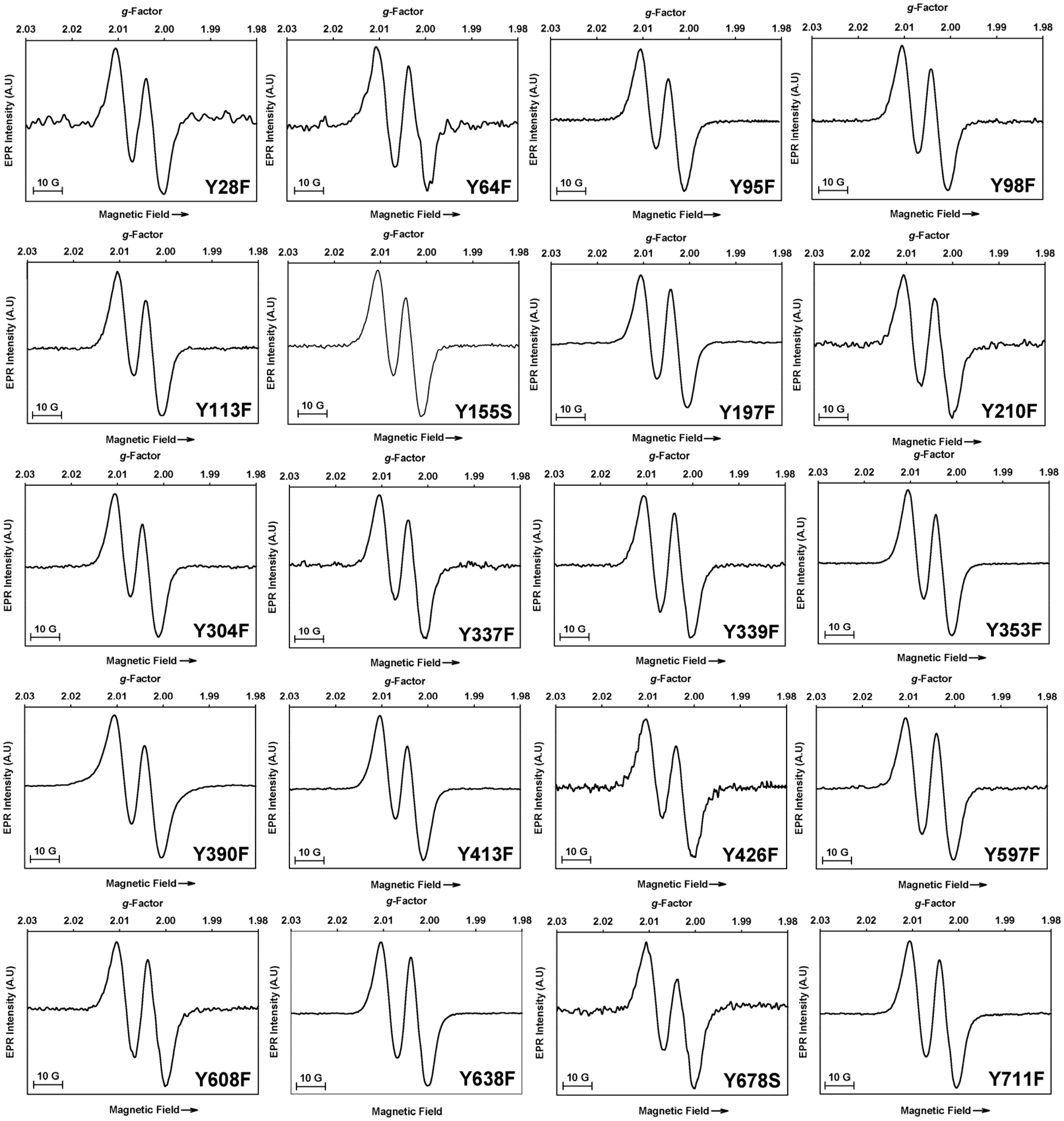

Figure 2.S1. X-band RFQ-EPR spectra of tyrosine mutants in KatG (50 µM) each treated with 8000-fold molar excess of H_2O_2 at pH 8.5 frozen manually within 1.5 sec after mixing. Experimental conditions: T = 77 K; microwave frequency = 9.45 GHz; microwave power = 0.1 mW; modulation amplitude = 1 G; average of 9 scans.

Chapter 3

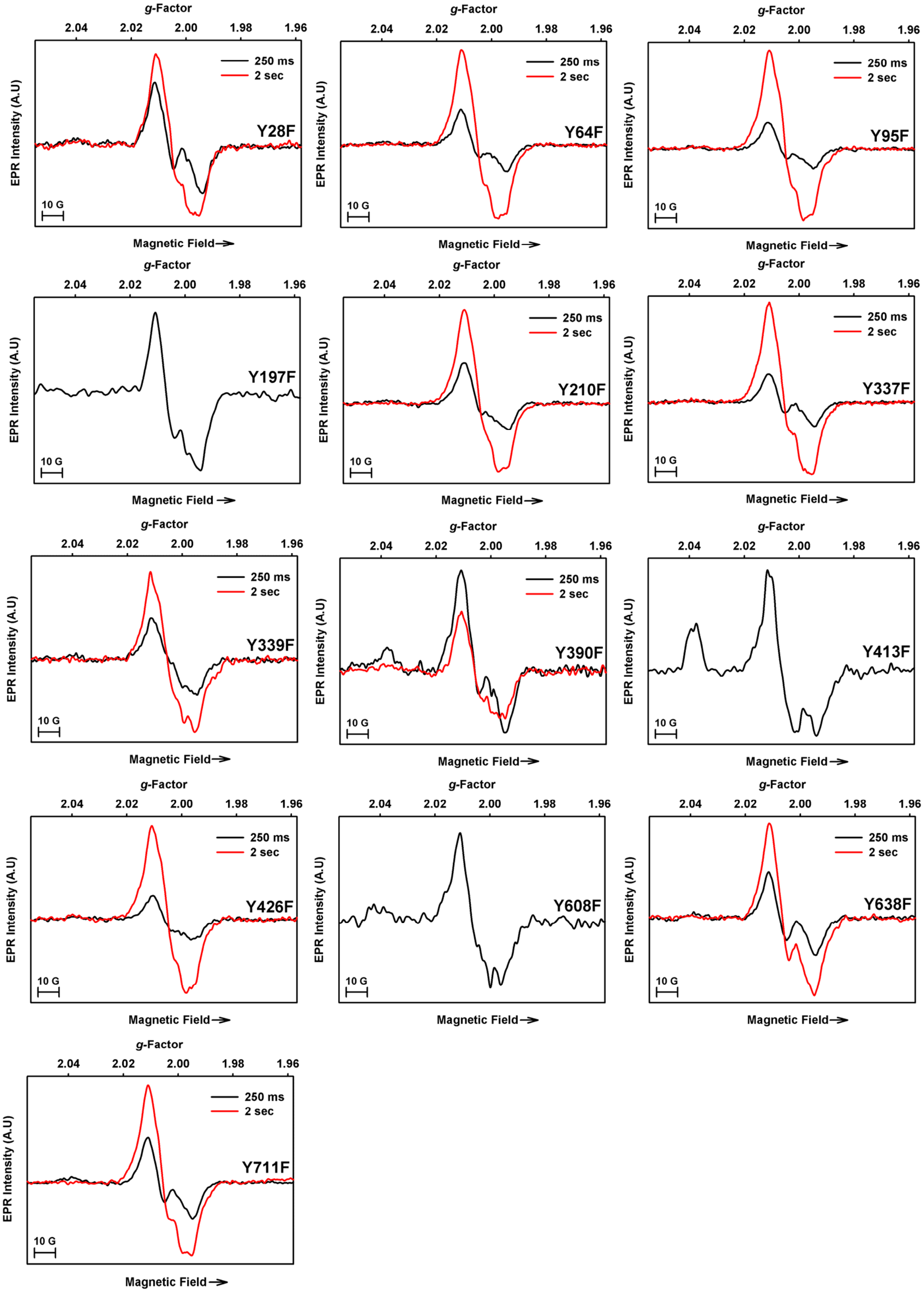

Figure 3.S1. X-band RFQ-EPR spectra of KatG[Y28F], [Y64F], [Y95F], [Y197F], [Y210F], [Y337F], [Y339F], [Y390F], [Y413F], [Y426F], [Y608F], [Y638F], and [Y711F] (50 µM) each treated with 3-fold molar excess of PAA at pH 7.2 frozen at the indicated times after mixing. Experimental conditions: T = 77 K; microwave frequency = 9.44 GHz; microwave power = 0.1 mW; modulation amplitude = 1 G; average of 6 scans.

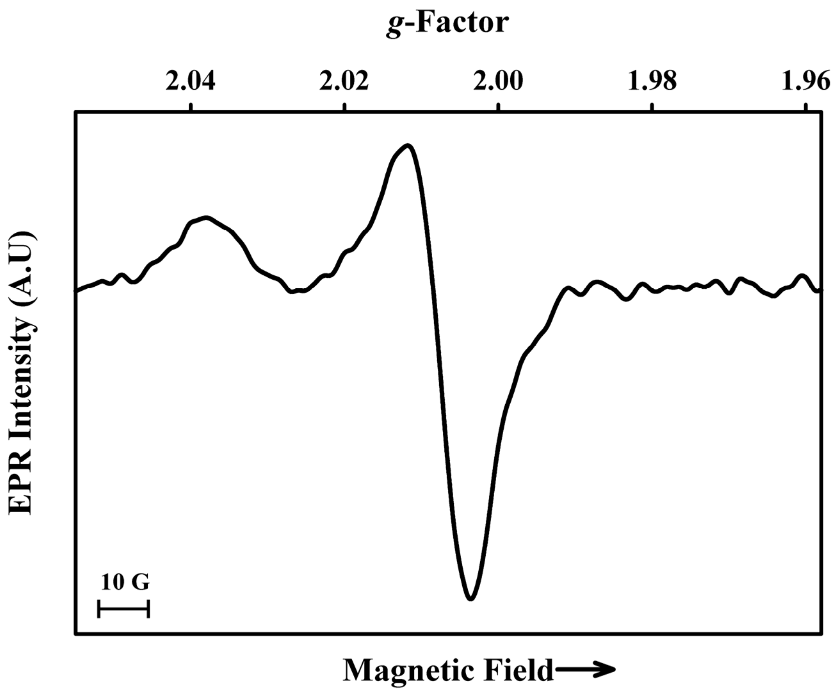

Figure 3S.2. X-band EPR spectrum of the peroxyl radical obtained from KatG[S315G] (50 µM) treated with 3-fold molar excess of PAA at pH 7.2 frozen ~1.5 sec after mixing. Experimental conditions: T = 77 K; microwave frequency = 9.44 GHz; microwave power = 0.1 mW; modulation amplitude = 1 G; average of 9 scans.

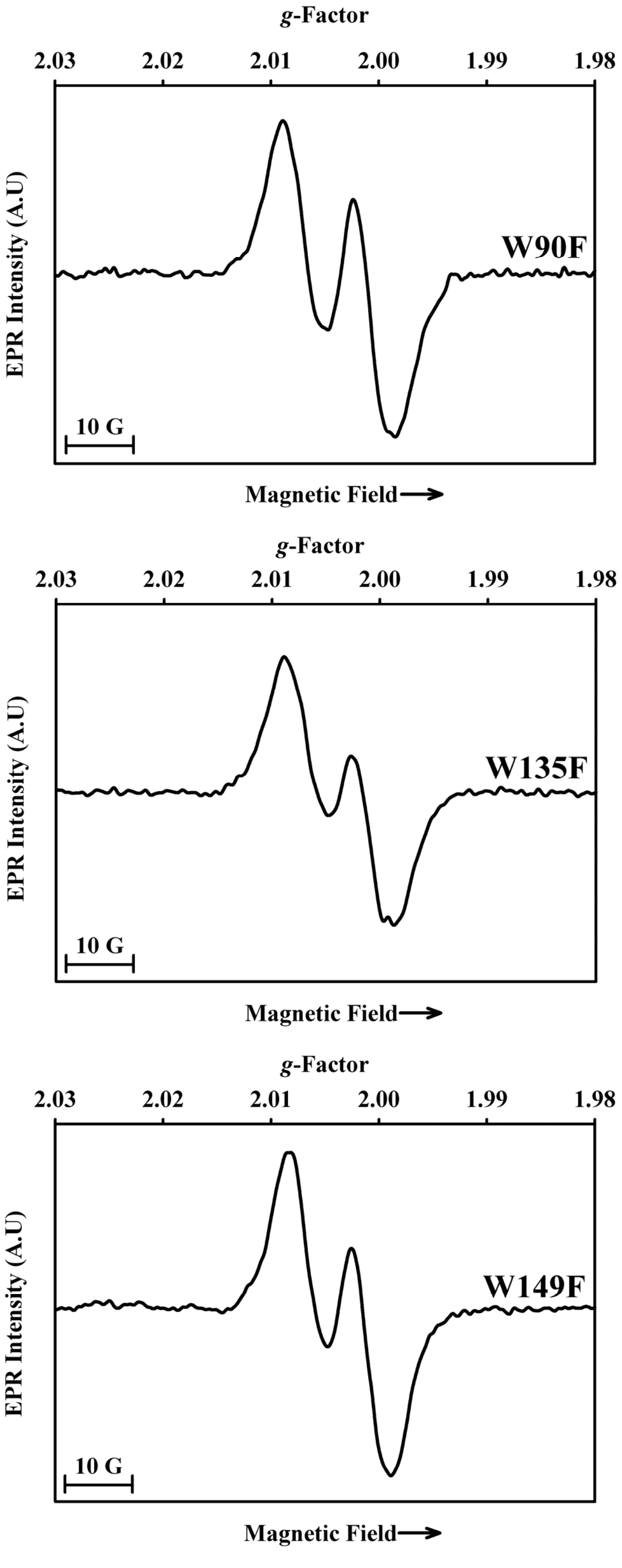

Figure 3.S3. X-band RFQ-EPR spectra of KatG[W90F], [W135F], and [W149F] (50 μM) each treated with 8000-fold molar excess of H_2O_2 at pH 8.5 frozen manually within 1.5 sec after mixing. Experimental conditions: T = 77 K; microwave frequency = 9.45 GHz; microwave power = 0.1 mW; modulation amplitude = 1 G; average of 9 scans.

Appendix C

Author's other contributions.

During the period of dissertation studies, the author carried out other experiments related to KatG and melanin research that were not addressed here and also, participated in other collaborative projects, some of which were published while others are still in progress.

In one of the published contributions [122], room-temperature spin-trapping EPR experiments were performed by the author to study the protection of DNA by the Lsr2 protein in *Mtb* against reactive oxygen intermediates. In spin-trapping, an EPR silent compound reacts with reactive short-lived free radicals to form a more persistent spin adduct. From the spectrum of the spin adduct, the structure of the reactive free radical can be deduced indirectly.

In another collaborative study related to oxidative damage and tissue injury mediated by the formation of free radicals [123], the author carried out enzyme kinetic experiment using double-mixing stopped-flow spectrophotometry to determine the rate of formation of Compound I in the mammalian peroxidase enzyme myeloperoxidase, and the rate of reduction of Compound I to Compound II by sulfite/bisulfite ions. This process produces sulfite anion radical ($SO_3^{\bullet-}$) that reacts rapidly with oxygen to form peroxymonosulfate ($^{-}O_3SOO^{\bullet}$) and sulfate ($SO_4^{\bullet-}$) anion radicals. The ultimately formed $SO_4^{\bullet-}$ is a very strong oxidant that can oxidize macromolecules such as proteins, thereby introducing cellular damage by propagating protein radical formation.

In a recently-published study involving trimeric aniline (TANI) [124], room-temperature EPR measurements were performed by the author to monitor the radical cation evolution in the organic oligomer as a result of acid doping. The EPR data helped explain the step-wise protonation process through unpaired spin quantification and provided additional characterization for a conducting polymer with potential applications in the field of sensors and electrochromic materials.

Altogether, 6 published papers and 1 manuscript (in review at the time of this writing) were the result of the past few years of doctoral research:

1. Colangeli, R.; Haq, A.; Arcus, V. L.; Summers, E.; Magliozzo, R. S.; McBride, A.; Mitra, A. K.; Radjainia, M.; Khajo, A.; Jacobs Jr., W. R.; Salgame, P.; and Alland, D. The multifunctional histone-like protein Lsr2 protects mycobacteria against reactive oxygen intermediates. *Proc. Natl. Acad. Sci., U S A* **2009**; 106(11): 4414-4418.

2. Zhao, X.; Suarez, J.; Khajo, A.; Yu, S.; Metlitsky, L.; and Magliozzo, R. S. A radical on the Met-Tyr-Trp modification required for catalase activity in catalase-peroxidase is established by isotopic labeling and site-directed mutagenesis. *J. Am. Chem. Soc.* **2010**; *132* (24), 8268–8269.

3. Khajo, A.; Bryan, R. A.; Friedman, M.; Burger, R. M.; Levitsky, Y.; Casadevall, A.; Magliozzo, R. S.; and Dadachova, E. Protection of melanized Cryptococcus neoformans from lethal dose gamma irradiation involves changes in melanin's chemical structure and paramagnetism. *PLoS ONE* **2011**; 6(9): e25092.

4. Ranguelova, K.; Rice, A. B.; Khajo, A.; Triquigneaux, M. ; Garantziotis, S.; Magliozzo, R. S.; and Mason, R. P. Formation of Reactive Sulfite-Derived Free Radicals by the Activation of Human Neutrophils: An ESR Study. *Free Rad. Biol. Med.* **2012**; 52(8), 1264-1271.

5. Zhang, Q.; Khajo, A.; Sai, T.; de Albuquerque, I.; Magliozzo, R.; and Levon, K. Intramolecular Transport of Charge Carriers in Trimeric Aniline upon a Three-Step Acid Doping Process. *J. Phys. Chem. A* **2012**; 116, 7629-7635.

6. Zhao, X.; Khajo, A.; Jarrett, S.; Suarez, J.; Levitsky, Y.; Burger, R. M.; Jarzecki, A. A.; and Magliozzo, R. S. Specific function of the Met-Tyr-Trp adduct radical and residues Arg418 and Asp137 in the atypical catalase reaction of catalase-peroxidase KatG. *J. Biol. Chem.* 2012; in press. http://www.jbc.org/cgi/doi/10.1074/jbc.M112.401208

7. Zhang, L.; Andersen, E. M. E.; Khajo, A.; Magliozzo, R. S. and Koder, R. L. Factors Affecting Gaseous Ligand Binding in an Artificial Neuroglobin. *Biochemistry* **2012**; in review.

References

[1] WHO. Global Tuberculosis Control. 2011.

[2] WHO. Initiative for Vaccine Research (IVR): Tuberculosis. 2007.

[3] Harries, A. D.; Dye, C. Tuberculosis. *Ann Trop Med Parasitol* **100:**415-431; 2006.

[4] Rothschild, B. M.; Martin, L. D.; Lev, G.; Bercovier, H.; Bar-Gal, G. K.; Greenblatt, C.; Donoghue, H.; Spigelman, M.; Brittain, D. *Mycobacterium tuberculosis* complex DNA from an extinct bison dated 17,000 years before the present. *Clin Infect Dis* **33:**305-311; 2001.

[5] eMedTV. Tuberculosis History. 2008.

[6] Robitzek, E. H.; Selikoff, I. J. Hydrazine derivatives of isonicotinic acid (rimifon marsilid) in the treatment of active progressive caseous-pneumonic tuberculosis; a preliminary report. *Am Rev Tuberc* **65:**402-428; 1952.

[7] CDC. Tuberculosis (TB). 2010.

[8] Phyu, S.; Ti, T.; Jureen, R.; Hmun, T.; Myint, H.; Htun, A.; Grewal, H. M.; Bjorvatn, B. Drug-resistant *Mycobacterium tuberculosis* among new tuberculosis patients, Yangon, Myanmar. *Emerging infectious diseases* **9:**274-276; 2003.

[9] Sepkowitz, K. A. AIDS, tuberculosis, and the health care worker. *Clin Infect Dis* **20:**232-242.; 1995.

[10] Sepkowitz, K. A. Tuberculosis control in the 21st century. *Emerging infectious diseases* **7:**259-262.; 2001.

[11] Middlebrook, G.; Cohn, M. L.; Schaeffer, W. B. *Am Rev Tuberc* **70:**852-872; 1954.

[12] Heym, B.; Cole, S. T. Isolation and characterization of isoniazid-resistant mutants of *Mycobacterium smegmatis* and *M. aurum*. *Res Microbiol* **143:**721-730; 1992.

[13] Zhang, Y.; Heym, B.; Allen, B.; Young, D.; Cole, S. The catalase-peroxidase gene and isoniazid resistance of *Mycobacterium tuberculosis*. *Nature* **358:**591-593.; 1992.

[14] Rawat, R.; Whitty, A.; Tonge, P. J. The isoniazid-NAD adduct is a slow, tight-binding inhibitor of InhA, the *Mycobacterium tuberculosis* enoyl reductase: adduct affinity and drug resistance. *Proc Natl Acad Sci U S A* **100:**13881-13886; 2003.

[15] Rozwarski, D. A.; Grant, G. A.; Barton, D. H. R.; Jacobs, W. R., Jr.; Sacchettini, J. C. Modification of the NADH of the isoniazid target (InhA) from *Mycobacterium tuberculosis*. *Science* **279:**98-102; 1998.

[16] Lei, B.; Wei, C. J.; Tu, S. C. Action mechanism of antitubercular isoniazid. Activation by *Mycobacterium tuberculosis* KatG, isolation, and characterization of inha inhibitor. *J Biol Chem* **275:**2520-2526; 2000.

[17] Quemard, A.; Sacchettini, J. C.; Dessen, A.; Vilcheze, C.; Bittman, R.; Jacobs, W. R., Jr.; Blanchard, J. S. Enzymatic characterization of the target for isoniazid in *Mycobacterium tuberculosis*. *Biochemistry* **34:**8235-8241; 1995.

[18] Claiborne, A.; Fridovich, I. Chemical and enzymatic intermediates in the peroxidation of o-dianisidine by horseradish peroxidase. 1. Spectral properties of the products of dianisidine oxidation. *Biochemistry* **18:**2324-2329; 1979.

[19] Claiborne, A.; Malinowski, D. P.; Fridovich, I. Purification and characterization of hydroperoxidase II of *Escherichia coli B*. *J Biol Chem* **254:**11664-11668; 1979.

[20] Welinder, K. G. Bacterial catalase-peroxidases are gene duplicated members of the plant peroxidase superfamily. *Biochim Biophys Acta* **1080:**215-220; 1991.

[21] Zhao, X.; Yu, H.; Yu, S.; Wang, F.; Sacchettini, J. C.; Magliozzo, R. S. Hydrogen peroxide-mediated isoniazid activation catalyzed by *Mycobacterium tuberculosis* catalase-peroxidase (KatG) and its S315T mutant. *Biochemistry* **45:**4131-4140; 2006.

[22] Heym, B.; Zhang, Y.; Poulet, S.; Young, D.; Cole, S. T. Characterization of the katG gene encoding a catalase-peroxidase required for the isoniazid susceptibility of *Mycobacterium tuberculosis*. *J Bacteriol* **175:**4255-4259; 1993.

[23] Cohn, M. L.; Oda, U.; Kovitz, C.; Middlebrook, G. Studies on isoniazid and tubercle bacilli. I. The isolation of isoniazid-resistant mutants in vitro. *Am Rev Tuberc* **70:**465-475; 1954.

[24] Ng, V. H.; Cox, J. S.; Sousa, A. O.; MacMicking, J. D.; McKinney, J. D. Role of KatG catalase-peroxidase in mycobacterial pathogenesis: countering the phagocyte oxidative burst. *Mol Microbiol* **52:**1291-1302; 2004.

[25] Zamocky, M.; Regelsberger, G.; Jakopitsch, C.; Obinger, C. The molecular peculiarities of catalase-peroxidases. *FEBS Lett* **492:**177-182.; 2001.

[26] Nagy, J. M.; Cass, A. E.; Brown, K. A. Purification and characterization of recombinant catalase-peroxidase, which confers isoniazid sensitivity in *Mycobacterium tuberculosis*. *J Biol Chem* **272:**31265-31271; 1997.

[27] Zamocky, M.; Furtmuller, P. G.; Obinger, C. Evolution of catalases from bacteria to humans. *Antioxid Redox Signal* **10:**1527-1548; 2008.

[28] Dunford, H. B. *Heme Peroxidases*. New York: Wiley-VCH; 1999.

[29] Jakopitsch, C.; Droghetti, E.; Schmuckenschlager, F.; Furtmuller, P. G.; Smulevich, G.; Obinger, C. Role of the main access channel of catalase-peroxidase in catalysis. *J Biol Chem* **280:**42411-42422; 2005.

[30] Jakopitsch, C.; Vlasits, J.; Wiseman, B.; Loewen, P. C.; Obinger, C. Redox intermediates in the catalase cycle of catalase-peroxidases from *Synechocystis* PCC 6803, *Burkholderia pseudomallei*, and *Mycobacterium tuberculosis*. *Biochemistry* **46:**1183-1193; 2007.

[31] Suarez, J.; Ranguelova, K.; Jarzecki, A. A.; Manzerova, J.; Krymov, V.; Zhao, X.; Yu, S.; Metlitsky, L.; Gerfen, G. J.; Magliozzo, R. S. An oxyferrous heme/protein-based radical intermediate is catalytically competent in the catalase reaction of *Mycobacterium tuberculosis* catalase-peroxidase (KatG). *J Biol Chem* **284:**7017-7029; 2009.

[32] Singh, R.; Switala, J.; Loewen, P. C.; Ivancich, A. Two [Fe(IV)=O Trp•] intermediates in *M. tuberculosis* catalase-peroxidase discriminated by multifrequency (9-285 GHz) EPR spectroscopy: reactivity toward isoniazid. *J Am Chem Soc* **129:**15954-15963; 2007.

[33] Colin, J.; Wiseman, B.; Switala, J.; Loewen, P. C.; Ivancich, A. Distinct role of specific tryptophans in facilitating electron transfer or as [Fe(IV)=O Trp•] intermediates in the peroxidase reaction of *Bulkholderia pseudomallei* catalase-peroxidase: a multifrequency EPR spectroscopy investigation. *J Am Chem Soc* **131:**8557-8563; 2009.

[34] Zhao, X.; Suarez, J.; Khajo, A.; Yu, S.; Metlitsky, L.; Magliozzo, R. S. A radical on the Met-Tyr-Trp modification required for catalase activity in catalase-peroxidase is established by isotopic labeling and site-directed mutagenesis. *J Am Chem Soc* **132:**8268-8269; 2010.

[35] George, P.; Irvine, D. H. A possible structure for the higher oxidation state of metmyoglobin. *The Biochemical journal* **60:**596-604; 1955.

[36] Gibson, J. F.; Ingram, D. J.; Nicholls, P. Free radical produced in the reaction of metmyoglobin with hydrogen peroxide. *Nature* **181:**1398-1399; 1958.

[37] Ivancich, A.; Jouve, H. M.; Sartor, B.; Gaillard, J. EPR investigation of compound I in Proteus mirabilis and bovine liver catalases: formation of porphyrin and tyrosyl radical intermediates. *Biochemistry* **36:**9356-9364; 1997.

[38] Ivancich, A.; Mazza, G.; Desbois, A. Comparative electron paramagnetic resonance study of radical intermediates in turnip peroxidase isozymes. *Biochemistry* **40:**6860-6866.; 2001.

[39] Larsson, A.; Sjoberg, B. M. Identification of the stable free radical tyrosine residue in ribonucleotide reductase. *Embo J* **5:**2037-2040.; 1986.

[40] Karthein, R.; Dietz, R.; Nastainczyk, W.; Ruf, H. H. Higher oxidation states of prostaglandin H synthase. EPR study of a transient tyrosyl radical in the enzyme during the peroxidase reaction. *Eur J Biochem* **171:**313-320.; 1988.

[41] Blodig, W.; Smith, A. T.; Winterhalter, K.; Piontek, K. Evidence from spin-trapping for a transient radical on tryptophan residue 171 of lignin peroxidase. *Arch Biochem Biophys* **370:**86-92.; 1999.

[42] Chouchane, S.; Girotto, S.; Yu, S.; Magliozzo, R. S. Identification and Characterization of Tyrosyl Radical Formation in *Mycobacterium tuberculosis* Catalase-Peroxidase (KatG). *J Biol Chem* **277:**42633-42638; 2002.

[43] Ranguelova, K.; Girotto, S.; Gerfen, G. J.; Yu, S.; Suarez, J.; Metlitsky, L.; Magliozzo, R. S. Radical sites in *Mycobacterium tuberculosis* KatG identified using electron paramagnetic resonance spectroscopy, the three-dimensional crystal structure, and electron transfer couplings. *J Biol Chem* **282:**6255-6264; 2007.

[44] Chouchane, S.; Lippai, I.; Magliozzo, R. S. Catalase-peroxidase (*Mycobacterium tuberculosis* KatG) catalysis and isoniazid activation. *Biochemistry* **39:**9975-9983; 2000.

[45] Weast, R. C. *CRC Handbook of Chemistry and Physics 61st Ed 1980-1981.* Chemical Rubber; 1981.

[46] Sprecher, M.; Srinivasan, P. R.; Sprinson, D. B.; Davis, B. D. The Biosynthesis of Tyrosine from Labeled Glucose in *Escherichia coli*. *Biochemistry* **4:**2855-2860; 1965.

[47] Vlasits, J.; Jakopitsch, C.; Bernroitner, M.; Zamocky, M.; Furtmüller, P. G.; Obinger, C. Mechanisms of catalase activity of heme peroxidases. *Arch Biochem Biophys* **500:**74-81; 2010.

[48] Jakopitsch, C.; Auer, M.; Ivancich, A.; Ruker, F.; Furtmuller, P. G.; Obinger, C. Total conversion of bifunctional catalase-peroxidase (KatG) to monofunctional peroxidase by exchange of a conserved distal side tyrosine. *J Biol Chem* **278:**20185-20191; 2003.

[49] Jakopitsch, C.; Ivancich, A.; Schmuckenschlager, F.; Wanasinghe, A.; Poltl, G.; Furtmuller, P. G.; Ruker, F.; Obinger, C. Influence of the unusual covalent adduct on the kinetics and formation of radical intermediates in *synechocystis* catalase peroxidase: a stopped-flow and EPR characterization of the MET275, TYR249, and ARG439 variants. *J Biol Chem* **279:**46082-46095; 2004.

[50] Yu, S.; Girotto, S.; Zhao, X.; Magliozzo, R. S. Rapid Formation of Compound II and a Tyrosyl Radical in the Y229F Mutant of *Mycobacterium tuberculosis* Catalase-peroxidase Disrupts Catalase but Not Peroxidase Function. *J Biol Chem* **278:**44121-44127; 2003.

[51] Ghiladi, R. A.; Medzihradszky, K. F.; Ortiz de Montellano, P. R. Role of the Met-Tyr-Trp Cross-Link in *Mycobacterium tuberculosis* Catalase-Peroxidase (KatG) As Revealed by KatG(M255I). *Biochemistry* **44:**15093-15105; 2005.

[52] Ghiladi, R. A.; Knudsen, G. M.; Medzihradszky, K. F.; de Montellano, P. R. The Met-Tyr-Trp cross-link in *Mycobacterium tuberculosis* catalase-peroxidase (KatG): autocatalytic formation and effect on enzyme catalysis and spectroscopic properties. *J Biol Chem* **280:**22651-22663; 2005.

[53] Carpena, X.; Wiseman, B.; Deemagarn, T.; Herguedas, B.; Ivancich, A.; Singh, R.; Loewen, P. C.; Fita, I. Roles for Arg426 and Trp111 in the modulation of NADH oxidase activity of the catalase-peroxidase KatG from *Burkholderia pseudomallei* inferred from pH-induced structural changes. *Biochemistry* **45:**5171-5179; 2006.

[54] Cade, C. E.; Dlouhy, A. C.; Medzihradszky, K. F.; Salas-Castillo, S. P.; Ghiladi, R. A. Isoniazid-resistance conferring mutations in *Mycobacterium tuberculosis* KatG: catalase, peroxidase, and INH-NADH adduct formation activities. *Protein Sci* **19:**458-474; 2010.

[55] Jakopitsch, C.; Auer, M.; Regelsberger, G.; Jantschko, W.; Furtmuller, P. G.; Ruker, F.; Obinger, C. Distal site aspartate is essential in the catalase activity of catalase-peroxidases. *Biochemistry* **42:**5292-5300; 2003.

[56] Zhao, X.; Yu, S.; Ranguelova, K.; Suarez, J.; Metlitsky, L.; Schelvis, J. P.; Magliozzo, R. S. Role of the oxyferrous heme intermediate and distal side adduct radical in the catalase activity of *Mycobacterium tuberculosis* KatG revealed by the W107F mutant. *J Biol Chem* **284:**7030-7037; 2009.

[57] Keilin, D.; Hartree, E. F. Purification of horse-radish peroxidase and comparison of its properties with those of catalase and methaemoglobin. *The Biochemical journal* **49:**88-104; 1951.

[58] Ranguelova, K.; Suarez, J.; Metlitsky, L.; Yu, S.; Brejt, S. Z.; Zhao, L.; Schelvis, J. P.; Magliozzo, R. S. Impact of distal side water and residue 315 on ligand binding to ferric *Mycobacterium tuberculosis* catalase-peroxidase (KatG). *Biochemistry* **47:**12583-12592; 2008.

[59] Yu, S.; Girotto, S.; Lee, C.; Magliozzo, R. S. Reduced Affinity for Isoniazid in the S315T Mutant of *Mycobacterium tuberculosis* KatG Is a Key Factor in Antibiotic Resistance. *J Biol Chem* **278:**14769-14775; 2003.

[60] Jakopitsch, C.; Wanasinghe, A.; Jantschko, W.; Furtmuller, P. G.; Obinger, C. Kinetics of interconversion of ferrous enzymes, compound II and compound III, of wild-type *synechocystis* catalase-peroxidase and Y249F: proposal for the catalatic mechanism. *J Biol Chem* **280:**9037-9042; 2005.

[61] Adediran, S. A.; Lambeir, A. M. Kinetics of the reaction of compound II of horseradish peroxidase with hydrogen peroxide to form compound III. *Eur J Biochem* **186:**571-576; 1989.

[62] Nakajima, R.; Yamazaki, I. The mechanism of oxyperoxidase formation from ferryl peroxidase and hydrogen peroxide. *J Biol Chem* **262 ,:**2576-2581; 1987.

[63] Zhao, X.; Girotto, S.; Yu, S.; Magliozzo, R. S. Evidence for radical formation at Tyr-353 in *Mycobacterium tuberculosis* catalase-peroxidase (KatG). *J Biol Chem* **279:**7606-7612; 2004.

[64] Erman, J. E.; Vitello, L. B.; Mauro, J. M.; Kraut, J. Detection of an oxyferryl porphyrin pi-cation-radical intermediate in the reaction between hydrogen peroxide and a mutant yeast cytochrome c peroxidase. Evidence for tryptophan-191 involvement in the radical site of compound I. *Biochemistry* **28:**7992-7995; 1989.

[65] Vidossich, P.; Alfonso-Prieto, M.; Carpena, X.; Loewen, P. C.; Fita, I.; Rovira, C. Versatility of the electronic structure of compound I in catalase-peroxidases. *J Am Chem Soc* **129:**13436-13446; 2007.

[66] Girotto, S. Application of EPR spectroscopy to study the resting state structure and the mechnism of *Mycobacterium tuberculosis* catalase peroxidase KatG. Ph. D. thesis. *The Graduate Center of the City University of New York;* 2004.

[67] Konovalova, T. A.; Kispert, L. D.; van Tol, J.; Brunel, L.-C. Multifrequency High-Field Electron Paramagnetic Resonance Characterization of the Peroxyl Radical Location in Horse Heart Myoglobin Oxidized by H_2O_2. *The Journal of Physical Chemistry B* **108:**11820-11826; 2004.

[68] Yu, M. A.; Egawa, T.; Shinzawa-Itoh, K.; Yoshikawa, S.; Yeh, S. R.; Rousseau, D. L.; Gerfen, G. J. Radical formation in cytochrome c oxidase. *Biochim Biophys Acta* **1807:**1295-1304; 2011.

[69] Svistunenko, D. A. Reaction of haem containing proteins and enzymes with hydroperoxides: the radical view. *Biochim Biophys Acta* **1707:**127-155; 2005.

[70] Ivancich, A.; Jakopitsch, C.; Auer, M.; Un, S.; Obinger, C. Protein-based radicals in the catalase-peroxidase of *synechocystis* PCC6803: a multifrequency EPR investigation of wild-type and variants on the environment of the heme active site. *J Am Chem Soc* **125:**14093-14102; 2003.

[71] Wengenack, N. L.; Rusnak, F. Evidence for Isoniazid-Dependent Free Radical Generation Catalyzed by *Mycobacterium tuberculosis* KatG and the Isoniazid-Resistant Mutant KatG(S315T). *Biochemistry* **40:**8990-8996; 2001.

[72] Broussy, S.; Bernardes-Genisson, V.; Coppel, Y.; Quemard, A.; Bernadou, J.; Meunier, B. 1H and 13C NMR characterization of pyridinium-type isoniazid-NAD adducts as possible inhibitors of InhA reductase of *Mycobacterium tuberculosis*. *Org Biomol Chem* **3:**670-673; 2005.

[73] Ghiladi, R. A.; Medzihradszky, K. F.; Rusnak, F. M.; Ortiz de Montellano, P. R. Correlation between isoniazid resistance and superoxide reactivity in *mycobacterium tuberculosis* KatG. *J Am Chem Soc* **127:**13428-13442; 2005.

[74] Suarez, J.; Ranguelova, K.; Schelvis, J. P.; Magliozzo, R. S. Antibiotic resistance in *Mycobacterium tuberculosis*: peroxidase intermediate bypass causes poor isoniazid activation by the S315G mutant of *M. tuberculosis* catalase-peroxidase (KatG). *J Biol Chem* **284:**16146-16155; 2009.

[75] Hazbon, M. H.; Brimacombe, M.; Bobadilla del Valle, M.; Cavatore, M.; Guerrero, M. I.; Varma-Basil, M.; Billman-Jacobe, H.; Lavender, C.; Fyfe, J.; Garcia-Garcia, L.; Leon, C. I.; Bose, M.; Chaves, F.; Murray, M.; Eisenach, K. D.; Sifuentes-Osornio, J.; Cave, M. D.; Ponce de Leon, A.; Alland, D. Population genetics study of isoniazid resistance mutations and evolution of multidrug-resistant *Mycobacterium tuberculosis*. *Antimicrob Agents Chemother* **50:**2640-2649; 2006.

[76] Metcalfe, C.; Macdonald, I. K.; Murphy, E. J.; Brown, K. A.; Raven, E. L.; Moody, P. C. E. The Tuberculosis Prodrug Isoniazid Bound to Activating Peroxidases. *Journal of Biological Chemistry* **283:**6193-6200; 2008.

[77] Schulz, C. E.; Devaney, P. W.; Winkler, H.; Debrunner, P. G.; Doan, N.; Chiang, R.; Rutter, R.; Hager, L. P. Horseradish peroxidase compound I: evidence for spin coupling between the heme iron and a 'free' radical. *FEBS Lett* **103:**102-105; 1979.

[78] Mauro, J. M.; Fishel, L. A.; Hazzard, J. T.; Meyer, T. E.; Tollin, G.; Cusanovich, M. A.; Kraut, J. Tryptophan-191----phenylalanine, a proximal-side mutation in yeast cytochrome c peroxidase that strongly affects the kinetics of ferrocytochrome c oxidation. *Biochemistry* **27:**6243-6256; 1988.

[79] Khajo, A.; Bryan, R. A.; Friedman, M.; Burger, R. M.; Levitsky, Y.; Casadevall, A.; Magliozzo, R. S.; Dadachova, E. Protection of melanized *Cryptococcus neoformans* from lethal dose gamma irradiation involves changes in melanin's chemical structure and paramagnetism. *PLoS ONE* **6:**e25092; 2011.

[80] Wakamatsu, K.; Ito, S. Advanced chemical methods in melanin determination. *Pigment Cell Res* **15:**174-183; 2002.

[81] Meredith, P.; Riesz, J. Radiative relaxation quantum yields for synthetic eumelanin. *Photochem Photobiol* **79:**211-216; 2004.

[82] Steinert, M.; Engelhard, H.; Flugel, M.; Wintermeyer, E.; Hacker, J. The Lly protein protects *Legionella pneumophila* from light but does not directly influence its intracellular survival in *Hartmannella vermiformis*. *Appl Environ Microbiol* **61:**2428-2430; 1995.

[83] Wang, Y.; Casadevall, A. Decreased susceptibility of melanized *Cryptococcus neoformans* to UV light. *Appl Environ Microbiol* **60:**3864-3866; 1994.

[84] Zughaier, S. M.; Ryley, H. C.; Jackson, S. K. A melanin pigment purified from an epidemic strain of *Burkholderia cepacia* attenuates monocyte respiratory burst activity by scavenging superoxide anion. *Infect Immun* **67:**908-913; 1999.

[85] Turick, C. E.; Caccavo, F., Jr.; Tisa, L. S. Electron transfer from *Shewanella algae* BrY to hydrous ferric oxide is mediated by cell-associated melanin. *FEMS Microbiol Lett* **220:**99-104; 2003.

[86] Turick, C. E.; Tisa, L. S.; Caccavo, F., Jr. Melanin production and use as a soluble electron shuttle for Fe(III) oxide reduction and as a terminal electron acceptor by *Shewanella algae* BrY. *Appl Environ Microbiol* **68:**2436-2444; 2002.

[87] Turick, C. E.; Beliaev, A. S.; Zakrajsek, B. A.; Reardon, C. L.; Lowy, D. A.; Poppy, T. E.; Maloney, A.; Ekechukwu, A. A. The role of 4-hydroxyphenylpyruvate dioxygenase in

enhancement of solid-phase electron transfer by *Shewanella oneidensis* MR-1. *FEMS Microbiol Ecol* **68:**223-225; 2009.

[88] Meredith, P.; Sarna, T. The physical and chemical properties of eumelanin. *Pigment Cell Res* **19:**572-594; 2006.

[89] Dadachova, E.; Bryan, R. A.; Huang, X.; Moadel, T.; Schweitzer, A. D.; Aisen, P.; Nosanchuk, J. D.; Casadevall, A. Ionizing radiation changes the electronic properties of melanin and enhances the growth of melanized fungi. *PLoS ONE* **2:**e457; 2007.

[90] Dadachova, E.; Bryan, R. A.; Howell, R. C.; Schweitzer, A. D.; Aisen, P.; Nosanchuk, J. D.; Casadevall, A. The radioprotective properties of fungal melanin are a function of its chemical composition, stable radical presence and spatial arrangement. *Pigment Cell Melanoma Res* **21:**192-199; 2008.

[91] Dadachova, E.; Casadevall, A. Ionizing radiation: how fungi cope, adapt, and exploit with the help of melanin. *Curr Opin Microbiol* **11:**525-531; 2008.

[92] Schweitzer, A. D.; Howell, R. C.; Jiang, Z.; Bryan, R. A.; Gerfen, G.; Chen, C. C.; Mah, D.; Cahill, S.; Casadevall, A.; Dadachova, E. Physico-chemical evaluation of rationally designed melanins as novel nature-inspired radioprotectors. *PLoS ONE* **4:**e7229; 2009.

[93] Sarna, T.; Pilas, B.; Land, E. J.; Truscott, T. G. Interaction of radicals from water radiolysis with melanin. *Biochim Biophys Acta* **883:**162-167; 1986.

[94] Korytowski, W.; Sarna, T. Bleaching of melanin pigments. Role of copper ions and hydrogen peroxide in autooxidation and photooxidation of synthetic dopa-melanin. *J Biol Chem* **265:**12410-12416; 1990.

[95] Sarna, T.; Swartz, H. A. The physical properties of melanin. In: Nordlund, J. J.; Biossy, R. E.; Hearing, V. J.; King, R. A.; Ortonne, J.-P., eds. *The Pigment System: Physiology and Pathophysiology*. Oxford: Oxford University Press; 1998: 333-358.

[96] Sarna, T.; Plonka, P. M. Biophysical studies of melanin: paramagnetic, ion-exchange and redox properties of melanin pigments and their photoreactivity. In: Eaton, S. S.; Eaton, G. R.; Berliner, L. J., eds. *Biomedical ESR. Biological Magnetic Resonance Series*. The Netherlands, New York, Boston: Kluwer Academic Publishers; 2005: 125-146.

[97] Felix, C. C.; Hyde, J. S.; Sarna, T.; Sealy, R. C. Interactions of Melanin with Metal Ions. Electron Spin Resonance Evidence for Chelate Complexes of Metal Ions with Free Radicals. *J Am Chem Soc* **100:**3922-3926; 1978.

[98] Sealy, R. C.; Hyde, J. S.; Felix, C. C.; Menon, I. A.; Prota, G. Eumelanins and pheomelanins: characterization by electron spin resonance spectroscopy. *Science* **217:**545-547; 1982.

[99] Pasenkiewicz-Gierula, M.; Sealy, R. C. Analysis of the ESR spectrum of synthetic dopa melanin. *Biochim Biophys Acta* **884:**510-516; 1986.

[100] Pan, Y. M.; Nilges, M. J.; Mashkovtsev, R. I. Radiation-induced defects in quartz: a multifrequency EPR study and DFT modelling of new peroxy radicals *Mineralogical Magazine* **73:**519-535; 2009.

[101] Bolton, J. R.; Borg, D. C.; Swartz, H. M. *Biological Applications of Electron Spin Resonance.* New York: Wiley & Sons; 1972.

[102] Box, H.; Lilga, K.; Budzinski, E.; Derr, R. Hydroxyl radicals in X-Irradiated single crystals of ice *J Chem Phys* **50:**5422-5423; 1969.

[103] Bednarek, J.; Plonka, A.; Hallbrucker, A.; Mayer, E.; Symons, M. C. R. Hydroperoxyl radical generation by γ-irradiation of glassy water at 77 K. *J Am Chem Soc* **118:**9387-9390; 1996.

[104] Arena, V. Ionizing radiation and life: An introduction to radiation biology and biological radiotracer methods. St. Louis: Mosby; 1971: 298-326.

[105] Napolitano, A.; Pezella, A.; Vincensi, M. R.; Prota, G. Oxidative degradation of melanins to pyrrole acids: A model study. *Tetrahedron* **51:**5913-5920; 1995.

[106] Kwon, T. W.; Watts, B. M. Determination of Malonaldehyde by Ultraviolet Spectrophotometry. *J Food Sci* **28:**627-630; 1963.

[107] Bird, R. P.; Draper, H. H. Comparative studies on different methods of malonaldehyde determination. *Methods Enzymol* **105:**299-305; 1984.

[108] Guzman-Chozas, M.; Vicario, I. M.; Guillen-Sans, R. Spectrophotometric profiles of off-flavor aldehydes by using their reactions with 2-thiobarbituric acid. *J Agric Food Chem* **45:**2452-2457; 1997.

[109] Grotto, D.; Maria, L. S.; Valentini, J.; Paniz, C.; Schmitt, G.; Garcia, S. C.; Pomblum, V. J.; Rocha, J. B. T.; Farina, M. Importance of the lipid peroxidation biomarkers and methodological aspects for malondialdehyde quantification. *Quim Nova* **32:**169-174; 2009.

[110] Halmann, M.; Bloch, S. Glyoxal and malonaldehyde formation by ultraviolet irradiation of aqueous formaldehyde. *Biosystems* **11:**227-232; 1979.

[111] Kosugi, H.; Kikugawa, K. Reaction of thiobarbituric acid with saturated aldehydes. *Lipids* **21:**537-542; 1986.

[112] Pascutti, P. G.; Ito, A. S. EPR study of melanin-protein interaction: photoinduced free radicals and progressive microwave power saturation. *J Photochem Photobiol B* **16:**257-266; 1992.

[113] Eisenman, H. C.; Nosanchuk, J. D.; Webber, J. B.; Emerson, R. J.; Camesano, T. A.; Casadevall, A. Microstructure of cell wall-associated melanin in the human pathogenic fungus *Cryptococcus neoformans*. *Biochemistry* **44:**3683-3693; 2005.

[114] Yordanov, N. D.; Ranguelova, K. Quantitative electron paramagnetic resonance and spectrophotometric determination of the free radical 4-hydroxy-2,2,6,6-tetramethylpiperidinyloxy. *Spectrochim Acta A Mol Biomol Spectrosc* **56A:**373-378; 2000.

[115] Jacobson, E. S.; Ayers, D. J.; Harrell, A. C.; Nicholas, C. C. Genetic and phenotypic characterization of capsule mutants of *Cryptococcus neoformans*. *J Bacteriol* **150:**1292-1296; 1982.

[116] Bryan, R. A.; Zaragoza, O.; Zhang, T.; Ortiz, G.; Casadevall, A.; Dadachova, E. Radiological studies reveal radial differences in the architecture of the polysaccharide capsule of *Cryptococcus neoformans*. *Eukaryot Cell* **4:**465-475; 2005.

[117] Wang, Y.; Casadevall, A. Susceptibility of melanized and nonmelanized *Cryptococcus neoformans* to nitrogen- and oxygen-derived oxidants. *Infect Immun* **62:**3004-3007; 1994.

[118] Wang, Y.; Aisen, P.; Casadevall, A. Melanin, melanin "ghosts," and melanin composition in *Cryptococcus neoformans*. *Infect Immun* **64:**2420-2424; 1996.

[119] Usatyi, A. F.; Verein, N. V. EPR-based dosimetry of large dimensional radiation fields (Chernobyl experience and new approaches). *Appl Radiat Isot* **47:**1351-1356; 1996.

[120] Ito, S.; Wakamatsu, K. Chemical degradation of melanins: application to identification of dopamine-melanin. *Pigment Cell Res* **11:**120-126; 1998.

[121] Burger, R. M.; Peisach, J.; Blumberg, W. E.; Horwitz, S. B. Iron-bleomycin interactions with oxygen and oxygen analogues. Effects on spectra and drug activity. *J Biol Chem* **254:**10906-10912; 1979.

[122] Colangeli, R.; Haq, A.; Arcus, V. L.; Summers, E.; Magliozzo, R. S.; McBride, A.; Mitra, A. K.; Radjainia, M.; Khajo, A.; Jacobs, W. R., Jr.; Salgame, P.; Alland, D. The multifunctional

histone-like protein Lsr2 protects mycobacteria against reactive oxygen intermediates. *Proc Natl Acad Sci U S A* **106:**4414-4418; 2009.

[123] Ranguelova, K.; Rice, A. B.; Khajo, A.; Triquigneaux, M.; Garantziotis, S.; Magliozzo, R. S.; Mason, R. P. Formation of reactive sulfite-derived free radicals by the activation of human neutrophils: An ESR study. *Free Radical Biology and Medicine* **52:**1264-1271; 2012.

[124] Zhang, Q.; Khajo, A.; Sai, T.; de Albuquerque, I.; Magliozzo, R. S.; Levon, K. Intramolecular Transport of Charge Carriers in Trimeric Aniline upon a Three-Step Acid Doping Process. *J Phys Chem A* **116:**7629-7635; 2012.